

**YALOVA UNIVERSITY ★ GRADUATE SCHOOL OF SCIENCE ENGINEERING AND  
TECHNOLOGY**

**PRODUCTION OF BIO – BASED POROUS CARBON  
MATERIAL FROM LIGNOCELLULOSICS**



**M.Sc. THESIS**

**Sümevra Seniha BARAN**

**Department of Energy Systems Engineering**

**Energy Systems Engineering Programme**

**JUNE 2019**



**YALOVA UNIVERSITY ★ GRADUATE SCHOOL OF SCIENCE ENGINEERING AND  
TECHNOLOGY**

**PRODUCTION OF BIO – BASED POROUS CARBON  
MATERIAL FROM LIGNOCELLULOSICS**

**M.Sc. THESIS**

**Sümevra Seniha BARAN  
(165103001)**

**Department of Energy Systems Engineering**

**Energy Systems Engineering Programme**

**Thesis Advisor: Assoc. Prof. Dr. Sibel BAŞAKÇILARDAN KABAĞCI**

**JUNE 2019**



**YALOVA ÜNİVERSİTESİ ★ FEN BİLİMLERİ ENSTİTÜSÜ**

**LİGNOSELÜLOZİKLERDEN BİYO-KÖKENLİ PORÖZ KARBON  
MATERYALİN ÜRETİLMESİ**

**YÜKSEK LİSANS TEZİ**

**Sümevra Seniha BARAN  
(165103001)**

**Enerji Sistemleri Mühendisliđi Anabilim Dalı**

**Enerji Sistemleri Mühendisliđi Programı**

**Tez Danışmanı: Doç. Dr. Sibel BAŞAKÇILARDAN KABAĞCI**

**HAZİRAN 2019**



Sümeýra Seniha Baran, a M.Sc. student of YALOVA UNIVERSITY Graduate School of Science Engineering and Technology student ID 165103001, successfully defended the thesis entitled "PRODUCTION OF BIO – BASED CARBON MATERIAL FROM LIGNOCELLULOSICS", which she prepared after fulfilling the requirements specified in the associated legislations, in front of the jury whose signatures are below.

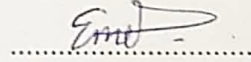
**Thesis Advisor :** Assoc. Prof. Dr. Sibel BAŞAKÇILARDAN  
KABAKCI  
Yalova University



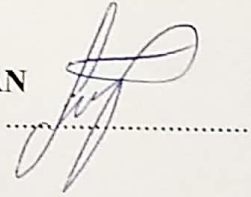
**Jury Members :** Dr. Pelin BARAN  
Yalova University



Dr. Emel TOPUZ  
Gebze Technical University



**Assoc. Prof. Dr. Sibel BAŞAKÇILARDAN**  
KABAKCI  
Yalova University



**Date of Submission :** 17 May 2019  
**Date of Defense :** 19 June 2019







*To the people whom I love,*



## **FOREWORD**

I would like to extend my gratitude to my respectable thesis advisor Assoc. Prof. Dr. Sibel BAŞAKÇILARDAN KABAKCI who meticulously managed this thesis, helped me in solving all my problems with her the knowledge and experience and never spared her support, attention and time from me.

I would like to thank Yalova University Scientific Research Unit for supported this thesis with the project numbered 2018/YL/0004. I also would like to thank the Scientific and Technological Research Council of Turkey (TÜBİTAK) for supported me and my thesis with 2210/C Priority Areas Graduate Scholarship.

I would like to thank my colleague Medya Hatun TANIŞ for her help and friendship both inside and outside the laboratory.

Finally, I would like to thank with my deepest feelings my dear mother Ayşe Nur BARAN, father Orhan Baran, sister Esma BARAN and brother Enes BARAN, who have brought me to this day, who provide all kinds of opportunities with their unlimited self-sacrifice and make always feel their love, interest and support.

June 2019

Sümevra Seniha BARAN  
Energy Systems Engineer, B.Sc.



## TABLE OF CONTENTS

	<u>Page</u>
<b>FOREWORD</b> .....	<b>ix</b>
<b>TABLE OF CONTENTS</b> .....	<b>xi</b>
<b>ABBREVIATIONS</b> .....	<b>xiii</b>
<b>LIST OF TABLES</b> .....	<b>xv</b>
<b>LIST OF FIGURES</b> .....	<b>xvii</b>
<b>SUMMARY</b> .....	<b>xix</b>
<b>ÖZET</b> .....	<b>xxi</b>
<b>1. BIOMASS</b> .....	<b>1</b>
1.1 Structural Composition of Lignocellulosic Biomass .....	2
1.1.1 Cellulose.....	4
1.1.2 Hemicellulose.....	5
1.1.3 Lignin .....	6
1.1.4 Extractives .....	7
1.2 Biomass Conversion Technologies .....	7
<b>2. HYDROTHERMAL CARBONIZATION</b> .....	<b>11</b>
2.1 Products .....	11
2.2 Reaction Mechanisms .....	12
2.3 Parameters That Affect Hydrothermal Carbonization.....	13
2.4 History and Applications of Hydrothermal Carbonization .....	19
<b>3. FUNCTIONALIZED CARBON MATERIALS</b> .....	<b>25</b>
3.1 Activated Carbon.....	26
3.1.1 Activation .....	27
3.1.1.1 Physical activation.....	27
3.1.1.2 Chemical activation.....	34
3.1.1.3 Physicochemical activation .....	46
3.1.2 History and applications of activated carbon .....	47
<b>4. MATERIALS AND METHODS</b> .....	<b>53</b>
4.1 Lignocellulosic biomass .....	53
4.2 Equipments.....	53
4.3 Methods .....	53
4.3.1 Hydrothermal carbonization.....	53
4.3.2 Chemical activation and carbonization .....	54
4.3.3 Characterizations .....	54
4.3.3.1 Elemental analysis.....	54
4.3.3.2 Proximate analysis.....	55
4.3.3.3 Determination of extractives in biomass.....	55

4.3.3.4 Determination of klason lignin in biomass.....	55
4.3.3.5 Heating value.....	56
4.3.3.6 Fourier transform infrared spectroscopy (FT-IR) .....	56
4.3.3.7 Thermogravimetric and derivative thermogravimetric analyses (TGA/DTG).....	56
4.3.3.8 Scanning electron microscopy (SEM).....	57
4.3.3.9 Brunauer-Emmett-Teller (BET) surface area analysis .....	57
<b>5. RESULT AND DISCUSSION.....</b>	<b>59</b>
5.1 Fuel Characteristics of Lignocellulosic Biomass Samples and Their Hydrochars.....	59
5.2 Surface Characteristics of Hydrochars and Activated Hydrochars .....	75
<b>6. CONCLUSIONS.....</b>	<b>87</b>
<b>REFERENCES .....</b>	<b>89</b>
<b>CURRICULUM VITAE .....</b>	<b>115</b>



## ABBREVIATIONS

<b>AHC</b>	: Activated Hydrochar
<b>ASTM</b>	: American Society for Testing and Materials
<b>BC</b>	: Before Christian Era
<b>BET</b>	: Brunauer–Emmett–Teller
<b>CH<sub>4</sub></b>	: Methane
<b>CO</b>	: Carbon Monoxide
<b>CO<sub>2</sub></b>	: Carbon Dioxide
<b>FeCl<sub>2</sub></b>	: Iron(II) Chloride
<b>FeCl<sub>3</sub></b>	: Iron(III) Chloride
<b>FT-IR</b>	: Fourier Transform Infrared Spectroscopy
<b>H<sub>2</sub>SO<sub>4</sub></b>	: Sulfuric Acid
<b>H<sub>3</sub>PO<sub>4</sub></b>	: Phosphoric Acid
<b>HC</b>	: Hydrochar
<b>HTC</b>	: Hydrothermal Carbonization
<b>I<sub>sc</sub></b>	: Short – Circuit Current
<b>IUPAC</b>	: International Union of Pure and Applied Chemistry
<b>K<sub>2</sub>CO<sub>3</sub></b>	: Potassium Carbonate
<b>KOH</b>	: Potassium Hydroxide
<b>m<sub>i</sub></b>	: Initial Mass
<b>m<sub>t</sub></b>	: Tare Mass
<b>N/A</b>	: Not Available
<b>nd</b>	: Not Determined
<b>N<sub>2</sub>O</b>	: Nitrous Oxide
<b>Na<sub>2</sub>CO<sub>3</sub></b>	: Sodium Carbonate
<b>NaOH</b>	: Sodium Hydroxide
<b>rpm</b>	: Revolutions Per Minute
<b>S<sub>BET</sub></b>	: BET Surface Area
<b>SEM</b>	: Scanning Electron Microscopy
<b>S<sub>mic</sub></b>	: Micropore Area
<b>TAPPI</b>	: Technical Association of the Pulp and Paper Industry

<b>T<sub>b</sub></b>	: Burnout Temperature
<b>TG/DTG</b>	: Thermogravimetry/Derivative Thermogravimetry
<b>T<sub>i</sub></b>	: Ignition Temperature
<b>T<sub>max</sub></b>	: The Temperature at Maximum Weight Loss Rate
<b>V<sub>meso</sub></b>	: Mesopore Volume
<b>V<sub>mic</sub></b>	: Micropore Volume
<b>V<sub>oc</sub></b>	: Open – Circuit Current
<b>V<sub>total</sub></b>	: Total Pore Volume
<b>ZnCl<sub>2</sub></b>	: Zinc Chloride





## LIST OF TABLES

	<u>Page</u>
<b>Table 1.1</b> : Cellulose, hemicellulose and lignin contents of various lignocellulosic biomass.....	2
<b>Table 2.1</b> : The hydrothermal carbonization of many different biomasses with various temperatures, retention times and biomass/water ratios and hydrochar yields. ....	16
<b>Table 3.1</b> : Physical activation conditions and properties of activated carbons produced. ....	32
<b>Table 3.2</b> : Chemical activation conditions and properties of activated carbons produced. ....	42
<b>Table 5.1</b> : Extractives and klason lignin contents of raw biomasses. ....	59
<b>Table 5.2</b> : Proximate and ultimate analyses, biomass contents and heating values of lignocellulosic biomass samples and their corresponding hydrochars....	62
<b>Table 5.3</b> : The mass yields of lignocellulosic hydrochars and their corresponding activated hydrochars.....	63
<b>Table 5.4</b> : Combustion characteristics. ....	74
<b>Table 5.5</b> : Textural properties of activated hydrochars.....	85



## LIST OF FIGURES

	<u>Page</u>
<b>Figure 1.1</b> : The structure of cellulose (Tekin et al, 2014).....	5
<b>Figure 1.2</b> : The structures of <b>a)</b> D-galactopyranose, <b>b)</b> D-mannopyranose, <b>c)</b> D-glucopyranose, <b>d)</b> D-xylopyranose and <b>e)</b> L-arabinofuranose (Tekin et al, 2014; Holtzapple, 2003). .....	5
<b>Figure 1.3</b> : Structures of <b>a)</b> coniferyl alcohol, <b>b)</b> trans-p-coumaryl alcohol and <b>c)</b> sinapyl alcohol (Tekin et al, 2014).....	6
<b>Figure 1.4</b> : The biomass conversion technologies (Adapted from Adams et al, 2018).....	7
<b>Figure 2.1</b> : The Van Krevelen diagram of various biomasses and their hydrochars. ....	14
<b>Figure 3.1</b> : Structures of <b>a)</b> graphite and <b>b)</b> activated carbon (McDougall, 1991)..	26
<b>Figure 5.1</b> : The <b>a)</b> TG and <b>b)</b> DTG curves of pyrolysis of wood dust and wood dust hydrochar.....	64
<b>Figure 5.2</b> : The <b>a)</b> TG and <b>b)</b> DTG curves of pyrolysis of walnut shell and walnut shell hydrochar. ....	65
<b>Figure 5.3</b> : The <b>a)</b> TG and <b>b)</b> DTG curves of pyrolysis of tea stalk and tea stalk hydrochar.....	65
<b>Figure 5.4</b> : The <b>a)</b> TG and <b>b)</b> DTG curves of pyrolysis of olive pomace and olive pomace hydrochar. ....	66
<b>Figure 5.5</b> : The <b>a)</b> TG and <b>b)</b> DTG curves of pyrolysis of apricot seed and apricot seed hydrochar.....	67
<b>Figure 5.6</b> : The <b>a)</b> TG and <b>b)</b> DTG curves of pyrolysis of hazelnut husk and hazelnut husk hydrochar.....	67
<b>Figure 5.7</b> : The <b>a)</b> TG and <b>b)</b> DTG curves of combustion of wood dust and wood dust hydrochar. ....	69
<b>Figure 5.8</b> : The <b>a)</b> TG and <b>b)</b> DTG curves of combustion of walnut shell and walnut shell hydrochar. ....	70
<b>Figure 5.9</b> : The <b>a)</b> TG and <b>b)</b> DTG curves of combustion of tea stalk and tea stalk hydrochar.....	70
<b>Figure 5.10</b> : The <b>a)</b> TG and <b>b)</b> DTG curves of combustion of olive pomace and olive pomace hydrochar. ....	71
<b>Figure 5.11</b> : The <b>a)</b> TG and <b>b)</b> DTG curves of combustion of apricot seed and apricot seed hydrochar.....	72
<b>Figure 5.12</b> : The <b>a)</b> TG and <b>b)</b> DTG curves of combustion of hazelnut husk and hazelnut husk hydrochar.....	73
<b>Figure 5.13</b> : Comparative FT-IR spectra of the biomasses, hydrochars and activated hydrochars of <b>a)</b> wood dust, <b>b)</b> walnut shell, <b>c)</b> tea stalk, <b>d)</b> olive pomace, <b>e)</b> apricot seed and <b>f)</b> hazelnut husk.....	76

<b>Figure 5.14</b> : SEM images of <b>(a-c)</b> raw wood dust, <b>(d-f)</b> wood dust hydrochar and <b>(g-i)</b> wood dust activated hydrochar with x200, x1000 and x5000 magnifications. ....	77
<b>Figure 5.15</b> : SEM images of <b>(a-c)</b> raw walnut shell, <b>(d-f)</b> walnut shell hydrochar and <b>(g-i)</b> walnut shell activated hydrochar with x200, x1000 and x5000 magnifications. ....	78
<b>Figure 5.16</b> : SEM images of <b>(a-c)</b> raw tea stalk, <b>(d-f)</b> tea stalk hydrochar and <b>(g-i)</b> tea stalk activated hydrochar with x200, x1000, x5000 and x10k. ....	79
<b>Figure 5.17</b> : SEM images of <b>(a-c)</b> raw olive pomace, <b>(d-f)</b> olive pomace hydrochar and <b>(g-i)</b> olive pomace activated hydrochar with x200, x1000 and x5000 magnifications. ....	80
<b>Figure 5.18</b> : SEM images of <b>(a-c)</b> raw apricot seed, <b>(d-f)</b> apricot seed hydrochar and <b>(g-i)</b> apricot seed activated hydrochar with x200, x1000, x5000, x10k and x20k magnifications.....	81
<b>Figure 5.19</b> : SEM images of <b>(a-c)</b> raw hazelnut husk, <b>(d-f)</b> hazelnut husk hydrochar and <b>(g-i)</b> hazelnut husk activated hydrochar with x200, x1000 and x5000 magnifications. ....	82
<b>Figure 5.20</b> : The N <sub>2</sub> <b>a)</b> adsorption and <b>b)</b> desorption isotherms of activated hydrochars. ....	83

# **PRODUCTION OF BIO-BASED CARBON MATERIAL FROM LIGNOCELLULOSICS**

## **SUMMARY**

Fossil resources are directing the economy today. The limited reserves of fossil resources, environmental pollution and greenhouse gas emissions caused by the use of fossil fuels, and the desire of countries to decrease the dependence of crude oil have led to a search for alternatives. Bio-based economy, which bases on producing value-added products (including bio-based chemicals, functional materials and biofuels) from biomass, has a great impact on reducing the dependency on fossil fuels. Moreover, adapting bio-based economy increases resource efficiency, reduces emissions and accelerates rural development. Among the biomass sources, lignocellulosic biomass such as agricultural residues/wastes and forestry residues/wastes require special attention. There are several conversion methods to produce different platform molecules, which can be used directly as an end-product or an intermediate product to produce the desired product. Hydrothermal carbonization (HTC) is among the thermochemical conversion methods, which gives opportunity to produce different value-added products including bio-based chemicals, carbon-rich materials and fuels with higher energy densities.

This thesis presents hydrothermal carbonization as a method a) to obtain solid fuels with better properties compared to their original feedstock, b) to obtain a precursor for producing bio-based activated carbon. Therefore, this study comprises two parts: 1) producing hydrochars of selected lignocellulosics, and comparing the fuel properties of the lignocellulosics with their corresponding hydrochars, 2) activation of those hydrochars with KOH to produce porous activated carbons, and assessment of porous structure based on the type of lignocellulosic feedstock.

Wood dust, walnut shell, tea stalk, olive pomace, apricot seed and hazelnut husk were used as lignocellulosic biowastes, which were hydrothermally carbonized at 220°C for 90 min. Hydrochars of those lignocellulosics were activated by chemical activation with KOH at 600°C.

As the wood dust, walnut shell, tea stalk, olive pomace, apricot seed and hazelnut husk biomass samples and their corresponding hydrochar were compared, the improvement of the fuel quality after HTC was remarkable. All hydrochars represented lower volatile matter content and hydrogen content. Fixed carbon content of all hydrochars were higher than their original raw sample, resulting higher net calorific values. The percentage increase in heating values were ranked between 30% (olive pomace) and 14% (wood dust). Among the hydrochars, olive pomace presented the best improvement in terms of high heating value (6106 cal/g) and low ash percentage (5.5%). All of the hydrochars had the heating values as high as bituminous coal.

Activated hydrochars demonstrated BET surface areas of between 308.9 m<sup>2</sup>/g and 666.7 m<sup>2</sup>/g (activated hydrochar of wood dust and tea stalk), and total pore volumes

of between 0.25 cm<sup>3</sup>/g and 0.73 cm<sup>3</sup>/g (activated hydrochar of olive pomace and wood dust). The average pore size distribution of the activated hydrochars was ranging between 1.05 nm (olive pomace) and 4.74 nm (wood dust). All agricultural based activated hydrochars had similar average pore size distribution of between 1.05 nm and 1.25 nm, which fell in the range of microporous structure. With the average pore size of 4.74 nm, activated hydrochar of wood dust was classified under the mesoporous structure.

This thesis clearly points out that:

- The type of lignocellulosic biomass affects the amount and characteristics of its corresponding hydrochar.
- HTC is a very effective method to decrease the moisture and volatile matter content of lignocellulosics.
- HTC is a very effective method to increase the fixed carbon content and heating value of the lignocellulosics.
- After HTC, all hydrochars represent similar pyrolysis and combustion profile, the only difference is the shifting of the characteristic temperatures (the temperatures of maximum mass loss rate, ignition temperature and burnout temperature) to higher values.
- HTC is a very effective method to enhance the fuel properties of the lignocellulosics.
- HTC, alone, also produces hydrochars with higher porous structure compared to their raw feedstock.
- Activating HTC with KOH dramatically affects the microporous structure formation.
- The type of lignocellulosic material (mainly the structure of lignin) has a great impact on porous structure.

# LİGNOSELÜLOZİKLERDEN BİYO-KÖKENLİ KARBON MATERYALİN ÜRETİLMESİ

## ÖZET

Fosil kaynaklar bugün ekonomiyi yönlendirmektedir. Fosil kaynakların sınırlı rezervleri, çevre kirliliği ve fosil yakıtların kullanımından kaynaklanan sera gazı emisyonları ve ülkelerin ham petrol bağımlılığını azaltma istekleri, alternatif arayışlarına yol açmıştır. Biyokütleden katma değerli ürünler (biyo-kökenli kimyasallar, fonksiyonel malzemeler ve biyoyakıtlar dahil olmak üzere) üretilmesine dayanan biyo-kökenli ekonomi, fosil yakıtlara bağımlılığı azaltmada büyük bir etkiye sahiptir. Ayrıca, biyo-kökenli ekonomiyi uyarlamak kaynak verimliliğini artırır, emisyonları azaltır ve kırsal kalkınmayı hızlandırır. Biyokütle kaynakları arasında, tarımsal artıklar/atıklar ve orman artıkları/atıkları gibi lignoselülozik biyokütle özel ilgi gerektirir. Doğrudan bir nihai ürün veya istenilen ürünü üretmek için bir ara ürün olarak kullanılabilen farklı platform moleküllerini üretmek için çeşitli dönüşüm yöntemleri vardır. Hidrotermal karbonizasyon (HTC), biyo-kökenli kimyasallar, karbon bakımından zengin materyaller ve daha yüksek enerji yoğunluğuna sahip yakıtlar dahil olmak üzere, çeşitli katma değeri yüksek ürünler üretme olanağı sağlayan termokimyasal dönüşüm yöntemleri arasındadır.

Bu tez, a) orijinal hammaddelerine göre daha iyi özelliklere sahip katı yakıtlar elde etmek, b) biyo-kökenli aktif karbon üretmek için bir öncü elde etmek için bir yöntem olarak hidrotermal karbonizasyonu sunmaktadır. Bu nedenle, bu çalışma iki bölümden oluşmaktadır: 1) seçilen lignoselüloziklerin hidrokoklarının üretilmesi ve lignoselüloziklerin yakıt özelliklerinin ilgili hidrokoklarıyla karşılaştırılması, 2) gözenekli aktif karbonlar üretmek için bu hidrokokların KOH ile aktivasyonu ve gözenekli yapının hammadde cinsine göre değerlendirilmesi. 220°C'de 90 dakika boyunca hidrotermal olarak karbonize edilen odun talaşı, ceviz kabuğu, çay sapı, zeytin küspesi, kayısı çekirdeği ve çotanak lignoselülozik biyo-atık olarak kullanılmıştır. Bu lignoselüloziklerin hidrokokları 600°C'de KOH ile kimyasal aktivasyonla aktive edildi.

Odun talaşı, ceviz kabuğu, çay sapı, zeytin küspesi, kayısı çekirdeği ve çotanak biyokütle örnekleri ve bunlara karşılık gelen hidrokoklar karşılaştırıldıklarında, HTC'den sonra yakıt kalitesindeki iyileşme dikkat çekicidir. Tüm hidrokoklar daha düşük uçucu madde içeriği ve hidrojen içeriği göstermiştir. Tüm hidrokokların sabit karbon içeriği orijinal ham numunelerinden daha yüksekti, bu da daha yüksek net kalorifik değerlere neden oldu. Isıl değerdeki yüzde artış %30 (zeytin küspesi) ile %14 (odun talaşı) arasındadır. Hidrokoklar arasında, zeytin küspesi yüksek ısıl değeri (6106 cal/g) ve düşük kül yüzdesi (%5.5) açısından en iyi iyileşmeyi göstermiştir. Tüm hidrokoklar bitümlü kömür kadar yüksek ısıl değerlere sahiptir.

Aktif hidrokoklar 308.9 m<sup>2</sup>/g ile 666.7 m<sup>2</sup>/g (odun talaşı ve çay sapı aktif hidrokokları) arasında BET yüzey alanları ve 0.25 cm<sup>3</sup>/g ile 0.73 cm<sup>3</sup>/g (zeytin küspesi ve odun talaşı aktif hidrokokları) arasında toplam gözenek hacimleri göstermiştir. Aktif

hidrokokların ortalama gözenek boyutu dağılımları 1.05 nm (zeytin küspesi) ve 4.74 nm (odun talaşı) arasında sıralanmaktadır. Tüm tarımsal kökenli aktif hidrokoklar mikro gözenekli yapıya denk gelen 1.05 nm ve 1.25 nm aralığında ortalama gözenek boyutu dağılımına sahiptir. 4.74 nm ortalama gözenek boyutu ile odun talaşı aktif hidrokoku mezo gözenekli yapı altında sınıflandırılmıştır.

Bu tez açıkça şunu belirtir:

- Lignoselülozik biyokütle türü, karşılık geldiği hidrokokun miktarını ve karakteristiklerini etkiler.
- HTC, lignoselüloziklerin nem ve uçucu madde içeriğini azaltmak için çok etkili bir yöntemdir.
- HTC, lignoselüloziklerin sabit karbon içeriğini ve ısıl değerini artırmak için çok etkili bir yöntemdir.
- HTC'den sonra, tüm hidrokoklar benzer piroliz ve yanma profili gösterir, tek fark karakteristik sıcaklıkların (maksimum kütle kaybı oranı, tutuşma sıcaklığı ve tükenme sıcaklığı) yüksek değerlere kaydırılmasıdır.
- HTC, lignoselüloziklerin yakıt özelliklerini geliştirmek için çok etkili bir yöntemdir.
- HTC, tek başına, ham hammaddelerine kıyasla daha yüksek gözenekli yapıya sahip hidrokoklar de üretir.
- HTC'nin KOH ile aktivasyonu, mikro gözenekli yapı oluşumunu önemli ölçüde etkiler.
- Lignoselülozik malzemenin türü (özellikle ligninin yapısı) gözenekli yapı üzerinde büyük bir etkiye sahiptir.



## **1. BIOMASS**

Fossil resources have been extensively used in the production of energy, valuable chemicals and materials for a very long time. But this finite resource has negative effects on environment. Very well-known environmental problems related with fossil resources include greenhouse gas emissions, air pollution, acid rains and soil pollution. Because of environmental impacts, the search for new resources for the production of energy, valuable chemicals and materials has been on the way. Biomass is the most suitable candidate to produce energy and value-added materials (Sindhu et al, 2016; Guney, 2013; Maniatis, 2001).

The biomass is a renewable energy source that encompasses all living and recently living (in the last 100 years) organisms and the wastes and residues of these organisms (Long et al, 2013). Due to photosynthesis, solar energy is stored in the structure as chemical energy. While photosynthesis, plants blend water in the soil and carbon dioxide in the air to shape carbohydrates which building blocks of biomass (Toklu, 2017).

The elemental composition of biomass mainly involves 30-40% of oxygen, 30-60% of carbon, 10-20% of hydrogen, 5-6% of ash and nitrogen and sulfur in trace amounts (Tekin et al, 2014).

Although the definition may seem narrow, there is a vast source of biomass with variable quantities. Examples of biomass sources include biodegradable products, wastes and residues of agricultural, forestry and related industries, as well as biodegradable fractions of industrial and domestic wastes and residues, energy crops and algae. Biomass is mainly classified as: i) agricultural wastes and residues; ii) energy crops; iii) forest wastes and residues; iv) industrial and domestic wastes and residues (Adams et al, 2018). Agricultural wastes and residues include straw, animal manure and seed, stone, shell, peel and husk of agricultural products. Energy crops contain miscanthus, wheat, maize, short rotation coppice willow, oilseed rape and switchgrass. Forestry wastes and residues involve arboricultural arisings, forest

residues, waste wood, sawmill by-product, stemwood, sawdust, bark, branch and stump. Industrial and domestic wastes and residues comprise municipal solid waste, food waste, landfill gas, sewage sludge and waste fats and oils (Goyal et al, 2008; Ullah et al, 2015; Adams et al, 2018).

### 1.1 Structural Composition of Lignocellulosic Biomass

Lignocellulosic biomass is mainly composed of cellulose (30-50%), hemicellulose (25-35%) and lignin (%20-30) (Turley, 2009). It also contains small amounts of pectin, protein, extractives and inorganic components (Ranzi et al, 2016; Coronella et al, 2014). The fraction of structural components vary with biomass type. Table 1.1 shows the cellulose, hemicellulose and lignin percentages (w%) in various lignocellulosic biomass.

**Table 1.1** : Cellulose, hemicellulose and lignin contents of various lignocellulosic biomass.

Biomass	Cellulose (%)	Hemicellulose (%)	Lignin (%)	Reference
Almond shell	30.70	32.60	35	Safari et al, 2016
Almond shell	32.5	25.5	24.8	Ledesma et al, 2018
Bamboo	34.9	16.2	28.3	Yang et al, 2016
Bamboo	47	25	21	Ando et al, 2000
Beech chips	40.8	21.2	23.8	Saleh et al, 2013
Beech wood	60.2	22	17.8	Dinjus et al, 2011
Calophyllum inophyllum L.	25.2	16.2	38.3	Yang et al, 2015b
Camellia oleifera seed shell	17.32	22	31.35	Guo et al, 2018
Cauliflower	77.2	11.6	11.2	Dinjus et al, 2011
Chinquapin	46	20	20	Ando et al, 2000
Cinnamomum camphora branch	27.8	18.4	27.7	Cao et al, 2016
Coconut shell	15.16	39.80	44.77	Islam et al, 2017a
Corn stalk	34.91	26.35	13.89	Kou et al, 2017
Corn stover	29.7	26.3	9.5	Reza et al, 2013
Corn cob	31.53	36.26	23.93	Zheng et al, 2014
Corn cob	36.8	40.5	20.7	Ding et al, 2013
Cotton stem	46.2	18.7	25.4	Gao et al, 2016b
Cow manure	27.4	12.2	13	Heilmann et al, 2014
Cultivated grass	31.2	17.2	9.3	Tsapekos et al, 2017

Cupressus funebris branches	23	19	18.3	Cao et al, 2016
Cupressus funebris leave	24.8	16.9	16.8	Cao et al, 2016
Digestate	44.6	18.9	21.4	Funke et al, 2013
Distylium racemosum branch	24.5	16.4	23.1	Cao et al, 2016
Distylium racemosum leave	23.7	16.3	23.8	Cao et al, 2016
Elephant grass	41.8	24.7	28	Nascimento and Rezende, 2017
Empty fruit bunch	55.82	30.35	N/A <sup>1</sup>	Jamari and Howse, 2012
Empty fruit bunch	59.7	22.1	18.1	Abdullah and Gerhauser, 2008
Giant reed	37.03	29.49	18.95	Kou et al, 2017
Grass	49.9	45.9	4.2	Dinjus et al, 2011
Hazelnut shell	24.2	28.2	48.5	Uzuner et al, 2018
Hazelnut shell	36.02	12.66	40.14	Gozaydın and Yuksel, 2017
Humulus lupulus	19.7	36.5	24.6	Yang et al, 2015b
Japan cedar	35	24	33	Ando et al, 2000
Loblolly pine	54	11.9	25	Yan et al, 2010
Loblolly pine	54	11.9	25	Reza et al, 2014b
Maize silage	25.5	0.5	25.5	Mumme et al, 2011
Meadow grass	36.1	29.8	19.9	Tsapekos et al, 2017
Miscanthus	48.5	20.1	22.4	Saleh et al, 2013
Miscanthus	44.4	30.2	14.2	Reza et al, 2013
Nut husks	12.4	20.9	53.2	Yang et al, 2015a
Olive tree pruning	46.16	25.46	15.37	Mamaní et al, 2019
Orange peel	12.9	8.8	1.3	Bicu and Mustata, 2013
Orange pomace	14.3	6.3	3.3	Erdogan et al, 2015
Palm shell	27.7	21.6	44	Abnisa et al, 2011
Pennisetum	41.82	21.93	16.52	Kou et al, 2017
Pine chips	38.6	20.5	29.2	Saleh et al, 2013
Pine wood dust	55.3	10.10	27.2	Gao et al, 2016b
Pine wood flour	53.12	N/A	28.86	Chen et al, 2014
Pinus branch	26.9	20.8	16.8	Cao et al, 2016
Pinus leave	22.9	15	31	Cao et al, 2016
Pittosporum tobira branch	26.7	21.2	14.5	Cao et al, 2016
Pittosporum tobira leave	18.2	17.6	10.6	Cao et al, 2016

Platanus branch	27.7	19.9	25.6	Cao et al, 2016
Platanus leave	22.7	16.1	23.6	Cao et al, 2016
Plumeria alba	33.9	22.7	25.2	Yang et al, 2015b
Pomegranate peel	7.9	8.1	22.1	Pereira et al, 2016
Pomegranate seeds	26.98	25.52	39.67	Ucar and Karagoz, 2009
Poplar sawdust	60.9	12.2	19	Funke et al, 2013
Potato peel	39	10	15	Sun et al, 2017
Poultry manure	12	20.2	2.3	Heilmann et al, 2014
Rice hull	39.8	14.9	11.3	Reza et al, 2013
Rice straw	37.5	32.8	16	Gao et al, 2016b
Salix babylonica branch	25.9	17	30.1	Cao et al, 2016
Silvergrass	44.07	26.19	17.07	Kou et al, 2017
Sludge from pulp and paper mill	8	19.5	32.5	Mäkelä et al, 2016
Spruce bark	24.1	12.9	36.8	Saleh et al, 2013
Spruce chips	45	18.4	27.6	Saleh et al, 2013
Straw	55.1	37.8	7.1	Dinjus et al, 2011
Straw	45.8	27.8	8.5	Funke et al, 2013
Swine manure	13.3	20.4	5.4	Heilmann et al, 2014
Switchgrass	36.45	27.84	17.83	Kou et al, 2017
Switchgrass	35.3	33.7	8.4	Reza et al, 2013
Walnut shell	27.9	30.2	39.1	Yang et al, 2014
Walnut shell	26.87	22.45	47.68	Kar, 2011
Walnut shell	36	25.43	38	Safari et al, 2016
Water hyacinth	23.5	33.6	8.6	Gao et al, 2016b
Wheat straw	39.80	27.30	19.30	Safari et al, 2016
Wheat straw	40.4	25.6	22.3	Gao et al, 2016b

<sup>1</sup>N/A = Not available

### 1.1.1 Cellulose

Cellulose ((C<sub>6</sub>H<sub>10</sub>O<sub>5</sub>)<sub>n</sub>) is a straight, long-chain and abundant natural polymer formed by glucose, the monomeric unit of a six-carbon sugar linked with β-1,4 glycosidic bonds of glucopyranose units and held together with hydrogen bonds (Kumar et al, 2018; Toor et al, 2014; Tekin et al, 2014; Pecha and Garcia-Perez, 2015). Hydrogen bonds provide rigidity and crystallinity to cellulose, and therefore cellulose has resistant to degradation (Coronella et al, 2014; Toor et al, 2014). The structure of cellulose is shown in Figure 1.1 (Tekin et al, 2014).

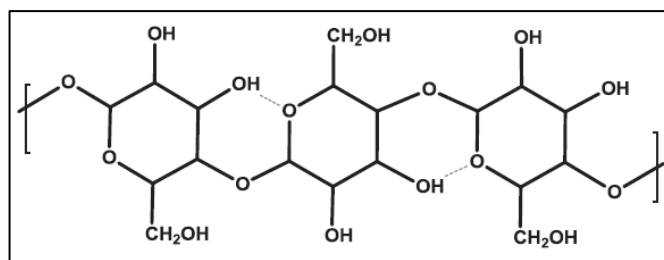


**Figure 1.1 :** The structure of cellulose (Tekin et al, 2014).

Cellulose is insoluble in the environment due to its high crystallinity, and it has also resistant to enzymatic reactions (Kumar et al, 2018; Toor et al, 2014). When lignin is removed from structure, cellulose is easily degraded by different enzymes. In terms of thermal decomposition, cellulose is partially decomposed at temperatures 250 – 300°C and completely decomposed at temperatures higher than 400°C (Libra et al, 2011; Tekin et al, 2014; Coronella et al, 2014).

### 1.1.2 Hemicellulose

Hemicellulose ( $C_5H_{10}O_5$ ) is an amorphous heteropolymer with branches comprised of hexoses such as D-galactopyranose, D-mannopyranose, D-glucopyranose and pentoses such as D-xylopyranose, L-arabinofuranose (Tekin et al, 2014; Kumar et al, 2018; Coronella et al, 2014). Figure 1.2 shows the hemicellulose branches. Hemicelluloses are linked to cellulose, proteins and lignins by covalent bond and hydrogen bond (Tekin et al, 2014; Holtzaple, 2003).

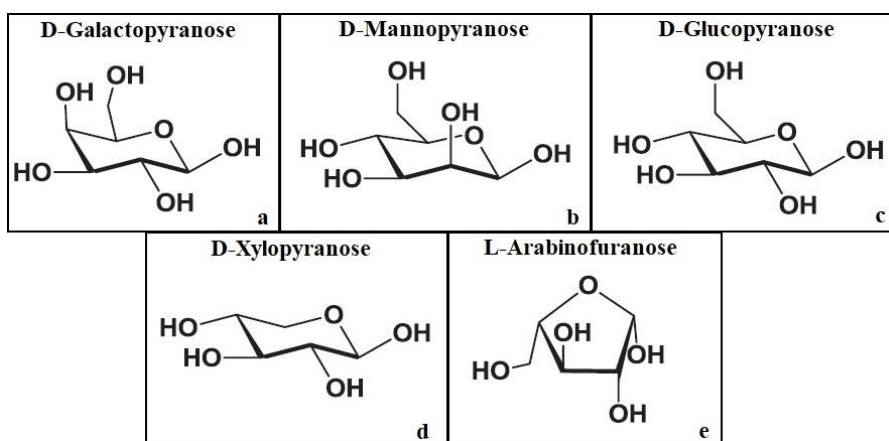


**Figure 1.2 :** The structures of **a)** D-galactopyranose, **b)** D-mannopyranose, **c)** D-glucopyranose, **d)** D-xylopyranose and **e)** L-arabinofuranose (Tekin et al, 2014; Holtzaple, 2003).

Hemicellulose has less crystallinity compared to cellulose due to its amorphous and branched structure and therefore its degradation is easier (Ranzi et al, 2016; Tekin et al, 2014). Moreover, hemicellulose is limited soluble in water due to its structure (Coronella et al, 2014). Thermal decomposition of hemicellulose occurs in a temperature range of 180-300°C (Toor et al, 2014; Kumar et al, 2018; Libra et al, 2011).

### 1.1.3 Lignin

Lignin is an aromatic and amorphous heteropolymer, which is found in all vascular plants. Lignin consists of phenyl propanoids, which has a phenolic structure with a side chain attached to it in para-position (Henriksson et al, 2010). The three main phenyl propanoids are coniferyl alcohol ( $C_{10}H_{12}O_3$ ), trans-p-coumaryl alcohol ( $C_9H_{10}O_2$ ) and sinapyl alcohol ( $C_{11}H_{14}O_4$ ) (Kumar et al, 2018; Kambo and Dutta, 2015; Toor et al, 2014; Pecha and Garcia-Perez, 2015). Figure 1.3 shows the monomers of lignin (Tekin et al, 2014).

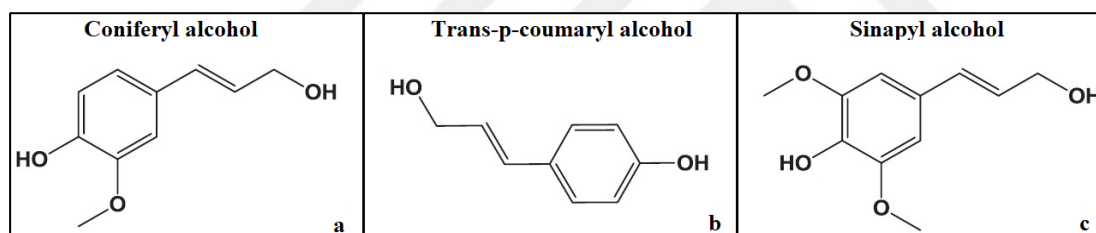


**Figure 1.3 :** Structures of **a)** coniferyl alcohol, **b)** trans-p-coumaryl alcohol and **c)** sinapyl alcohol (Tekin et al, 2014).

P-coumarly alcohol is mainly found in softwoods, and lignin of monocotyledons (Henriksson et al, 2010). Coniferyl alcohol is found in all kinds of lignin. Especially in softwoods, coniferyl alcohol is the most abundant monolignol. Sinapyl alcohol is found in all types of lignin expect softwoods (Henriksson et al, 2010).

Lignin is hydrophobic, insoluble in water and it is resistant to enzymatic and chemical decomposition due to covalent bonds which is randomly ordered (Tekin et al, 2014; Kumar et al, 2018; Toor et al, 2014; Turley, 2009). Thermal decomposition of lignin occurs in a temperature range of 180 – 700°C (Libra et al, 2011).

### 1.1.4 Extractives

Extractives are generally between 2% and 10% in lignocellulosic biomasses (Pecha and Garcia-Perez, 2015). Extractives are the materials that are soluble in polar solvents such as water and alcohol or non-polar solvents such as hexane or toluene. Extractives involve phenolics, waxes, resins, pectins, proteins, fats and inorganics (Tekin et al, 2014; Pattiya, 2018; Pecha and Garcia-Perez, 2015; Basu, 2013).

### 1.2 Biomass Conversion Technologies

There are several conversion technologies that can be used to produce energy, biofuel and value-added bio-based products from biomass. The process requirements and resultant product distributions are quite different. Figure 1.4 shows the biomass conversion technologies in brief. Biomass conversion technologies are mainly classified in three groups: Physicochemical, biochemical and thermochemical conversion technologies.

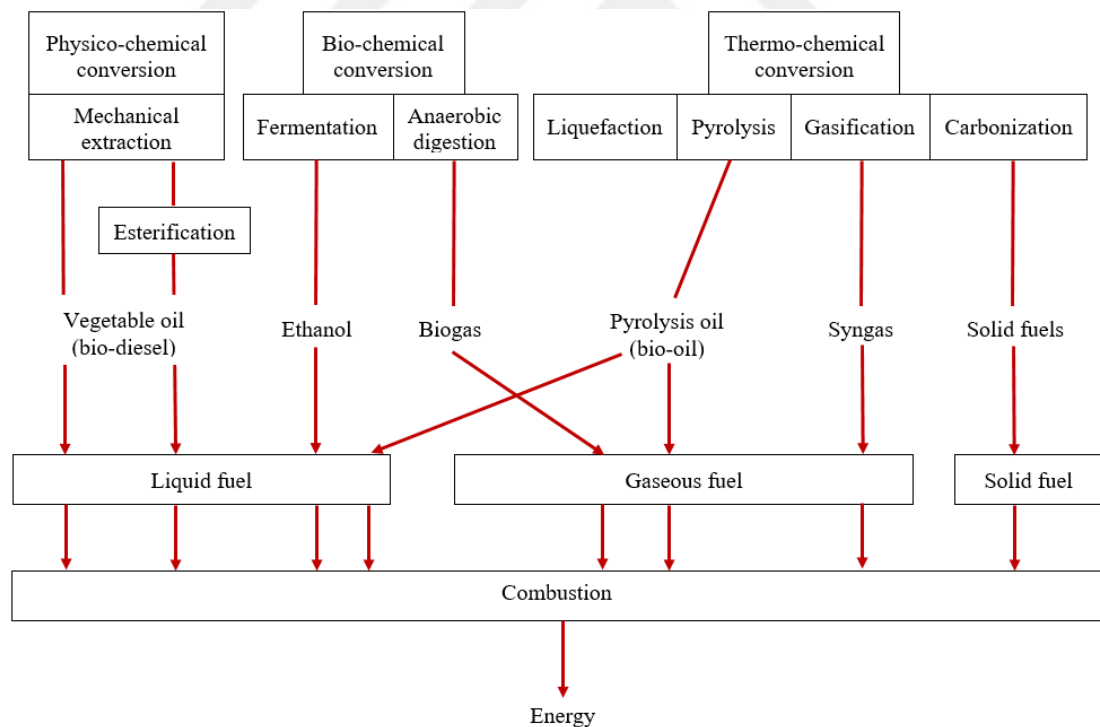


**Figure 1.4 :** The biomass conversion technologies (Adapted from Adams et al, 2018).

Physicochemical conversion involves the mechanical extraction with esterification process. Mechanical extraction is a process used to obtain bio-oil from oilseeds. Biodiesel is derived by esterification from the bio-oil (Adams et al, 2018).

Biochemical conversion technologies include anaerobic digestion and fermentation processes. Anaerobic digestion is a bacterial fermentation process, which occurs in the absence of oxygen. As the facultative and methanogenic bacteria degrades the substrate in the absence of oxygen, biogas formation is observed. Biogas is a gas mixture containing mainly methane and carbon dioxide but also hydrogen sulfide and moisture are also found in trace amounts. After purifying the biogas, it can be used as a fuel for engines, gas turbines and fuel cells. Fermentation is an enzymatic anaerobic process where bioethanol is obtained from simple sugars by using enzymes such as yeast. Based on the type of feedstock, a pretreatment is required to obtain simple sugars. In the case of lignocellulosic biomass, the main aim is to decrystallize cellulose and to break it down into glucose. Bio-ethanol is used as a fuel additive in vehicles (Adams et al, 2018; Ullah et al, 2015; Guney, 2013).

Thermochemical conversion is the process that involves the thermal decomposition of biomass. This technology involves combustion, pyrolysis, direct liquefaction, gasification and hydrothermal carbonization. Combustion is the most prevalent process for using to obtain heat and power by thermal degradation of biomass in the presence of oxidative environment (Ullah et al, 2015). Pyrolysis is the process of obtaining solid, liquid and gas products by thermal degradation of biomass at the temperature between 300°C and 800°C in non-reactive environment. The solid product is named char and can be used in the production of activated carbon. The liquid product consists of pyrolytic oil or bio-oil and tar. Bio-oil can consist of acids, esters, alcohols, ketones, phenols, alkenes, furans, sugars. The synthetic gas (syngas) consists of non-condensable gases (Akhtar and Saidina Amin, 2012; Goyal et al, 2008; Kambo and Dutta, 2015). Liquefaction is a process that involves the thermal decomposition and hydrogenation in a non-oxidative environment and under pressure. The quality of bio-oil can be improved (similar to the petroleum-derived products) by hydrothermal treatment (Kambo and Dutta, 2015; Libra et al, 2011; Arshadi and Sellstedt, 2008). Gasification is a process that thermally converts biomass into synthesis gas by partial oxidation (by using sub-stoichiometric air or oxygen, steam, carbon dioxide). Syngas consists of gases mainly carbon monoxide (CO), hydrogen (H<sub>2</sub>), methane (CH<sub>4</sub>) and



carbon dioxide (CO<sub>2</sub>). Syngas can be directly burned for electricity production or can be utilized as a feedstock for producing synthetic fuels (Libra et al, 2011; Ullah et al, 2015; Kambo and Dutta, 2015; Goyal et al, 2008). Hydrothermal carbonization is a thermochemical process that carried out under low temperature (between 130°C and 250°C), and autonomous (self-generated) pressure using water as a carbonization medium. The solid product which is named as hydrochar, is rich in carbon content. The liquid product consists of water, organic acids, phenolic groups and sugar and its derivatives, while the gas product consists mainly of carbon dioxide, methane and carbon monoxide. It is possible to use hydrothermal carbonization products as fuel and also in the production of valuable chemicals (Adams et al, 2018; Funke and Ziegler, 2010; Kambo and Dutta, 2015).





## **2. HYDROTHERMAL CARBONIZATION**

Hydrothermal carbonization is a recently used method for the production of biofuels and value-added materials from biomass. As stated before, hydrothermal carbonization is a process in which the biomass is carbonized in the presence of water at a definite temperature and pressure in a closed vessel (Lu and Berge, 2014). Based on the feedstock and final product requirements, this process proceeds at different temperatures (180 – 250°C) and under pressure (10-40 bar) to keep water in liquid state for a period of time ranging from a few minutes to many hours (Funke and Ziegler, 2010; Jain et al, 2016; Mumme et al, 2011). Water plays an essential role in hydrothermal carbonization as a solvent and reactant (Funke and Ziegler, 2010). In addition, hydrothermal carbonization has advantages such as high conversion efficiency, enable to use of wet biomass, suitable for use at a wide range of temperatures and varying retention time (Zhang et al, 2015; Pala et al, 2014). Because the hydrothermal carbonization reactions require water, wet biomass sources or moisture-rich biomass sources are preferable for hydrothermal carbonization.

### **2.1 Products**

The products obtained from hydrothermal carbonization are in solid, liquid and gaseous form. Carbon-rich solid fraction is named as hydrochar. The structure, composition and heating value of hydrochar depends on the severity of the reaction conditions. The oxygenated functional groups are higher in hydrochars (Funke and Ziegler, 2010). Hydrochar has higher carbon content, energy density, heating value but lower aromatization degree as compared to parent biomass (Román et al, 2013; Reza et al, 2014a; Jain et al, 2016; Kumar et al, 2018; Wang et al, 2018b). A significant effect of hydrothermal carbonization is the elimination of hydroxyl and carboxyl groups, which results a lower hydrophilic product as compared to raw biomass. Hydrochar shows brittle and hydrophobic characteristics. Also, it is separated from the liquid phase easily (Wang et al, 2018b; Zhao et al, 2014). Also, hydrochar is sterile due to heat treatment (He et al, 2013). The liquid fraction (hydrothermal carbonization liquid) includes hydrolysis products of hemicelluloses and dissolved inorganic species

(Nakason et al, 2018). This liquid fraction can be reused or further processed to produce bio-based chemicals. In addition, also there could be carbon dioxide dissolved in water as the liquid product (Butler, 2018). The obtained gas product contains mainly carbon dioxide but also may include carbon monoxide, methane and hydrogen in trace amounts (Basso et al, 2016; Funke and Ziegler, 2010).

## **2.2 Reaction Mechanisms**

Hydrothermal carbonization includes many reactions including hydrolysis, dehydration, decarboxylation, condensation polymerization, aromatization and recondensation simultaneously. During the hydrolysis, the ether and ester bonds are broken (Libra et al, 2011; Fakkaew et al, 2015). Dehydration is the process that involves the water removal, reducing H/C and O/C ratios. In addition, a reduction in the hydroxyl groups of the biomass occurs (Funke and Ziegler, 2010). During decarboxylation, partial removal of carboxyl groups occurs (Blazsó et al., 1986). By decomposition of the carbonyl and carboxyl groups above 150°C, CO and CO<sub>2</sub> are produced (Fang et al, 2017; Gao et al, 2016a; Zhang et al, 2015). Some compounds obtained by degradation of biomass with hydrothermal carbonization are highly reactive and can readily be polymerized. The compounds, which are produced by the degradation of hydroxyl and carboxyl groups, usually undergo polymerization reaction (Funke and Ziegler, 2010). Condensation polymerization is an undesirable reaction which causes precipitate formation in hydrothermal carbonization. The condensation polymerization process can continue for several minutes at above 300°C and for several months at room temperature for the lignin, while it can take longer for hemicellulose and cellulose (Masselter et al, 1995). Cellulose and hemicellulose in biomass slow down this reaction by stabilizing lignin. (Bobleter, 1994). Aromatization reaction occurs as a result of dehydration and decarboxylation reactions. Cellulose and hemicellulose can form aromatic structures as a result of the aromatization reaction under hydrothermal carbonization conditions (Tsukashima, 1967). Hydrochar is formed by the re-condensation reaction from degradation products of hydrothermal carbonization (Libra et al, 2011).

### 2.3 Parameters That Affect Hydrothermal Carbonization

Hydrothermal carbonization is affected by many parameters such as temperature, retention time, biomass/water ratio, biomass structure and pressure.

Among the parameters, temperature is the one which affects the product properties most. As the temperature increases, the amount of hydrochar decreases while liquid and gas production increase. The solid product is produced at 180-200°C, predominantly. Liquid product is mainly produced at 250-350°C. Gas product is produced at above 350°C, predominantly (Nizamuddin et al, 2017). Due to the energy provided by heat, the efficiency of biomass conversion (in terms of mass) increases with increasing temperature (Nizamuddin et al, 2017; Akhtar and Saidina Amin, 2012). Retention time is also quite essential to ensure that char conversion and hydrothermal carbonization reactions occur. Many researchers investigated the effects of temperature and retention time on hydrothermal carbonization. Basso et al. (2016) applied hydrothermal carbonization to grape marc at different temperatures between 180°C and 250°C for various retention times between 1 h and 3 h. Inoue et al. (2002) investigated hydrothermal carbonization of wood dust at different temperatures between 200-350°C for retention times between 0-1 h. Benavente et al. (2015) studied hydrothermal carbonization of industrial organic wastes of canned artichoke, olive mill and orange juice at various temperatures between 220 – 250°C for 2 – 24 h of retention times. Based on the studies provided above, risen temperature and retention time resulted in decreased hydrochar yield and increased gas products. In addition, while the heating value and carbon content of hydrochar increased, the hydrogen and oxygen contents of hydrochar decreased. The studies also concluded that the temperature was more effective than the retention time. Zhu et al. (2015) investigated hydrothermal carbonization of rice straw, bamboo, soybean straw, pomelo peel and pine needle with 1:10 of biomass/water ratio at 180°C to 300°C for 0.5 – 4 h. With the increase in temperature and retention time, pH values and hydrochar yields decreased. Similar observation was done by Jain et al. (2016) who concluded that organic acids were formed during HTC and this formation had a negative effect on hydrochar yield. Şimşir et al. (2017) examined the hydrothermal carbonization of wood chips at 200°C and at variable retention times ranging from 6 h to 48 h. As retention time was changed from 6 h to 48 h, the hydrochar yield was decreased from 60.6% to 51.8%. In most of the feedstocks, there is a direct relation between the retention time and heating value.

There is also observed in the study of Şimşir et al (2017), who observed 33.56% increase in heating value as the retention time was increased from 6 h to 48 h. As the retention time increased, the carbon content (48.72% to 61.92%) increased and the hydrogen (6.21% to 5.85%) and oxygen contents (44.94% to 32.34%) diminished. The atomic ratios of H/C and O/C of various biomass sources and their hydrochars are shown on the Van Krevelen diagram in Figure 2.1. As seen in Van Krevelen diagram, hydrothermal carbonization causes an increase in carbon content and a decrease in hydrogen and oxygen contents. In other words, H/C and O/C ratios are reduced, and thus fuel quality is improved. As it is seen from Figure 2.1, hydrochars of biomass exhibit H/C ratio and O/C ratio that are similar to high quality coal (Unur et al, 2013; Qian et al, 2018; Zeng et al, 2018; Basso et al, 2016; Hoekman et al, 2011; Ghanim et al, 2016; Reza et al, 2014).

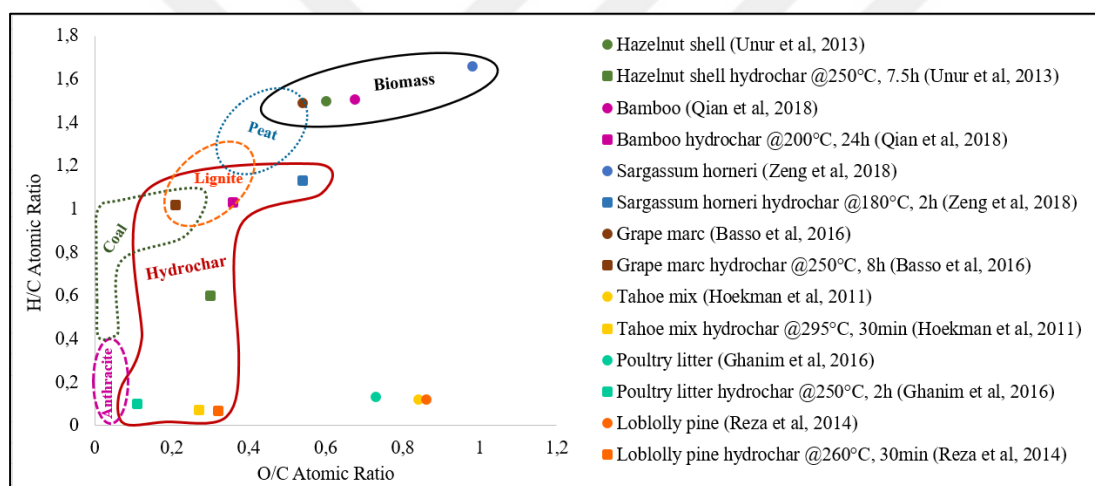


**Figure 2.1** : The Van Krevelen diagram of various biomasses and their hydrochars.

Nizamuddin et al. (2016) studied the effect of biomass/water ratio on hydrothermal carbonization of palm shell. At constant temperature (180°C) and retention time (30 min), hydrochars obtained at biomass to water ratio of 1.10 and 1.60 (w%) had 58.6% and 70.6% of hydrochar yields, respectively. At constant temperature (220°C) and retention time (75 min), hydrochars obtained with 1.10, 1.35 and 1.60 (w%) of biomass to water ratios had 50.3%, 54.5% and 56.9% of hydrochar yields, respectively. While the biomass to water ratio increased, the hydrochar yield also increased. Sabio et al. (2016) investigated hydrochars obtained from tomato-peel waste at 230°C for 5 and 15 h with different biomass/water ratios. Hydrochars, which were obtained at biomass to water ratios of 3.3 and 10 (w%) for 5 h, had 49.6% and 62.2% of hydrochar yields

and 31.2 MJ/kg and 28.3 MJ/kg of heating values. Hydrochars, which were obtained for 15 h with the same biomass to water ratios, had 27.6% and 35.4% of hydrochar yields and 32.9 MJ/kg and 34.8 MJ/kg of heating values, respectively. Kambo and Dutta (2015) examined hydrothermal carbonization of miscanthus at 190-260°C for 5-30 min with 1:6 and 1:12 of biomass/water ratios. As the temperature and retention time increased and the biomass/water ratio decreased, the hydrochar yield reduced (from 83.5% to 42.8%). In the same study, it was observed that biomass/water ratio had no effect on gross calorific value. Moreover, it was concluded that temperature was more effective than retention time. Both of the studies mentioned above showed that biomass/water ratio affected char yield while it had no considerable effect on heating value.

Another crucial parameter affecting hydrothermal carbonization is biomass structure. Lignocellulosics are generally composed of hemicellulose (25 – 35%), cellulose (30 – 50%) and lignin (20 – 30%). Due to its heterogeneous structure, each component reacts differently under hydrothermal conditions. In terms of thermal stability, hemicellulose has the least and lignin has the highest thermal stability (Grønli et al, 2002). Under hydrothermal conditions, rapid hemicellulose hydrolysis is observed (Libra et al, 2011). Falco et al. (2011) indicated that cellulose is not degraded at hydrothermal conditions where reaction temperatures are 220-230°C and the retention time is 240 min. At temperatures higher than 230°C, cellulose undergoes hydrolysis reaction (Reza et al, 2014a). In the case of lignin degradation, higher temperatures (>250 °C) are required, where the degree of degradation depends on the type of lignin (Yu et al, 2008; Funke and Ziegler, 2010). In addition, hemicellulose and cellulose enhance oil production, while lignin improves hydrochar production. It is possible to obtain hydrochar with high yield by hydrothermal carbonization from biomass having high lignin content (Gani and Naruse, 2007; Zhang et al, 2019). Zhong and Wei (2004) subjected to various wood feedstocks to hydrothermal treatment at 280°C for 70 min. The *cunninghamia lanceolata* with the highest lignin content of 32.44% had the highest heating values before and after hydrothermal treatment with 18.224 MJ/kg and 26.015 MJ/kg respectively. The high lignin content of biomass contributed to the increase in heating value by hydrothermal carbonization (Thomsen et al, 2008). Due to the reason that each lignocellulosic biomass has variable composition, the hydrochar yield and heating value of the hydrochars differ from feedstock to feedstock. In recent

publications, it is seen that several lignocellulosic feedstocks were hydrothermally carbonized. These studies include hydrothermal carbonization of coconut shell (Islam et al, 2017a), grape seeds (Fiori et al, 2014), hazelnut husk (Donar et al, 2016), olive residue (Weidner et al, 2013), peanut shell (Huff et al, 2014), tomato peel (Sabio et al, 2016), walnut shell (Yang et al, 2014), watermelon peel (Chen et al, 2017), pig manure (Liu et al, 2017), miscanthus (Kambo and Dutta, 2015; Reza et al, 2013), acacia wood (Wilk et al, 2019), beech wood chips (Simsir et al, 2017), bamboo (Yang et al, 2016), loblolly pine (Wu et al, 2017; Reza et al, 2014b), eucalyptus leaves (Liu et al, 2013), sewage sludge (He et al, 2013), municipal solid waste (Berge et al, 2011; Basso et al, 2015), food waste (Berge et al, 2011); microalgae (Heilmann et al, 2010). Table 2.1 shows a review of hydrothermal carbonization reaction conditions and hydrochar yield of several biomass resources.

**Table 2.1 :** Hydrothermal carbonization reaction conditions and hydrochar yield of several biomass resources.

Biomass	Biomass to water ratio (g/mL)	Temperature	Retention time	Hydrochar yield (%)	Reference
Acacia wood	1:8	200°C	4 h	70	Wilk et al, 2019
Bagasse	4:31	200°C	6 h	47.75	Fang et al, 2015
Bagasse	1:15	300°C	5 h	27.78	Sun et al, 2014
Bamboo	1:3	300°C	30 min	32.73	Huff et al, 2014
Bamboo	1:15	300°C	5 h	48.42	Sun et al, 2014
Bamboo	3:7	260°C	10 min	47.1	Yang et al, 2016
Barley straw	4:25	250°C	2 h	37	Sevilla et al, 2011b
Beech wood chips	1.5:20	200°C	6 h	60.6	Simsir et al, 2017
Calophyllum inophyllum L.	1:4	180°C	10 min	70	Yang et al, 2015b
Coconut fiber	1:10	150°C	30 min	91	Liu et al, 2013
Coconut shell	1:20	200°C	2 h	77	Islam et al, 2017a
Corn stover	1:8	175°C	30 min	67.03	Hoekman et al, 2011
Corn stover	1:5	200°C	5 min	82	Reza et al, 2013
Digestate	1:17	190°C	6 h	66	Funke et al, 2013
Eucalyptus leaves	1:10	150°C	30 min	91	Liu et al, 2013
Eucalyptus sawdust	4:25	250°C	2 h	40	Sevilla et al, 2011b



Food waste	1:4	250°C	20 h	43.8	Berge et al, 2011
Grape marc	1:5	180°C	1 h	76	Basso et al, 2016
Grape seeds	3:10	180°C	1 h	80.3	Fiori et al, 2014
Grindelia	1:5	200°C	5 min	59	Reza et al, 2015
Hazelnut shell	1:10	180°C	4 h	66	Donar et al, 2016
Hazelnut shell	1:25	280°C	2 h	65.40	Gozaydın and Yuksel, 2017
Herbal tea waste	N/A <sup>1</sup>	120°C	30 min	89.88	Zhuang et al, 2019
Hickory wood	5:29	200°C	6 h	54.60	Fang et al, 2015
Hickory wood	1:15	300°C	5 h	43.68	Sun et al, 2014
Humulus lupulus	1:4	180°C	10 min	50	Yang et al, 2015b
Loblolly pine	1:8	175°C	30 min	77.71	Hoekman et al, 2011
Loblolly pine	1:5	200°C	5 min	88.3	Reza et al, 2014b
Loblolly pine	4:75	240°C	6 h	48.54	Wu et al, 2017
Maize silage	1.5:1	190°C	2 h	71.8	Mumme et al, 2011
Microalgae	1:12.35	203°C	2 h	39	Heilmann et al, 2010
Microalgae	1:1	180°C	30 min	74.53	Lee et al, 2018a
Miscanthus	1:6	190°C	5 min	83.5	Kambo and Dutta, 2015
Miscanthus	1:5	200°C	5 min	79	Reza et al, 2013
Miscanthus	1:10	180°C	4 h	80	Wilk and Magdziarz, 2017
Mixed wood	1:8	215°C	30 min	69.1	Hoekman et al, 2011
Municipal solid waste	1:10	180°C	1 h	80	Basso et al., 2015
Municipal solid waste	1:4	250°C	20 h	63.2	Berge et al, 2011
Nut husks	1:4	180°C	10 min	95.1	Yang et al, 2015a
Olive mill waste	N/A	220°C	2 h	18.4	Benavente et al, 2015
Olive residue	1:10	180°C	4 h	53	Donar et al, 2016
Olive residue	3:10	180°C	8 h	75.4	Weidner et al, 2013
Orange peel	1:10	200°C	20 h	37	Fernandez et al, 2015
Orange pomace	1:8	175°C	2 h	54	Erdogan et al, 2015

Palm empty fruit bunch	1:10	150°C	20 min	76	Parshetti et al, 2013
Palm shell	8:5	180°C	30 min	70.6	Nizamuddin et al, 2016
Paper	1:4	250°C	20 h	29.2	Berge et al, 2011
Peanut hull	55:313	200°C	6 h	50.55	Fang et al, 2015
Peanut hull	1:15	300°C	5 h	38	Xue et al, 2012
Peanut shell	1:3	300°C	30 min	50.07	Huff et al, 2014
Penicillin mycelial waste	N/A	120°C	30 min	67.51	Zhuang et al, 2018
Pig manure	1:6	180°C	1.5 h	56.7	Liu et al, 2017
Pine wood	1:3	300°C	30 min	49.51	Huff et al, 2014
Pine wood	1:8	200°C	4 h	79	Wilk et al, 2019
Pinyon/juniper	1:8	175°C	30 min	77.38	Hoekman et al, 2011
Plumeria alba	1:4	180°C	10 min	53	Yang et al, 2015b
Poplar wood chips	1:5	220°C	4 h	60	Stemann et al, 2013
Poplar wood chips	3:10	180°C	8 h	89.9	Weidner et al, 2013
Poultry litter	1:5	150°C	30 min	87.17	Ghanim et al, 2016
Rabbitbrush	1:5	200°C	5 min	79	Reza et al, 2015
Rice hull	1:8	175°C	30 min	78.48	Hoekman et al, 2011
Rice hull	1:5	200°C	5 min	85	Reza et al, 2013
Rice straw	1:20	180°C	1.5 h	56	Liu et al, 2017
Salix psammophila wood	1:10	180°C	1 h	64.7	Zhu et al, 2015
Sewage sludge	N/A	200°C	12 h	60.4	He et al, 2013
Sugarcane bagasse	1:8	175°C	30 min	69.63	Hoekman et al, 2011
Switch grass	1:5	200°C	5 min	87	Reza et al, 2013
Tahoe mix chip	1:8	215°C	30 min	69.1	Hoekman et al, 2011
Tobacco stalk	1:10	180°C	2 h	80	Cai et al, 2016
Tomato peel	6.7:100	200°C	1.6 h	87.7	Sabio et al, 2016
Walnut shell	1:7	200°C	15 min	54	Yang et al, 2014
Waste lettuce	1:8	240°C	2 h	28.38	Li et al, 2019
Watermelon peel	N/A	190°C	12 h	94.76	Chen et al, 2017
Wheat straw	1:16	190°C	6 h	57	Funke et al, 2013
Wheat straw	3:10	180°C	8 h	80.1	Weidner et al, 2013

<sup>1</sup>N/A: Not available

As stated before, pressure is the another parameter that affects the hydrochar yield and hydrochar properties. But it is known that pressure is actually “self-pressure”, which is generated by the water in the reaction chamber. Hydrothermal carbonization is carried out under 10-40 bar which allows water to remain in the liquid phase. As a result of high temperature, a rise in pressure also occurs (Funke and Ziegler, 2010).

#### **2.4 History and Applications of Hydrothermal Carbonization**

The researches on hydrothermal carbonization have started at the beginning of the 1900s. The hydrothermal process was firstly described by Bergius in 1913 (Dinjus et al, 2011). In 1932, more systematic experiments were achieved by Berl et al. who hydrothermally carbonized cellulose and lignin at temperatures between 150 – 350°C under self-pressure. In the same year, Berl and Schmidt investigated a similar study that involved the hydrothermal carbonization of resin and wax at temperatures between 250 – 400°C (Funke and Ziegler, 2010; Titirici et al, 2007a). Schuhmacher et al. investigated the effect of pH on hydrothermal carbonization and determined that elemental composition was effected from changed pH, in 1960 (Titirici et al, 2007a). Hydrothermal degradation of organic substances and production of valuable materials were investigated widely by Bobleter et al. in many years (Mumme et al, 2011; Benavente et al, 2015). Bobleter, Pape and Concini carried out that essential characteristics of hydrothermal carbonization in many years (Mumme et al, 2011; Benavente et al, 2015). Bonn et al. (1983) investigated the hydrothermal carbonization of poplar wood and wheat straw at 200°C and 260°C in 1983. As the increase in temperature, degradation of poplar wood was increased, while there was no significant change in the wheat straw. Bonn et al. (1985) studied hydrothermal carbonization of poplar woods that had different ages and found that different ages of poplar wood processed in HTC caused different product contents. Overend et al. synthesized fuels from biomasses by hydrothermal processes in 1985 (Mumme et al, 2011). In 1989, Schwald and Bobleter (1989) studied on hydrothermal carbonization of cotton cellulose at different temperatures. Goudriaan and Peferoen (1990) investigated production of liquid fuels from biomass via hydrothermal carbonization in 1990.

Since the beginning of the 2000s, many scientists have extensively studied the production of carbonaceous materials from biomass sources by hydrothermal carbonization. In 2006, Cui et al. (2006) investigated the textural properties of starch

and rice grains, which were hydrothermally carbonized with iron oxide. Titirici et al. (2007b) studied carbon spheres which were synthesized by hydrothermal carbonization at 180°C for 24 h. Inoue et al. (2008) investigated characteristics of cellulose-based hydrochars, which were synthesized at different temperatures and retention times. Demir – Cakan et al. (2009) studied on synthesis of functional carbonaceous materials from the hydrochar of glucose and acrylic acid which were carbonized at 190°C for 16 h. Titirici and Antonietti (2010) extensively investigated functional carbon materials produced from hydrochars, and their study also discussed the potential end-uses.

Using raw biomass as a fuel is challenging due to its high moisture content and low heating value. As stated before, it is possible to increase the heating value by applying hydrothermal carbonization. Cai et al. (2016), Gao et al. (2016a) and Nakason et al. (2018) investigated the fuel properties of hydrochars obtained by hydrothermal carbonization from tobacco stalk, eucalyptus bark and cassava rhizome, respectively. After hydrothermal carbonization, specific parameters such as volatile matter, moisture, hydrogen and oxygen contents decreased while heating value, fixed carbon and carbon contents increased. Therefore it is possible to conclude that fuel properties are enhanced after HTC.

Wang et al. (2011b; 2013) and Tusi et al. (2013; 2017) examined the use of hydrochar in the fuel cell. By using hydrochar in an electrode, catalytic activity and gas diffusion efficiency were increased.

Ding et al. (2012; 2013b), Falco et al. (2013), Feng et al. (2014), Gao et al. (2015), Sevilla et al. (2014) and Wei et al. (2011) studied the use of hydrochars derived from rice husk, spruce and corncob,  $\beta$ -cyclodextrins, glucose, microalgae, eucalyptus wood sawdust in supercapacitors. The specific capacitance and efficiency of supercapacitors increased due to developed porosity and surface functional groups by hydrothermal carbonization and the supercapacitors had long-term cycle life and high electrochemical stability.

Tang et al. (2012a), Hu et al. (2008b) and Unur et al. (2013) investigated the use of hydrochars of D-glucose, glucose and hazelnut shell, respectively, in an anode electrode of lithium-ion batteries. Similarly, Tang et al. (2012b) examined the usage of D-glucose hydrochar in anode material of sodium-based battery. Their results

indicated that due to surface properties and functional groups of hydrochars, electrochemical performance, cycle stability, storage capacity, rate capability properties were better for both sodium and lithium based batteries, compared to non-hydrochar applications.

Briscoe et al. (2015) used carbon dots obtained from chitin, chitosan and glucose by hydrothermal carbonization in solar cells. The solar cells with hydrochars had higher short-circuit current ( $I_{sc}$ ) and open-circuit voltage ( $V_{oc}$ ) and therefore had higher efficiency. Due to better surface properties as a result of hydrothermal carbonization, hydrochars increased the efficiency of solar cell.

Sevilla and Fuertes (2011) and Sevilla et al. (2011b) investigated CO<sub>2</sub> capture and adsorption properties of hydrochars obtained from eucalyptus sawdust and barley straw. Porous hydrochars had high CO<sub>2</sub> adsorption capability and also they had the ability to select CO<sub>2</sub> from other gases because of their CO<sub>2</sub> selectivity. Moreover, hydrochars could be reused.

Sevilla et al. (2011a) studied H<sub>2</sub> storage properties of potato starch, cellulose and eucalyptus sawdust hydrochars. Compared to non-hydrochar applications, their H<sub>2</sub> adsorption capacities were higher. This is mainly due to the porous structure of hydrochar.

Ruan et al. (2014) researched carbon nanoparticles derived from cocoon silk by hydrothermal carbonization. The obtained nanoparticles showed strong visible blue fluorescence at the various excitation wavelengths. Carbon nanoparticles were used to visualize heart. By the imaging studies with the obtained nanoparticles, they determined that high-quality imaging could be performed without adversely affecting the heart. The use of biocompatible and harmless nanoparticles of hydrochars for bioimaging is promising.

Kammann et al. (2012) studied the greenhouse gas fluxes effects of beetroot chips and bark chip hydrochars mixed with the soil. Malghani et al. (2013) investigated the effect of corn silage hydrochar mixed with the soil on greenhouse gases emissions. It was determined that the hydrochars decreased only N<sub>2</sub>O emissions at the beginning and then caused an increase. Besides, CO<sub>2</sub> and NH<sub>4</sub> emissions were increased. The hydrochars decomposed rapidly in the soil, which may be stimulated greenhouse gas emissions such as CH<sub>4</sub>, CO<sub>2</sub>. Moreover, the hydrophobicity and elemental components

of hydrochars were also quite important. The studies have shown that hydrochars had stability problems and therefore careful soil selection and fertilizer use were required. Bargmann et al. (2013) who synthesized hydrochar from beet-root chips investigated the effect of hydrochar (as a soil additive) on growth of spring barley, phaseolus bean, leek. George et al. (2012) studied the effects of hydrochars obtained from spent brewer's grains and yeast on growth of *medicago sativa*. While the growth of spring barley and phaseolus bean increased, the growth of leek and *medicago sativa* were adversely affected by the use of hydrochars. Besides, hydrochars affected the pH of the soil. These could also adversely affect plant growth. Soil pH, soil type, hydrochar characteristics, the structure of the plant to be grown were quite significant. The growth process for each plant might be different, even if all conditions are the same. Moreover, hydrochars had a positive effect on soil aggregation and can be used as a soil improver.

Abel et al. (2013) examined the effects of hydrochar derived from maize silage on water repellency and retention of sandy soil. Hydrochar increased water retention capacity of sandy soils with low water retention capacity. Hydrophobicity and fungal colonization caused by hydrothermal carbonization improved the water repellency. Hydrochars have great potential in soil amendments with the advantages they provided.

Chung et al. (2015; 2016) investigated hydrochars obtained from sewage sludge and swine feces for removal of adenovirus and rotavirus. Takaya et al. (2016) researched ammonium and phosphate adsorption capacity of oak wood hydrochar. Hydrochars were used as adsorbents for removal of virus and contaminants and due to hydrophobicity and meso/macro pore structure of hydrochars, adsorption capacity developed.

Hammud et al. (2015) studied the pine needles hydrochars for Malachite Green removal. Fernandez et al. (2015) examined the orange peel hydrochars for removal of organic pollutant. Flora et al. (2013) researched the adsorption capacity of hydrochar obtained from food waste by hydrothermal carbonization with acidic and alkaline media. Kumar et al. (2011) investigated the removal of uranium with switchgrass hydrochar. Based on the studies provided above, the adsorption capacity was quite

affected by the pH of the hydrochars and the hydrochars were highly effective adsorbents for the removal of various pollutants.

The production of various carbon materials such as carbon spheres, film, tubes, sheets and fiber can be produced by hydrothermal carbonization under different reaction conditions. Demir-Cakan et al. (2009) obtained raspberry – like carbon nanospheres as a result of the hydrothermal reaction of glucose in the presence of acrylic acid. Gogotsi and Yoshimura (1994) investigated the hydrothermal carbonization of tyrano fibers at 300°C and as a result, obtained highly flexible carbon film. Libera and Gogotsi (2001) obtained graphite tubes by hydrothermal carbonization of polyethylene sheets in the presence of nickel. Liu et al. (2012) investigated the electrical characteristics of deflated-balloon-like and wrinkled carbon nanosheets obtained from glucose by hydrothermal carbonization and they determined that carbon nanosheets which obtained with HTC had better conductivity and capacity. Calderon Moreno and Yoshimura (2001) examined the multi-walled carbon nanotubes produced from amorphous carbon by hydrothermal carbonization at 800°C under 100 MPa. Qian et al. (2006) investigated the production of tellurium and carbon-rich nanofibers, as a result of hydrothermal carbonization of glucose with sodium tellurite. Makowski et al. (2008) studied the hydrothermal carbonization of furfural at 190°C for 14 h in the presence of palladium metal. As a result of hydrothermal carbonization, well-defined and hydrophobic spherical carbon particles were obtained. Titirici et al. (2007b) investigated the acquiring of hydrophobic carbon spheres with the hydrothermal carbonization of glucose in the presence of silica. Titirici et al. (2007c) hydrothermally carbonized pine needles, pine cones, and oak leaves for 16 h at 200°C and as a result, they obtained sponge-like and porous carbon material. Titirici et al. (2006) examined the production of hollow carbon spheres with hydrothermal carbonization for 24 h at 180°C of glucose in the presence of metal oxide. The obtained carbonaceous materials can be used for different purposes and also in the production of activated carbon by various modifications.





### 3. FUNCTIONALIZED CARBON MATERIALS

Due to their versatile applications, functional carbon materials such as carbon nanotube, carbon nanofiber, carbon nanocoil, carbon aerogel and activated carbon have been extensively investigated in recent years.

It is possible to use functional carbon materials in many application such as aircraft, aerospace, construction and automotive industry, vehicle tires, bio-imaging, medicine, removal of heavy metal, pharmaceutical and dye, CO<sub>2</sub> capture and storage, hydrogen storage, supercapacitors, fuel cells, lithium-ion batteries and solar cells (Inagaki et al, 2014; Yazdani and Brown, 2016; Zhu et al, 2018). Depending on the purpose of use, functional carbon materials with desired properties can be produced.

Carbon nanotube can be obtained with laser vaporization, chemical vapour deposition or catalytic combustion (Edelstein, 2001). It has high crystallinity, mesoporous structure, inert surface morphology, high chemical and mechanical stability, good electrical properties and poor catalytic activity (Zhang and Zhao, 2009; You and Kamarudin, 2017; Zhu et al, 2018; Liang et al, 2012). Carbon nanofiber are cylindrical nanostructures having graphene layers and can be obtained with degradation in the presence of transition metal of carbon precursor (Liang et al, 2012). Carbon nanofiber usually has good chemical stability and high electrical properties (You and Kamarudin, 2017). Carbon nanocoil can be obtained via carbon dioxide laser deposition (Liang et al, 2012). Carbon nanocoil has good structural properties, while it does not have resistance to excessive reaction conditions (You and Kamarudin, 2017). The carbon aerogel can be obtained by consecutive sol-gel and pyrolysis processes (Zhang and Zhao, 2009; Liang et al, 2012). Carbon aerogel usually has a mesoporous structure, hydrophobic surface morphology, high mechanical stability and flexibility (You and Kamarudin, 2017). Activated carbon is produced by activating the carbon precursor. Activated carbon has a hydrophobic surface, high surface area and porosity, controllable surface morphology and functional groups, good mechanical and chemical stability and enhanced electrical properties. Due to several properties listed, activated carbons are used in many applications (Sevilla and Fuertes, 2011; Zhang and Zhao, 2009; González-García, 2018).

### 3.1 Activated Carbon

The structure of activated carbon is quite similar to graphite. Structures of graphite and activated carbon are shown in Figure 3.1. Graphite is composed of layers with regular hexagonal carbon rings, while activated carbon exhibits a more irregular structure. Along with activation, the hexagonal carbon rings undergo degradation and are randomly oriented. Due to structural defects, activated carbons have more functional groups. The unlinked carbon groups in the edge regions of the graphite crystallites in the structure of the activated carbon are usually bonded to heteroatoms such as oxygen, hydrogen, nitrogen, sulphur leading to the formation of surface functional groups. Among these groups, oxygen-containing surface groups are the most common (McDougall, 1991; Menéndez-Díaz and Martín-Gullón, 2006; Delgado et al, 2012). Apart from oxygen-containing surface groups, the activated carbon has also other functional groups such as carboxylic, carbonyl and phenolic groups. Activated carbon has both the acidic and basic characteristics due to the nature of its functional groups (Menéndez-Díaz and Martín-Gullón, 2006).

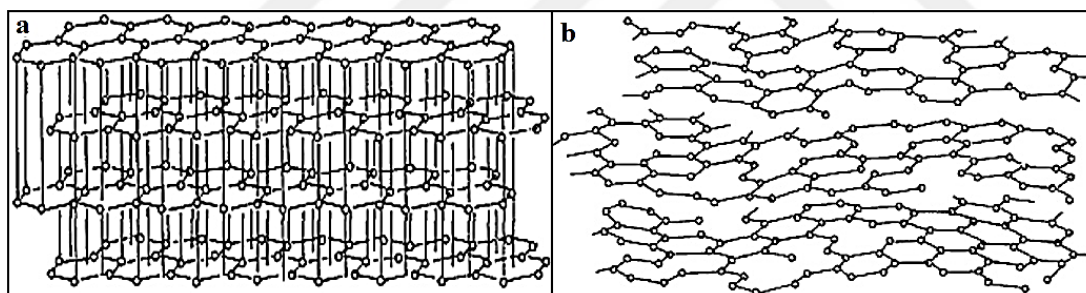


**Figure 3.1 :** Structures of **a)** graphite and **b)** activated carbon (McDougall, 1991).

Activated carbon is a functional carbon material with high surface area, superior porosity, hydrophobicity, controllable oxygenated functional groups, tailor-made surface morphology and pore structure, chemical and structural resistances, high stability, good corrosion resistance and electrical conductivity (Sevilla and Fuertes, 2011; Pandolfo and Hollenkamp, 2006; Zhang and Zhao, 2009; Delgado et al, 2012; Sevilla and Mokaya, 2014; Ao et al, 2018; Tran et al, 2017; Chomiak et al, 2017; González-García, 2018; Parshetti et al, 2015; Tan et al, 2016; Wang et al, 2014).

The textural properties of activated carbon such as BET surface and micropore areas, total, micro, meso and macro pore volumes can be obtained in a wide range according to application (Sevilla and Mokaya, 2014). It is possible to synthesize activated carbon

with tailor-made porous structure with various pore size. According to IUPAC (1985), the pores are classified by their size into three groups. The pores with a size greater than 50 nm, between 2 nm and 50 nm and less than 2 nm are called macropore, mesopore and micropore, respectively. Activated carbon with up to 2 nm pore size (micropore) is quite suitable using as adsorbent (Kaźmierczak et al, 2013), while activated carbon with micro and meso pores is convenient for use in supercapacitors (Chang and Zainal, 2019).

### **3.1.1 Activation**

There are three methods of activation: Physical, chemical and physicochemical. Starting from the char or hydrochar of biomass or coal, it is possible to produce activated carbon by applying the most suitable activation method.

#### **3.1.1.1 Physical activation**

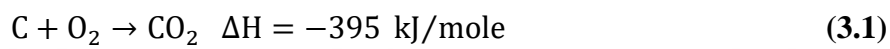
Physical activation, also called thermal activation, consists of two stages: carbonization and activation. In the first stage called carbonization, the precursor is subjected to pyrolysis in an inert atmosphere at a temperature between 300°C and 800°C. During carbonization, carbonaceous char is obtained which is rich in aromatic components and rudimentary porous due to the released volatile fractions and the broken weak bonds. During the decomposition, the pores of material are blocked due to the repolymerization of the tar and its condensation on the char surface and therefore, the obtained char has low porosity. Activation stage is required for opening the blocked pores and increasing the porosity.

In the second stage of activation, the char is subjected to heat treatment at a temperature between 700°C and 1000°C with an activating agent such as carbon dioxide, steam, air and oxygen. The removal of tar and the development of porosity and pores are carried out by activation (Pallarés et al, 2018).

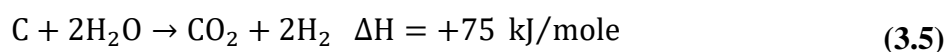
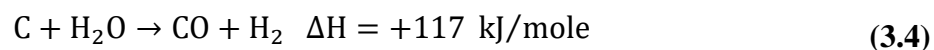
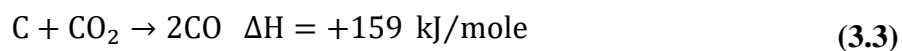
However, physical activation can also be carried out in a single stage where carbonization and activation processes occur simultaneously (Paraskeva et al, 2008). The precursor is heated to a predetermined temperature under a nitrogen atmosphere and the process is continued by changing the nitrogen gas with the gas, which is the activating agent, when the desired temperature is reached. The 2-stage activation

contains the cooling process under nitrogen atmosphere, while one-stage activation does not involve this process (Rashidi and Yusup, 2017).

Air, oxygen, carbon dioxide (CO<sub>2</sub>) and steam are used as activating agents. The use of air or oxygen as an activating agent is not common, because carbon-oxygen reactions are exothermic and can cause thermal leakage and excessive burn-off. However, it is possible to use at lower activation temperatures (Gañan et al, 2004). Exothermic reactions of carbon precursor material, which are carried out simultaneously with oxygen and contributing to porosity, are shown in Equations 3.1 and 3.2 (Plaza et al, 2014).



Carbon dioxide and steam show endothermic reactions and are easier to control. Carbon dioxide is highly preferred as it can be easily controlled due to its low reactivity at high temperatures (Pallarés et al, 2018). However, when steam is used as the activation agent, the activation takes place in a shorter time than with the carbon dioxide due to the reactivity of the steam (Nowicki et al, 2010; Ahmed, 2017). Endothermic reactions of carbon precursor material, which are carried out simultaneously with carbon dioxide and steam and contributing to porosity, are shown in Equations 3.3, 3.4 and 3.5, respectively (Plaza et al, 2014; Manyà et al, 2018; Sartova et al, 2019).



The parameters affecting the development of porous structure are activation agent, carbonization and activation conditions. CO<sub>2</sub>, steam, air and oxygen may, therefore, be suitable activating agents depending on the choice of the precursor material and process conditions (Chang et al, 2000; Aworn et al, 2008; Rambabu et al, 2015).

Pyrolysis temperature and retention time affect the composition and porosity of activated carbon. As the temperature increases, the hydrogen and oxygen components decrease, and therefore the H/C ratio decreases. The production of aromatic and carbon-rich material is a result of the reduction of the H/C ratio by pyrolysis. In addition, the surface area and total pore volume increase with increasing pyrolysis temperature up to a specific value (800°C – 850°C), while the pyrolysis at temperatures (850°C – 900°C) causes degradation with shrinkage of the material structure and decrease in surface area. Also, as pyrolysis period generally increases porosity but it is not as effective as temperature (Ioannidou and Zabaniotou, 2007).

Activation temperature and time are one of the most critical parameters affecting the structural and surface properties of activated carbon. The temperature increase up to a certain value (800°C – 850°C) increases the surface area of the activated carbon and improves its porosity. However, as a result of activation at temperatures above 850°C, the structure deteriorates and the porosity is reduced by the blocking of the pores with the components that have low melting temperatures (Pallarés et al, 2018). Sánchez et al. (2001) investigated physical activation of quercus agrifolia wood waste using CO<sub>2</sub> as an activating agent at 800°C, 840°C and 880°C. The least activation ratio was obtained at the longest activation time and 800°C, while the activation ratio increased with temperature. BET surface areas increased up to 840°C, while at 880°C the surface area was not changed. BET surface areas were obtained 931 m<sup>2</sup>/g, 1201 m<sup>2</sup>/g and 1197 m<sup>2</sup>/g at the 800°C, 840°C and 880°C, respectively. El-Hendawy et al. (2001) examined the physical activation of corncob with steam as an activating agent at various temperatures between 500°C and 850°C. While BET surface area and porosity increased up to 700°C, it was determined that porosity and surface area tend to decrease after this temperature. BET surface areas of activated carbons derived by activation at 500°C, 600°C, 700°C and 850°C were 39 m<sup>2</sup>/g, 618 m<sup>2</sup>/g, 786 m<sup>2</sup>/g and 607 m<sup>2</sup>/g, respectively. Additionally, activated carbon yields decreased with increasing activation temperature. Rezma et al. (2017) physically activated palm waste with CO<sub>2</sub> at 750°C, 850°C and 950°C. It was observed that BET surface areas were increased from 353 m<sup>2</sup>/g to 546 m<sup>2</sup>/g with an increase in temperature from 750°C to 850°C and more porous structure was observed at higher temperatures. However, at 950°C, the BET surface area was significantly reduced and BET surface area was observed 214 m<sup>2</sup>/g. It indicated that the material may be decomposed at high

temperature. Pallarés et al. (2018) investigation physical activation of barley straw with CO<sub>2</sub> at various temperatures (600-900°C) and times (1-2 h). It has been observed that the surface characteristics enhanced with the increasing temperature from 700°C to 800°C, but in the activation at 900°C, the components with low melting temperature blocked the pores formed and resulted a decrease in porosity. Lua and Guo (2001) examined the physical activation of oil palm stones with CO<sub>2</sub> at various temperatures and times. BET and micropore surface areas and percentage micropore fraction increased with the increase in activation temperature and time. However, at high temperature (900°C) as the retention time was changed from 15 min to 60 min, micropore fraction was decreased. The micropore fractions of activated carbons synthesized at 900°C for 15, 30 and 60 min were 74%, 70.2% and 44.1%, respectively. It can be concluded that at high temperature activation, the material is degraded, the pores are blocked and the formation of meso and macro pores developed.

Another important parameter affecting the physical activation is the gas, which is used as an activating agent. As mentioned above, carbon dioxide and steam show endothermic reactions with precursor and are easy to control, while air and oxygen show exothermic reactions with precursor and are more difficult to control (Gañan et al, 2004; Pallarés et al, 2018). Activation with carbon dioxide promotes the formation of microporosities, while activation with steam supports the formation of meso and macro porosity (González-García, 2018; Chen et al, 2011). In addition, activation with carbon dioxide provides uniform porosity compared to steam (Khezami et al, 2007). Pallarés et al. (2018) studied physical activation of barley straw with CO<sub>2</sub> and steam at almost similar conditions. As a result, it was stated that activation with CO<sub>2</sub> was more effective than steam in increasing the surface area and porosity. In the activation with CO<sub>2</sub>, the BET surface area and micropore volume were 789 m<sup>2</sup>/g and 0.327 cm<sup>3</sup>/g, while in the activation with steam the BET surface area and micropore volume were 540 m<sup>2</sup>/g and 0.230 cm<sup>3</sup>/g. Barroso-Bogeat et al. (2015) investigated physical activation of vine shoot with air, CO<sub>2</sub> and steam at same conditions and determined that electrical conductivity of activated carbons was ranked from highest to lowest as the activation agents were air, CO<sub>2</sub> and steam. That occurred as a result of the different reactions of each activating agent with carbon surface. According to studies of Pallarés et al. (2018) and Barroso-Bogeat et al. (2015), it is possible to use activating agents in various applications under suitable conditions.

In literature, it is possible to see several studies that concentrate on the physical activation of various biomass samples, such as coconut shell (Yang et al, 2010), corncob (Aworn et al, 2008; El-Hendawy et al, 2001), cotton ball (Sartova et al, 2019), horse manure (Hao et al, 2013), macadamia nut shell (Aworn et al, 2008), pistachio-nut shell (Yang and Lua, 2003), rice husk (Aworn et al, 2008), vine shoots (Barroso-Bogeat et al, 2015), walnut shell (Nowicki et al, 2010), eucalyptus sawdust (Couto et al, 2012), olive-tree wood (Ould-Idriss et al, 2011), quercus agrifolia wood waste (Sánchez et al, 2001), sawdust (Aworn et al, 2008), beer waste (Hao et al, 2013), sludge from paper and pulp mill (Hao et al, 2013). Table 3.1 gives a brief review of physical activation conditions and properties of activated carbons produced.



**Table 3.1 : Physical activation conditions and properties of activated carbons produced.**

Biomass	Pre – carbonization		Pre-carbonization conditions		Activating agent	Activation conditions		S <sub>BET</sub> <sup>1</sup> (m <sup>2</sup> /g)	S <sub>mic</sub> <sup>2</sup> (m <sup>2</sup> /g)	V <sub>total</sub> <sup>3</sup> (cm <sup>3</sup> /g)	V <sub>meso</sub> <sup>4</sup> (cm <sup>3</sup> /g)	V <sub>mic</sub> <sup>5</sup> (cm <sup>3</sup> /g)	Pore size (nm)	Application	Reference
	HTC	Pyrolysis	Temp. (°C)	Time (h)		Temp. (°C)	Time (min)								
Bagasse	No	Yes	500	1	Steam	800	N/A <sup>6</sup>	595	N/A	0.3953	0.1330	0.2653	2.68	Carbon material	Aworn et al, 2008
Barley malt bagasse	No	Yes	800	2	CO <sub>2</sub>	900	60	80.5	N/A	0.0468	N/A	N/A	1.16	Methylene blue adsorption	Franciski et al, 2018
Barley straw	No	Yes	500	1	CO <sub>2</sub>	800	60	789	778	0.3495	N/A	0.327	1.77	Carbon material	Pallarés et al, 2018
Barley straw	No	Yes	500	1	Steam	700	60	552	540	0.2576	N/A	0.230	1.87	Carbon material	Pallarés et al, 2018
Beer waste	Yes	No	N/A	N/A	CO <sub>2</sub>	800	120	622	573	0.317	N/A	0.204	N/A	CO <sub>2</sub> adsorption	Hao et al, 2013
Coconut shell	No	Yes	1000	2	CO <sub>2</sub>	900	210	2288	N/A	1.30	0.287	1.012	N/A	Carbon material	Yang et al, 2010
Coconut shell	No	Yes	1000	2	Steam	900	75	2079	N/A	1.21	0.239	0.974	N/A	Carbon material	Yang et al, 2010
Coconut shell	No	Yes	1000	2	CO <sub>2</sub> + Steam	900	75	2194	N/A	1.30	0.283	1.010	N/A	Carbon material	Yang et al, 2010
Corncob	No	Yes	500	1	Steam	800	N/A	675	N/A	0.3590	0.0373	0.3590	2.13	Carbon material	Aworn et al, 2008
Corncob	No	Yes	500	2	Steam	700	60	786	N/A	0.430	0.121	0.252	1.09	Methylene blue adsorption	El-Hendawy et al, 2001
Corncob	No	Yes	800	N/A	Steam	800	120	998	819	0.511	0.117	0.382	1.52	Carbon material	Chang et al, 2000
Corncob	No	Yes	800	N/A	CO <sub>2</sub>	800	120	670	578	0.342	0.056	0.284	1.48	Carbon material	Chang et al, 2000
Cotton ball	No	Yes	500	N/A	Steam	800	8	N/A	N/A	2.415	N/A	N/A	N/A	Removal of pollutant	Sartova et al, 2019
Eucalyptus sawdust	No	Yes	500	3	CO <sub>2</sub>	850	60	528	N/A	N/A	N/A	N/A	N/A	Methylene blue adsorption	Couto et al, 2012
Grass cuttings	Yes	No	N/A	N/A	CO <sub>2</sub>	800	120	841	742	0.379	N/A	0.281	N/A	CO <sub>2</sub> adsorption	Hao et al, 2013
Horse manure	Yes	No	N/A	N/A	CO <sub>2</sub>	800	120	749	344	0.816	N/A	0.141	N/A	CO <sub>2</sub> adsorption	Hao et al, 2013



Macadamia nut shell	No	Yes	500	1	Steam	800	N/A	844	N/A	0.4852	0.0941	0.3911	2.30	Carbon material	Aworn et al, 2008
Oil palm shell	No	Yes	900	1	CO <sub>2</sub>	850	420	1118	N/A	0.51	N/A	0.42	2.04	Methane adsorption	Arami-Niya et al, 2010
Oil palm stones	No	Yes	600	2	CO <sub>2</sub>	900	30	1136	958	N/A	N/A	N/A	N/A	Gas-phase adsorption	Lua and Guo, 2001
Olive-tree wood	No	Yes	600	2	Air	400	120	481	N/A	N/A	0.046	0.226	N/A	Carbon material	Ould-Idriss et al, 2011
Palm wastes	No	Yes	1000	8	CO <sub>2</sub>	850	30	546	540	0,24	N/A	0.23	0.9	Carbon material	Rezma et al, 2017
Pistachio-nut shell	No	Yes	500	2	CO <sub>2</sub>	800	120	1014	N/A	N/A	N/A	0.205	N/A	Carbon material	Yang and Lua, 2003
Quercus agrifolia wood waste	No	Yes	450	2	CO <sub>2</sub>	840	N/A	1201	N/A	0.671	0.159	0.512	N/A	Carbon material	Sánchez et al, 2001
Rice husk	No	Yes	500	1	Steam	800	N/A	74	N/A	0.0532	0.0206	0.0326	2.90	Carbon material	Aworn et al, 2008
Rice husk	No	Yes	500	1	CO <sub>2</sub>	800	N/A	39	N/A	0.0296	0.0123	0.0173	3.01	Carbon material	Aworn et al, 2008
Rubber seed shell	No	Yes	N/A	N/A	Steam	880	60	948	N/A	0.988	N/A	0.615	3.65	Carbon material	Sun and Jiang, 2010
Sawdust	No	Yes	500	1	Steam	800	N/A	613	N/A	0.4926	0.2242	0.2684	3.22	Carbon material	Aworn et al, 2008
Sludge from paper and pulp mill	Yes	No	N/A	N/A	CO <sub>2</sub>	800	120	489	291	0.387	N/A	0.117	N/A	CO <sub>2</sub> adsorption	Hao et al, 2013
Vine shoots	No	Yes	600	2	Air	275	60	322	N/A	0.77	0.03	0.16	N/A	Semiconductor	Barroso-Bogeat et al, 2015
Vine shoots	No	Yes	900	2	CO <sub>2</sub>	750	60	293	N/A	0.62	0.07	0.14	N/A	Semiconductor	Barroso-Bogeat et al, 2015
Walnut shell	No	Yes	400	2	CO <sub>2</sub>	800	60	469	456	0.25	N/A	0.23	2.14	Adsorbent	Nowicki et al, 2010

<sup>1</sup>S<sub>BET</sub> = BET Surface area, <sup>2</sup>S<sub>mic</sub> = Micropore area, <sup>3</sup>V<sub>total</sub> = Total pore volume, <sup>4</sup>V<sub>meso</sub> = Mesopore volume, <sup>5</sup>V<sub>mic</sub> = Micropore volume; <sup>6</sup>N/A = Not available

### 3.1.1.2 Chemical activation

Chemical activation is an one-step thermochemical process, which is carried out at a definite temperature in the presence of a chemical activating agent under an inert gas atmosphere. Biomass, which is used as a precursor, can be subjected to a pre-carbonization process such as hydrothermal carbonization and pyrolysis before activation. The poor porosity of hydrochar can be improved by chemical activation through its oxygenated functional groups. Oxygen functional groups of hydrochar increase the effectiveness of the chemical activating agent and contribute to the development of surface properties (Jain et al, 2015; Wang et al, 2018a; Lima et al, 2019). Activating agent is mixed with precursor by using either dry mixing or liquid impregnation methods. In the dry mixing method, the precursor and activating agent are directly mixed and then activated. In the wet impregnation method, the precursor is subjected to the liquid solution of the activating agent and after the impregnation, the slurry is dried (Wang and Kaskel, 2012; Rashidi and Yusup, 2017). The prepared mixture of precursor and activating agent is subjected to heat treatment (temperature between 400 – 950°C) under an inert atmosphere such as nitrogen and argon (Wang and Kaskel, 2012). To remove the activating agent, activated carbon is washed with acid/base solution and deionized water based on the activating agent.

Chemical activation has significant advantages compared to physical activation. Chemical activation can be carried out at lower temperatures and shorter times and it is possible to obtain activated carbon having higher surface area and porosity (Ding et al, 2013a; Tang et al, 2018; Nowicki et al, 2010). Also, it is easier to control the reaction and porosity development by chemical activation (Kwiatkowski and Broniek, 2017). Nowicki et al. (2010) compared chemically activated (activating agent: KOH) and physically activated (with CO<sub>2</sub>) walnut shell. The chemical activation with KOH was carried out at 800°C for 30 min and the BET surface area of the activated carbon was observed as 2263 m<sup>2</sup>/g. The physical activation with CO<sub>2</sub> was also carried out at 800°C for 60 min and the BET surface area was found as 697 m<sup>2</sup>/g. In addition, the micropore area and volume of activated carbon obtained by chemical activation were quite high compared to those obtained by physical activation. Due to high surface area and porosity obtained with a shorter activation time, chemical activation may be preferred.

Despite these advantages, chemical activation requires the removal of the activating agent to prevent the pores from blocking. Therefore, after activation, washing with selected acid/base solutions and deionized water is quite important. Chemical activating agents generally are corrosive and after activation, its removal and recovery are the disadvantages of chemical activation (Albanese et al, 2019).

The parameters, which affect the formation of porous structure, are type of precursor and activating agent, impregnation ratio, pre-carbonization and activation conditions (Kwiatkowski and Broniek, 2017).

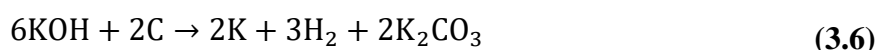
Alkali hydroxides such as NaOH (Qian et al, 2018; Cazetta et al, 2011; Pezoti et al, 2016), KOH (Yang et al, 2019; Parshetti et al, 2015; Lin et al, 2019),  $K_2CO_3$  (Marques et al, 2018; Couto et al, 2012; Tzvetkov et al, 2016); inorganic acids such as  $H_2SO_4$  (Wang et al, 2011a),  $H_3PO_4$  (Vernersson et al, 2002; Hao et al, 2014; Kumar and Jena, 2016); alkali earth metal salts such as  $ZnCl_2$  (Boyjoo et al, 2017; Duan et al, 2019; Arami-Niya et al, 2010),  $FeCl_2$  (Fu et al, 2017),  $FeCl_3$  (Tian et al, 2019) are used as activating agents. Using chemical activation agents, increase the number of functional groups, surface area and porosity (Tan et al, 2017; Lee et al, 2018b). Chemical activating agents cause dehydration and degradation of the precursor carbon material. Various cross-linking reactions occur during activation, and porosity increases while pore size decreases (Danish and Ahmad, 2018; Sevilla and Mokaya, 2014).

KOH develops micro-pores with heterogeneous distribution, while  $ZnCl_2$  improves larger micropores and small mesopores and  $H_3PO_4$  enhances macropores with large mesopores (Sevilla and Mokaya, 2014). While KOH, NaOH,  $H_3PO_4$  are corrosive and toxic (Adinata et al, 2007; Yakout and Sharaf El-Deen, 2016; Kumar and Jena, 2016),  $K_2CO_3$  is not hazardous and can be used in applications of the food industry (Adinata et al, 2007). In addition,  $ZnCl_2$  is not suitable for use in the food and pharmaceutical industry (Rashidi and Yusup, 2017; Yakout and Sharaf El-Deen, 2016), and it is not also appropriate for use with hydrochar as it fails to improve the hydrochar structure (Liu et al, 2018). Despite its advantages and disadvantages, it is possible to use activating agents with appropriate activation conditions according to various application areas.

Each activating agent exhibits a different reaction mechanism with carbon precursor. Acidic activation agents, such as  $H_3PO_4$  and  $H_2SO_4$ , are highly effective in breaking

down the hemicellulose, cellulose and lignin components of biomass. The reaction between  $\text{H}_3\text{PO}_4$  and precursor begins as they are mixed and it continues throughout the activation. Because of the resistance of cellulose to phosphoric acid, hemicellulose and lignin begin to decompose firstly. The ether linkages in the lignin structure are broken and the degradation of the precursor occurs. Dehydration, degradation, and condensation reactions take place simultaneously during activation (Yakout and Sharaf El-Deen, 2016). Due to the reason that  $\text{H}_2\text{SO}_4$  is easily decomposed into sulfur dioxide and water, it tends to release an oxygen atom to compose  $\text{H}_2\text{SO}_3$  and hence it behaves as a severe oxidizing agent (Chen et al, 2011).

In KOH activation, primarily potassium reacts with carbon precursor to form a porous network. Subsequently, steam and carbon dioxide react with carbonaceous precursor at elevated temperatures and in fact, this is similar to a physical activation process that contributes to the development of carbon porosity. Finally, metallic potassium causes breakage and separation between the carbon layers, resulting in the formation of micropores (Sevilla and Mokaya, 2014; Wang and Kaskel, 2012).  $\text{K}_2\text{CO}_3$ , a by-product, which is formed by oxidation of C atoms to CO or  $\text{CO}_2$ , increases porosity. Also, due to the release of the CO and  $\text{CO}_2$  gases formed as a result of the reactions, the activated carbon yields decrease and the porosity increases. Chemical reactions between the carbon precursor and KOH are shown in Equations 3.6 – 3.10 (Mamaní et al, 2019; Gao et al, 2015; Liu et al, 2019; Tan et al, 2017; Unur, 2013; Sevilla and Mokaya, 2014).



The reaction mechanism is also valid if NaOH is used instead of KOH. As a result of the reaction between NaOH and the carbon precursor, the ester linkages between carbohydrates and lignin breaks, the structure decomposed and the porosity increases

(Kumar and Jena, 2016). Although the reaction mechanisms are similar, NaOH is effective in structurally irregular precursors, while KOH is highly effective in all types of structures and therefore, it has a broader application area (Liu et al, 2019).

Marques et al. (2018) carried out chemical activation of apple tree branches with the same ratios of  $K_2CO_3$  and KOH at  $800^\circ C$ . The activated carbons obtained by activation in the presence of  $K_2CO_3$  and KOH had BET surface areas of  $1959\text{ m}^2/\text{g}$  and  $2472\text{ m}^2/\text{g}$ , respectively. Activated carbons obtained under the same activation conditions had different surface areas due to different reaction mechanisms of KOH and  $K_2CO_3$  activations. The reactions between the carbon matrix and activating agent took place at between  $400^\circ C$  and  $600^\circ C$  for KOH and between  $600^\circ C$  and  $800^\circ C$  for  $K_2CO_3$ . Köseoğlu and Akmil-Başar (2015) studied the chemical activation of orange peel in the presence of  $ZnCl_2$  and  $K_2CO_3$  at  $500^\circ C$  and  $1000^\circ C$ , respectively. Activated carbons obtained in the presence of  $ZnCl_2$  and  $K_2CO_3$  had almost the same BET surface areas with  $1215\text{ m}^2/\text{g}$  and  $1228\text{ m}^2/\text{g}$ , respectively. Although they had a similar surface area, porosity and pore size,  $ZnCl_2$  reacted with the precursor at lower temperatures, while the  $K_2CO_3$  was required higher temperatures. Olivares-Marín et al. (2006a; 2006b) investigated the chemical activation of cherry stone with KOH and  $ZnCl_2$  at  $900^\circ C$  and  $500^\circ C$  for 2 h, respectively. The active carbons obtained by two studies showed similar BET surface area and micropore volume, while the activated carbon obtained with KOH had a higher total pore volume. Activated carbons obtained with KOH and  $ZnCl_2$  had  $1624\text{ m}^2/\text{g}$  and  $1566\text{ m}^2/\text{g}$  of BET surface areas, respectively and  $0.69\text{ m}^3/\text{g}$  of micropore volume. In addition, activated carbons obtained with KOH and  $ZnCl_2$  had total pore volumes of  $2.88\text{ cm}^3/\text{g}$  and  $1.20\text{ cm}^3/\text{g}$ , respectively. However, activated carbon obtained with KOH at the higher temperature, whereas in the presence of  $ZnCl_2$ , activated carbon obtained at the lower temperature. It is possible to use each activating agent according to various applications and activation conditions.

Activation temperature is one of the most critical parameters that affects the structural and surface properties of activated carbon. Olivares-Marín et al. (2006a) did a chemical activation of cherry stones in the presence of KOH at temperatures between  $400^\circ C$  and  $900^\circ C$ . BET surface areas of activated carbons at  $400^\circ C$ ,  $500^\circ C$ ,  $600^\circ C$ ,  $700^\circ C$ ,  $800^\circ C$  and  $900^\circ C$  were determined as  $7\text{ m}^2/\text{g}$ ,  $279\text{ m}^2/\text{g}$ ,  $588\text{ m}^2/\text{g}$ ,  $888\text{ m}^2/\text{g}$  and  $1167\text{ m}^2/\text{g}$ , respectively. Surface areas and microporous volumes of activated

carbons obtained by activation in the presence and absence of KOH at 900°C were obtained as 1624 m<sup>2</sup>/g, 0.69 cm<sup>3</sup>/g and 230 m<sup>2</sup>/g, 0.11 cm<sup>3</sup>/g respectively. With the use of the activating agent, porosity and surface area increased significantly. Carvalho et al. (2003) studied chemical activation of cork waste with KOH at temperatures for 2 h. Activated carbons obtained at temperatures of 500°C, 600°C, 700°C, 800°C and 900°C had BET surface areas of 507 m<sup>2</sup>/g, 723 m<sup>2</sup>/g, 1063 m<sup>2</sup>/g, 1336 m<sup>2</sup>/g and 1415 m<sup>2</sup>/g, respectively. Sevilla and Fuertes (2011) researched activated carbon derived from eucalyptus sawdust by chemical activation with KOH at various temperatures. BET surface areas of activated carbons obtained by activation at temperatures of 600°C, 700°C and 800°C were determined as 1260 m<sup>2</sup>/g, 1390 m<sup>2</sup>/g and 1940 m<sup>2</sup>/g, respectively. According to studies of Olivares-Marín et al. (2006a), Carvalho et al. (2003) and Sevilla and Fuertes (2011), with risen temperatures BET surface areas and micropore volumes increased and porosity enhanced. Chandra et al. (2009) subjected to durian shell to chemical activation with KOH at various temperatures. BET surface area increased with rising temperature from 400°C to 500°C, while BET surface area decreased at temperatures between 600°C and 800°C. The improvement in the BET surface area with the increased temperature indicated the released of volatiles and therefore, enhanced porosity. 600°C – 800°C temperature range, the decreased in the BET surface area due to the increased in temperature was caused by the sintering effect of the volatile matters, shrinkage of the carbon structure and blocking and contraction of some pores (Paraskeva et al, 2008; Chandra et al, 2009).

Activation period is another important parameter affecting the properties of activated carbon. Ding et al. (2013b) studied chemical activation of corncob by using KOH (KOH/biomass: 4) at 800°C for 0.5, 1 and 2 h. The BET surface area, total pore and micropore volumes increased from 2705 m<sup>2</sup>/g to 3220 m<sup>2</sup>/g, from 1.95 cm<sup>3</sup>/g to 2.35 cm<sup>3</sup>/g and from 0.32 cm<sup>3</sup>/g to 0.36 cm<sup>3</sup>/g, respectively, with an extension of retention time. Carvalho et al. (2003) examined the chemical activation of cork waste with KOH at 800°C for 0, 2 and 16 h. As the activation period was extended two hours, the BET surface area of activated carbon was improved from 1039 m<sup>2</sup>/g to 1336 m<sup>2</sup>/g, while the BET surface area decreased to 1275 m<sup>2</sup>/g for 16 h of activation. According to studies of Ding et al. (2013b) and Carvalho et al. (2003), BET surface areas, total pore and micropore volumes generally increased with retention time. However, in the long

activation times like 16 hours, reduction in the BET surface area due to shrinkage and blocking of pores might occur.

Another important parameter affecting the chemical activation is the activating agent to biomass ratio. Chandra et al. (2009) examined activated carbon derived from durian shell with various ratios of KOH. Activated carbons obtained with ratios of 0.25 and 0.50 had 560 m<sup>2</sup>/g and 674 m<sup>2</sup>/g of BET surface areas and 0.16 cm<sup>3</sup>/g and 0.34 cm<sup>3</sup>/g of micropore volumes, respectively. Idrees et al. (2018) studied the chemical activation of packing waste by using different KOH/biomass ratios at 700°C for 60 min. As the KOH/biomass ratio was selected as 1, 2, 3 and 4, BET surface area of activated carbons were found as 761 m<sup>2</sup>/g, 963 m<sup>2</sup>/g, 1283 m<sup>2</sup>/g and 1383 m<sup>2</sup>/g, respectively. It can be concluded that increasing the KOH/biomass ratio positively affects porous structure formation. Sevilla and Fuertes (2011) investigated eucalyptus sawdust activated carbons derived by chemical activation where the KOH/biomass ratio was 2 and 4. BET surface areas of activated carbons obtained with rising ratios from 2 to 4 increased from 1940 m<sup>2</sup>/g to 2850 m<sup>2</sup>/g. Tseng and Tseng (2005) subjected to corncob to chemical activation with KOH at 780°C for 1 h. BET surface areas of activated carbons obtained with rising KOH to biomass ratios of between 0 and 6 increased from 309 m<sup>2</sup>/g to 2595 m<sup>2</sup>/g and porosity increased. Cazetta et al. (2011) carried out chemical activation of coconut shell at 700°C for 1 h with various ratios of NaOH. As a result of activations with 1, 2 and 3 of NaOH to biomass ratios, the BET surface area, total pore, mesopore and micropore volumes developed. However, activated carbon yield decreased with increased NaOH. Activated carbons obtained with 1, 2 and 3 of ratios had BET surface areas of 783 m<sup>2</sup>/g, 1842 m<sup>2</sup>/g and 2825 m<sup>2</sup>/g, mesopore volumes of 0.356 cm<sup>3</sup>/g, 0.775 cm<sup>3</sup>/g and 1.143 cm<sup>3</sup>/g and micropore volumes of 0.022 cm<sup>3</sup>/g, 0.152 cm<sup>3</sup>/g and 0.355 cm<sup>3</sup>/g, respectively. Activated carbon yields decreased from 28.9% to 18.8%. Olivares-Marín et al. (2006b) investigated the chemical activation of cherry stone with various ratios of ZnCl<sub>2</sub> to biomass at 500°C for 2 h. Activated carbons obtained with 1, 2, 3 and 4 of ratios had BET surface areas of 567 m<sup>2</sup>/g, 1086 m<sup>2</sup>/g, 1566 m<sup>2</sup>/g ve 1971 m<sup>2</sup>/g, respectively. Carvalho et al. (2003) investigated the chemical activation of cork waste with various ratios of KOH at 800°C for 2 h. As the surface area increased with increasing KOH/cork waste ratio, it had no significant effect on pore diameter and microporosity. Activated carbons obtained by activation with ratios of 0.1, 0.25, 0.5 and 1 had BET surface areas of 427 m<sup>2</sup>/g, 1044 m<sup>2</sup>/g, 1190

$\text{m}^2/\text{g}$  and  $1336 \text{ m}^2/\text{g}$ , respectively. When the ratios were 2 and 4, the surface areas of activated carbons reduced from  $1104 \text{ m}^2/\text{g}$  to  $251 \text{ m}^2/\text{g}$ , respectively. According to studies, the surface area and porosity generally increased by the rising activating agent to biomass ratio. However, as in research of Carvalho et al. (2003), the use of a high amount of activating agent may result in a decrease in porosity due to occluding of pores formed.

The pre-carbonization processes such as hydrothermal carbonization and pyrolysis prior to activation improve the structure of raw precursor and provide a better quality precursor for activation. Zeng et al. (2019) subjected to *sargassum horneri* to hydrothermal carbonization and chemical activation with KOH, respectively. Raw biomass, hydrochar and activated hydrochar had BET surface areas of  $0.43 \text{ m}^2/\text{g}$ ,  $26.64 \text{ m}^2/\text{g}$  and  $1221 \text{ m}^2/\text{g}$  and micropore volumes of  $0 \text{ cm}^3/\text{g}$ ,  $0.0007 \text{ cm}^3/\text{g}$  and  $0.38 \text{ cm}^3/\text{g}$ , respectively. Raw biomass, hydrochar and activated hydrochar had average pore sizes of  $21.77 \text{ nm}$ ,  $13.96 \text{ nm}$  and  $2.16 \text{ nm}$ , respectively. After hydrothermal carbonization and activation, gradually, surface areas and micropore volumes increased, while the average pore diameter decreased. The poor porosity of hydrochar was enhanced with activation. Hao et al. (2014) carried out hydrothermal carbonization and then activation ( $\text{H}_3\text{PO}_4$ ) to beer waste. The lower BET surface area of hydrochar with  $6 \text{ m}^2/\text{g}$  increased to  $1070 \text{ m}^2/\text{g}$  by activation. In addition, the activation further reduced the H/C and O/C ratios, which were slightly reduced by hydrothermal carbonization. The H/C and O/C ratios obtained with hydrothermal carbonization were 1.21 and 0.46, and these ratios were 0.44 and 0.28 after activation, respectively. Pezoti et al. (2016) applied pyrolysis to guava seed and then activated with NaOH. The low surface area and porosity of biochar, which was obtained by pyrolysis, were developed after activation. Biochar had the microporous volume of  $0.005 \text{ cm}^3/\text{g}$  and the BET surface area of  $18.08 \text{ m}^2/\text{g}$ , while BET surface area and microporous volume of activated carbon increased to  $2573 \text{ m}^2/\text{g}$  and  $1.07 \text{ cm}^3/\text{g}$ , respectively. Also, the average pore diameter was reduced from  $4.42 \text{ nm}$  to  $1.96 \text{ nm}$  by activation.

Chemical activation can be applicable to various biomass resources, such as cherry stones (Olivares-Marín et al, 2006a; Olivares-Marín et al, 2006b), coconut shell (Islam et al, 2017a; Chen et al, 2016; Cazetta et al, 2011), corn cob (Duan et al, 2019; Li et al, 2017; Ding et al, 2013b), durian shell (Chandra et al, 2009), fox nut shell (Kumar and Jena, 2016), grape stalk (Shahraki et al, 2018), guava seed (Pezoti et al, 2016),



hazelnut husk (Unur et al, 2013), horse chestnut seed (Tzvetkov et al, 2016), jackfruit peel (Prahas et al, 2008), tomato stem (Fu et al, 2017), walnut shell (Nowicki et al, 2010), apple tree branch (Marques et al, 2018), bamboo (Qian et al, 2018), eucalyptus sawdust (Couto et al, 2012; Sevilla and Fuertes, 2011), fir wood (Wu and Tseng, 2008), olive tree pruning (Mamaní et al, 2019), beer waste (Hao et al, 2014), Coca Cola® waste (Boyjoo et al, 2017), factory-rejected tea (Islam et al, 2015a), packaging waste (Idrees et al, 2018); algae (Fan et al, 2015). Moreover, hydrochar can be used as the precursor in the production of activated carbon.

Table 3.2 summarizes the studies, which investigated the chemical activation of biomass sources.



**Table 3.2 :** Chemical activation conditions and properties of activated carbons produced.

Biomass	Pre – carbonization		Pre – carbonization conditions		Activating agent	Activating agent: Precursor ratio (w/w)	Activation conditions		S <sub>BET</sub> <sup>1</sup> (m <sup>2</sup> /g)	S <sub>mic</sub> <sup>2</sup> (m <sup>2</sup> /g)	V <sub>total</sub> <sup>3</sup> (cm <sup>3</sup> /g)	V <sub>meso</sub> <sup>4</sup> (cm <sup>3</sup> /g)	V <sub>mic</sub> <sup>5</sup> (cm <sup>3</sup> /g)	Pore size (nm)	Application	Reference
	HTC	Pyrolysis	Temp. (°C)	Time (h)			Temp. (°C)	Time (min)								
Apple tree branch	No	Yes	N/A <sup>6</sup>	0.5	K <sub>2</sub> CO <sub>3</sub>	4	800	240	1705	N/A	0.82	0.05	N/A	N/A	Removal of pharmaceuticals	Marques et al, 2018
Arundo donax	No	No	N/A	N/A	H <sub>3</sub> PO <sub>4</sub>	1.5	500	60	1151	N/A	1.00	0.44	0.56	1.7	Porous carbon material	Vernersson et al, 2002
Bamboo	Yes	No	200	24	NaOH	N/A	N/A	60	1.398	N/A	0.005	N/A	N/A	3.80	Methylene blue adsorption	Qian et al, 2018
Beer waste	Yes	No	N/A	N/A	H <sub>3</sub> PO <sub>4</sub>	4	600	60	1073	238	0.978	N/A	0.10	N/A	CO <sub>2</sub> adsorption	Hao et al, 2014
Brewers draff	No	Yes	650	N/A	KOH	N/A	N/A	60	11.6	N/A	8.74	N/A	N/A	N/A	Copper removal	Trakal et al, 2014
Brown algae	Yes	No	200	12	KOH	3	900	60	2421	1798	1.61	0.74	0.87	2.5	Supercapacitor	Fan et al, 2015
Camellia leaves	Yes	No	240	5	KOH	3	800	60	1823	1307	1.07	N/A	0.70	2.17	CO <sub>2</sub> adsorption	Yang et al, 2019
Camellia oleifera seed shell	Yes	No	230	12	KOH	4	650	120	1882	N/A	0.072	N/A	N/A	2.17	Removal of hexavalent chromium and methylene blue	Guo et al, 2018
Cherry stones	No	No	N/A	N/A	KOH	3	900	120	1624	N/A	2.88	0.28	0.69	N/A	Porous carbon material	Olivares-Marin et al, 2006a
Cherry stones	No	No	N/A	N/A	ZnCl <sub>2</sub>	3	500	120	1566	N/A	1.20	0.15	0.69	N/A	Porous carbon material	Olivares-Marin et al, 2006b
Coca Cola® waste	Yes	No	200	4	ZnCl <sub>2</sub>	3	600	120	1994	N/A	0.87	0.51	0.26	0.6	CO <sub>2</sub> adsorption, supercapacitors	Boyjoo et al, 2017
Coconut shell	Yes	No	200	2	NaOH	3	600	60	876	557	N/A	N/A	0.27	2.01	Methylene blue adsorption	Islam et al, 2017a
Coconut shell	No	Yes	350	2	KOH	3	700	240	1937	N/A	0.78	N/A	N/A	N/A	CO <sub>2</sub> capture	Chen et al, 2016

Coconut shell	No	Yes	500	2	NaOH	3	700	90	2825	N/A	1.50	0.36	1.14	2.27	Methylene blue adsorption	Cazetta et al, 2011
Cork waste	No	No	N/A	N/A	KOH	1	900	120	1415	N/A	0.59	N/A	N/A	0.69	Porous carbon material	Calvalho et al, 2003
Corn cob	No	Yes	400	0.5	ZnCl <sub>2</sub>	3	600	120	1270	701	0.67	N/A	0.28	2.10	Removal of mercury	Duan et al, 2019
Corn cob	Yes	No	200	5	N/A	N/A	650	120	143	N/A	0.18	N/A	0.00	5.12	Lithium-ion capacitor	Li et al, 2017
Corn cob	Yes	No	95	6	KOH	6	800	60	3611	1756	1.68	N/A	0.35	2.96	Porous carbon material	Ding et al, 2013b
Corn straw	Yes	No	200	5	N/A	N/A	650	120	367	N/A	0.22	N/A	0.12	2.37	Removal of pollutants	Liu et al, 2018
Cotton stalk	No	No	N/A	N/A	H <sub>3</sub> PO <sub>4</sub>	1.5	600	120	1400	N/A	0.79	0.17	0.62	N/A	Porous carbon material	Nahil and Williams, 2012
Cotton waste	No	No	N/A	N/A	FeCl <sub>3</sub>	1	400	60	504	353	0.30	N/A	0.17	2.38	Methylene blue adsorption	Tian et al, 2019
Durian shell	No	No	N/A	N/A	KOH	2	500	60	992	849	0.41	N/A	0.37	N/A	Porous carbon material	Chandra et al, 2009
Empty fruit bunch	Yes	No	250	0.3	KOH	5	600	30	2239	N/A	0.88	N/A	0.19	1.09	CO <sub>2</sub> capture	Parshetti et al, 2015
Eucalyptus sawdust	No	No	N/A	N/A	K <sub>2</sub> CO <sub>3</sub>	1	500	180	539	N/A	N/A	N/A	N/A	N/A	Methylene blue adsorption	Couto et al, 2012
Eucalyptus sawdust	Yes	No	230	2	KOH	4	800	60	2850	2720	1.35	N/A	1.23	0.35	CO <sub>2</sub> capture	Sevilla and Fuertes, 2011
Factory-rejected tea	Yes	No	200	5	NaOH	3	800	60	369	N/A	0.21	N/A	N/A	2.30	Methylene blue adsorption	Islam et al, 2015a
Fir wood	No	Yes	450	1.5	NaOH	4	N/A	N/A	2406	N/A	1.32	N/A	N/A	2.2	Dye adsorption	Wu and Tseng, 2008
Fox nut shell	No	No	N/A	N/A	H <sub>3</sub> PO <sub>4</sub>	1.5	700	60	2636	2042	1.53	0.21	1.32	2.32	Hexavalent chromium adsorption	Kumar and Jena, 2016
Furfural redisue	No	No	N/A	N/A	KOH	2	600	90	767	N/A	0.08	N/A	N/A	3.63	Porous carbon material	Lin et al, 2019
Furfural redisue	No	No	N/A	N/A	ZnCl <sub>2</sub>	3	600	90	1422	N/A	0.59	N/A	N/A	2.86	Porous carbon material	Lin et al, 2019

Glucose	Yes	No	190	48	NaOH	N/A	800	180	335	140	0.22	N/A	0.05	2.59	Removal of heavy metal	Tran et al, 2017
Glucose	Yes	Yes	180 800	7 1	KOH	2	800	60	1197	928	0.74	N/A	0.48	1.3- 8.0	Supercapacitor	Gao et al, 2015
Grape stalk	No	No	N/A	N/A	KOH	6	400	120	834	N/A	0.53	0.23	0.30	1.73	Adsorbent	Shahraki et al, 2018
Guava seed	No	Yes	500	2	NaOH	3	750	90	2573	N/A	1.26	0.18	1.07	1.96	Removal of pharmaceuticals	Pezoti et al, 2016
Hazelnut husk	Yes	No	250	7.5	KOH	4	600	120	1700	N/A	0.79	N/A	N/A	N/A	Lithium ion batteries	Unur et al, 2013
Hemp (Cannabis sativa L.) stem	Yes	Yes	160 600	12 2	KOH	5	800	210	3062	1600	1.72	0.60	0.83	2.25	CO <sub>2</sub> and CH <sub>4</sub> adsorption	Wang et al, 2015
Horse chestnut seed	No	No	N/A	N/A	K <sub>2</sub> CO <sub>3</sub>	1	700	120	952	797	N/A	N/A	N/A	0.3	Malachite green oxalate adsorption	Tzvetkov et al, 2016
Jackfruit peel	No	No	N/A	N/A	H <sub>3</sub> PO <sub>4</sub>	4	550	60	1260	N/A	0.73	0.26	0.47	N/A	Porous carbon material	Prahas et al, 2008
Lentinus edodes	Yes	No	650	N/A	Na <sub>2</sub> CO <sub>3</sub> & K <sub>2</sub> CO <sub>3</sub>	4	800	180	1144	854	N/A	N/A	0.46	2.26	Supercapacitor	Tang et al, 2018
Oil palm shell	No	No	N/A	N/A	ZnCl <sub>2</sub>	0.65	500	120	1671	N/A	0.99	N/A	0.87	2.36	Methane adsorption	Arami-Niya et al, 2010
Olive stone	No	No	N/A	N/A	H <sub>3</sub> PO <sub>4</sub>	4	500	120	1218	N/A	0.6	0.1	0.5	1.1	Porous carbon material	Yakout and El-Deen, 2016
Olive tree pruning	No	Yes	500	2	KOH	7.35	800	82.50	3490	N/A	1.66	0.04	1.09	N/A	Porous carbon material	Mamaní et al, 2019
Orange peel	No	No	N/A	N/A	ZnCl <sub>2</sub>	1	500	60	1215	327	0.68	0.55	0.13	2.2	Porous carbon material	Köseoğlu and Akmil-Başar, 2015
Orange peel	No	No	N/A	N/A	K <sub>2</sub> CO <sub>3</sub>	1	950	60	1352	505	0.79	0.57	0.22	2.3	Porous carbon material	Köseoğlu and Akmil-Başar, 2015
Packaging waste	No	Yes	500	1	KOH	4	700	60	1383	N/A	0.74	0.10	0.63	N/A	CO <sub>2</sub> capture	Idrees et al, 2018
Palm date seed	Yes	No	200	5	NaOH	3	600	60	1282	770	0.66	N/A	0.38	2.07	Methylene blue adsorption	Islam et al, 2015b
Pecan nut shell	Yes	No	190	48	KOH	5	800	45	2342	N/A	1.31	0.54	0.77	2.24	Methylene blue adsorption	Lima et al, 2019

Rattan (Lacosperma secundiflorum)	Yes	No	200	5	NaOH	3	600	60	1135	N/A	0.44	N/A	0.17	3.55	Methylene blue adsorption	Islam et al, 2017b
Rice husk	No	Yes	400	1.5	NaOH	3	800	60	2681	2376	1.40	0.39	1.01	0.8- 1.0	Supercapacitor	Le Van and Luong Thi, 2014
Rice husk	Yes	No	95	6	KOH	6	800	90	3322	N/A	2.53	N/A	N/A	3.05	Electrochemical supercapacitor	Ding et al, 2013a
Rice husk	Yes	No	95	6	NaOH	3	800	90	2455	N/A	1.82	N/A	N/A	3.52	Electrochemical supercapacitor	Ding et al, 2013a
Rice husk	Yes	No	95	6	H <sub>3</sub> PO <sub>4</sub>	6	500	60	1498	N/A	1.27	N/A	N/A	3.39	Electrochemical supercapacitor	Ding et al, 2013a
Rice husk	Yes	No	95	6	KOH	5	800	90	3362	N/A	1.41	N/A	N/A	N/A	Porous carbon material	Wang et al, 2014
Rice husk	Yes	No	95	6	H <sub>2</sub> SO <sub>4</sub>	4	500	60	2530	N/A	1.98	N/A	N/A	N/A	Porous carbon material	Wang et al, 2011a
Sargassum horneri	Yes	No	180	2	KOH	1	600	120	1221	N/A	0.58	N/A	0.38	2.16	CO <sub>2</sub> capture	Zeng et al, 2018
Sisal waste	No	No	N/A	N/A	K <sub>2</sub> CO <sub>3</sub>	0.5	700	60	1038	N/A	0.49	0.04	N/A	N/A	Removal of pharmaceuticals	Mestre et al, 2011
Tapioca flour	Yes	No	250	8	KOH	3	800	60	986	899	0.57	N/A	0.46	1.66	Porous carbon material	Pari et al, 2014
Tobacco stem	Yes	No	180	10	KOH	2	800	60	2940	1885	2.13	N/A	1.17	N/A	Acetone adsorption	Ma et al, 2018
Tomato stem	No	No	N/A	N/A	FeCl <sub>2</sub>	2.5	700	60	971	838	0.58	N/A	0.43	2.78	Adsorbent	Fu et al, 2017
Walnut shell	No	Yes	400	1	KOH	4	800	30	2263	2249	1.10	N/A	1.07	1.94	Adsorbent	Nowicki et al, 2010
Waste vinasse	Yes	No	180	12	KOH	1	800	60	1042	N/A	0.69	1.12	0.57	N/A	Dye adsorption	Kazak et al, 2018

<sup>1</sup>S<sub>BET</sub> = BET Surface area, <sup>2</sup>S<sub>mic</sub> = Micropore area, <sup>3</sup>V<sub>total</sub> = Total pore volume, <sup>4</sup>V<sub>meso</sub> = Mesopore volume, <sup>5</sup>V<sub>mic</sub> = Micropore volume; <sup>6</sup>N/A = Not available

### 3.1.1.3 Physicochemical activation

Physicochemical activation involves both physical and chemical activation processes. The mixture of precursor and chemical activating agent is subjected to heat treatment under air, steam, CO<sub>2</sub> or by switching a physical activating agent to an inert atmosphere, such as nitrogen gas (Rashidi and Yusup, 2017). The problem of blockage of pores due to the chemical activating agent in the chemical activation can be solved with heat treatment under the steam or CO<sub>2</sub> atmosphere in the physicochemical activation (Chowdhury et al, 2013).

Benadjemia et al. (2011) carried out activation of artichoke leaves impregnated with H<sub>3</sub>PO<sub>4</sub> under air atmosphere for one hour. The obtained activated carbon had 2038 m<sup>2</sup>/g of BET surface area, 1258 m<sup>2</sup>/g of micropore area, 2.46 cm<sup>3</sup>/g of total pore volume and 0.61 m<sup>3</sup>/g of micropore volume. Salman (2014) performed activation of the palm oil fronds impregnated with KOH under CO<sub>2</sub> atmosphere. The obtained activated carbon had 1237 m<sup>2</sup>/g of BET surface area, 0.67 cm<sup>3</sup>/g of total pore volume and 2.16 nm of pore size. Arami-Niya et al. (2012) studied physicochemical activation of the oil palm shell. Oil palm shell was impregnated with H<sub>3</sub>PO<sub>4</sub> and the mixture subjected to chemical activation at 450°C for 2 h under nitrogen gas. Activated carbon, which was obtained by chemical activation, was subjected to physical activation under CO<sub>2</sub> atmosphere at 885°C for 135 min. The activated carbon obtained by physicochemical activation had 642 m<sup>2</sup>/g of BET surface area, 0.28 cm<sup>3</sup>/g of total pore volume, 0.26 cm<sup>3</sup>/g of micropore volume and 1.76 nm of pore size. However, the activated carbon obtained by only chemical activation had 615 m<sup>2</sup>/g of BET surface area, 0.28 cm<sup>3</sup>/g of total pore volume, 0.26 cm<sup>3</sup>/g of micropore volume and 1.83 nm of pore size. The surface area increased with additional physical activation, while it had no significant effects on pore diameter and pore volumes. Arami-Niya et al. (2011) investigated physicochemical activation of palm shell. Palm shell was impregnated with ZnCl<sub>2</sub> and H<sub>3</sub>PO<sub>4</sub> and mixtures subjected to chemical activation at 500°C and 450°C for 2 h under nitrogen gas, respectively. Activated carbons obtained by chemical activation with ZnCl<sub>2</sub> and H<sub>3</sub>PO<sub>4</sub> subjected to physical activation under CO<sub>2</sub> atmosphere at 850°C for 7 h and 5 h, respectively. The activated carbon obtained by activation in the presence of ZnCl<sub>2</sub> had a BET surface area of 1118 m<sup>2</sup>/g, a total pore volume of 0.51 cm<sup>3</sup>/g, 0.42 cm<sup>3</sup>/g of micropore volume and 2.24 nm of pore size. The

activated carbon obtained by activation in the presence of  $\text{H}_3\text{PO}_4$  had 1653  $\text{m}^2/\text{g}$  of BET surface area, 0.94  $\text{cm}^3/\text{g}$  of total pore volume, 0.89  $\text{cm}^3/\text{g}$  of micropore volume and 2.27 nm of pore size. The surface area and porosity enhanced with increased physical activation period in the presence of both chemical activating agents.

### **3.1.2 History and applications of activated carbon**

Carbonized wood or wood char, which can be considered as activated carbon, has been used for thousands of years.

The first application dated back to 3750 BC, the Egyptian and Sumerians used removal of copper, zinc and tin ores in bronze production and also used wood char as a smoke-free fuel. On 2650 BC, the Egyptians used bone char to wall paint to Perneb's grave. The first evidence of the medical usage of char was found on a papyrus document remaining from 1550 BC in Thebes, Greece. Then, around 400 BC, Hippocrates recommended that the water was filtered with wood char before it could be used to eliminate bad taste and odor and prevent various diseases. It is also known in the Phoenician ships that it is stored in carbonized barrels for the refinement of drinking water, from 450 BC. However, the application of the first known activated carbon as a gas phase adsorbent was carried out by Dr. D.M. Kehl with charcoal to reduce odours from the gangrene (Gupta, 2007; Menéndez-Díaz and Martín-Gullón, 2006; González-García, 2018).

Industrial activated carbon applications began in 1794 for colour removal in the sugar production industry. In 1811, bone char was found to be more effective than wood char, and studies on its recovery began. The first patent on the thermal recovery of activated carbon was taken in 1817. In 1841, a process for the production and recovery of bone char was developed in Germany (McDougall, 1991).

The gold adsorption ability of the activated carbon from chloride solutions was firstly reported in 1847 (McDougall, 1991). In 1880, Davis (1880) patented a process, that the wood char was used for the gold recovery from chloride solutions.

The first large-scale gas phase application took place in the middle of the 19th century. Wood char used filters were used in sewage ventilation systems of London to eliminate odors in 1854, while carbon filter gas masks were used in the chemical industry to prevent inhalation of mercury vapours in 1872.

The present form of the activated carbon was discovered by R. von Ostrejko at the end of the 1800s and he patented two different methods of producing activated carbon in 1901. Those methods are the skeletons of the current chemical and physical activation methods. At the same time, R. von Ostrejko also received patents for special equipment for the production of activated carbon. In 1910, Wijnberg and Sauer took patent rights and applied activated carbons to the sugar industry (Norit White Sugar Company). Later, during the First World War, the company started to produce its own activated carbon from the peat under the name of NV Nederlandse NORIT Maatschappij (Menéndez-Díaz and Martín-Gullón, 2006). On the other hand, the first commercial chemical activation was carried out using wood sawdust as precursor and  $ZnCl_2$  as the activating agent, in Aussig, the Czech Republic in 1914 (Menéndez-Díaz and Martín-Gullón, 2006).

The First World War encouraged the development of both production and application of activated carbon. The use of toxic gases against the French, British and Russians on different fronts by the German army posed a severe problem for the allies, and as a result, there was an urgent need to develop a gas mask. Professor Nikolai Zelinski suggested the use of activated carbons as filter attached to a gas mask (Menéndez-Díaz and Martín-Gullón, 2006; McDougall, 1991). Undoubtedly, the First World War was the starting point for the development of activated carbon, not only in the sugar industry, but also as an adsorbent for water treatment and removal of vapors in the gas phase.

As a matter of fact, lately, researches on the production and application of activated carbon have increased due to the recovery of valuable chemicals and stricter environmental regulations on both the water resources and the flue gas.

Ding et al. (2013a), Tang et al. (2018), Gao et al. (2015), Fan et al. (2015), Le Van and Luong Thi (2014) and Boyjoo et al. (2017) investigated the use of activated carbon, which were derived from rice husk hydrochar, lentinus edodes hydrochar, glucose hydrochar, brown algae, rice husk and Coca Cola waste, in supercapacitors, respectively. Their BET surface areas were  $3322 \text{ m}^2/\text{g}$ ,  $1144 \text{ m}^2/\text{g}$ ,  $1197 \text{ m}^2/\text{g}$ ,  $2421 \text{ m}^2/\text{g}$ ,  $2681 \text{ m}^2/\text{g}$  and  $1994 \text{ m}^2/\text{g}$ , while their specific capacitances were  $157.2 \text{ F/g}$ ,  $280 \text{ F/g}$ ,  $237 \text{ F/g}$ ,  $314 \text{ F/g}$ ,  $198.4 \text{ F/g}$  and  $352.7 \text{ F/g}$  at  $1 \text{ A/g}$ , respectively. The specific capacitance and efficiency of supercapacitors increased with enhanced porosity and



surface functional groups by activation and the supercapacitors had long-term cycle life and high electrochemical stability.

Unur et al. (2013) studied the synthesis of hydrochar from hazelnut shells and their activation with KOH in order to use as an anode electrode of the lithium-ion battery. Due to the structural changes, hydrothermally carbonized and activated hydrochar showed better electrochemical performance, cycle stability, storage capacity, rate capacity.

Parshetti et al. (2015), Zeng et al. (2018), Yang et al. (2019), Chen et al. (2016), Idrees et al. (2018) and Sevilla and Fuertes (2011) examined CO<sub>2</sub> capture and adsorption characteristics of activated carbons obtained in the presence of KOH as the activating agent from palm empty fruit bunch hydrochar, sargassum horneri, camellia leaves hydrochar, coconut shell, packaging waste and eucalyptus sawdust hydrochar, respectively. Their BET surface areas were 2511 m<sup>2</sup>/g, 1221 m<sup>2</sup>/g, 1823.77 m<sup>2</sup>/g, 1535 m<sup>2</sup>/g, 1383 m<sup>2</sup>/g, 2850 m<sup>2</sup>/g, while CO<sub>2</sub> adsorption capacities were 3.71 mmol/g, 101.7 mmol/g, 8.30 mmol/g, 4.8 mmol/g, 3.93 mmol/g and 3 mmol/g at room temperature and low pressure, respectively. After activation they had higher CO<sub>2</sub> uptakes together with higher surface areas and microporosities. With the presence of narrow micropores, there was a significant improvement of CO<sub>2</sub> adsorption. Porous activated carbons had high CO<sub>2</sub> adsorption capacity, good cycle stability, fast CO<sub>2</sub> uptake rate and also distinguished CO<sub>2</sub> from other gases because of their CO<sub>2</sub> selectivity. Besides, activated carbons could be reused by recovery processes.

Wang et al. (2015) and Arami – Niya et al. (2010) investigated methane (CH<sub>4</sub>) adsorption properties of activated carbon derived from hemp stem hydrochar and oil palm shell by chemical activation with KOH and ZnCl<sub>2</sub>, respectively. Activated hydrochar of hemp stem had 1397 m<sup>2</sup>/g of BET surface area, 0.54 cm<sup>3</sup>/g of micropore volume and 51 cm<sup>3</sup>/g of CH<sub>4</sub> uptake, while oil palm shell activated carbon had 1671.6 m<sup>2</sup>/g of BET surface area, 0.87 cm<sup>3</sup>/g of micropore volume and 12 cm<sup>3</sup>/g of CH<sub>4</sub> uptake. Porous activated carbons had high adsorption capacities of CH<sub>4</sub> at room temperature and low pressures.

Mestre et al. (2011), Pezoti et al. (2016) and Marques et al. (2018) examined activated carbons of sisal waste, guava seed and apple tree branches for removal of paracetamol and ibuprofen, amoxicillin and atenolol from liquid phases, respectively. Sisal waste

activated carbon had 1038 m<sup>2</sup>/g of BET surface area and 139.8 mg/g and 124.5 mg/g of pharmaceuticals adsorption capacity for ibuprofen and paracetamol, respectively. Guava seed activated carbon had 2573.6 m<sup>2</sup>/g of BET surface area and 570 mg/g of pharmaceuticals adsorption capacity for amoxicillin. Apple tree branches had 2371 m<sup>2</sup>/g of BET surface area and 555.5 mg/g of pharmaceuticals adsorption capacity for atenolol. With the increased in microporosity by activation, adsorption capacity of pharmaceuticals were enhanced.

Cazetta et al. (2011) investigated the use of activated carbon derived from coconut shell for methylene blue removal. Coconut shell activated carbon had 2825 m<sup>2</sup>/g of BET surface area and 916.26 mg/g of methylene blue adsorption capacity. Islam et al. (2015a) studied the use of factory-rejected tea activated hydrochar for methylene blue removal. Factory-rejected tea activated hydrochar had 368.92 m<sup>2</sup>/g of BET surface area and 487.4 mg/g of methylene blue adsorption capacity. Islam et al. (2017b) examined the use of activated carbon obtained from *rattan* hydrochar for methylene blue removal. Activated hydrochar of *rattan* had 1135 m<sup>2</sup>/g of BET surface area and 359 mg/g of methylene blue adsorption capacity. Islam et al. (2017a) researched the use of coconut shell activated hydrochar for methylene blue removal. It had 876.14 m<sup>2</sup>/g of BET surface area and 200 mg/g of methylene blue adsorption capacity. Islam et al. (2015b) studied the use of palm date seed activated carbon for methylene blue removal. Palm date seed activated carbon had 1282.49 m<sup>2</sup>/g BET surface area and 612.1 mg/g of methylene blue adsorption capacity. Tian et al. (2019) investigated the use of activated carbon obtained from cotton waste for methylene blue and eriochrome black removal. Cotton waste activated carbon had 1342 m<sup>2</sup>/g of BET surface area and 342.87 mg/g and 369.48 mg/g for methylene blue and eriochrome black adsorption capacity. Kazak et al. (2018) examined the use of waste vinasse activated hydrochar for Victoria Blue B removal. It had 1042 m<sup>2</sup>/g of BET surface area and 713.254 mg/g of Victoria Blue B adsorption capacity. Tzvetkov et al. (2016) the use of activated carbon derived from horse chestnut shell for malachite green oxalate removal. Horse chestnut shell activated carbon had 1040 m<sup>2</sup>/g of BET surface area and 250 mg/g malachite green oxalate adsorption capacity. Active carbons were highly effective in dye removal because of their various functional groups, high surface area and porosity. Trakal et al. (2014), Guo et al. (2018) and Kumar and Jena (2017) investigated the use of activated carbon derived from brewers draff, camellia oleifera seed shell, fox nut

shell for removals of copper and hexavalent chromium, respectively. Brewers druff activated carbon had 11.6 m<sup>2</sup>/g of BET surface area and 10.3 mg/g of copper adsorption capacity. Camellia oleifera seed shell activated carbon had 1882.41 m<sup>2</sup>/g of BET surface area and 165.1 mg/g of hexavalent chromium adsorption capacity. Fox nut shell activated carbon had 2636 m<sup>2</sup>/g of BET surface area and 74.95 mg/g of hexavalent chromium adsorption capacity. Activated carbons could interact with metal ions easily due to their functional groups and superior surface properties; thus the adsorption and removal of metal ions increased.





## **4. MATERIALS AND METHODS**

### **4.1 Lignocellulosic biomass**

Wood dust, walnut shell, tea stalk, olive pomace, apricot seed and hazelnut husk biomass samples were taken from the local markets and industries located in Marmara region. Before the hydrothermal carbonization experiments, biomass samples were crushed, grounded and sieved to have a particle size of less than 250  $\mu\text{m}$  (60 mesh).

### **4.2 Equipments**

The following equipment was used in this study:

- Autoclave: The autoclave is resistant to high temperature and pressure, the inner surface is ceramic and the outer surface is stainless steel vessel.
- Oven: Mikrotest
- Tubular furnace: Protherm
- Vibrating sieve: 60 mesh sieve, RETSCH AS 200

### **4.3 Methods**

#### **4.3.1 Hydrothermal carbonization**

For each biomass source (wood dust, walnut shell, tea stalk, olive pomace, apricot seed and hazelnut husk) 6 g biomass and 24 mL deionized water were mixed in autoclave. The biomass/deionized water ratio was chosen as 1 g: 4 mL to ensure safe operation. The autoclave was kept in oven for 90 min at 220°C. By the end of the carbonization period, the autoclave was immediately cooled and the mixture was filtered. The hydrochar samples were dried in oven at 105°C for 24 h. Hydrothermal carbonization of each biomass source was repeated 5 times to ensure the consistency of hydrochar yield. The amount of hydrochar yield was calculated by mass loss between biomass and hydrochar. Hydrochar yield was calculated with Equation 4.1:

$$\text{Hydrochar yield, \%} = \frac{M_{\text{Hydrochar, g}}}{M_{\text{Raw biomass, g}}} \times 100 \quad (4.1)$$

### 4.3.2 Chemical activation and carbonization

All hydrochars were activated by using the same method and activating agent (KOH). Dry hydrochar samples were mixed with KOH at a KOH/hydrochar ratio of 2 (w/w). The hydrochar-KOH mixture was placed in a ceramic boat and then placed in a horizontal tubular furnace. The mixture was heated at a heating rate of  $10^{\circ}\text{C}\cdot\text{min}^{-1}$  up to  $600^{\circ}\text{C}$ , and kept at the same temperature for 1 h. During the heating, activation and cooling steps, horizontal tubular furnace was continuously flushed with nitrogen gas. After activation, samples were washed with 0.1 M HCl and deionized water until there were no potassium ions in the filtrate. Activation of each hydrochar sample was repeated 5 times to ensure the consistency of activated hydrochar yield.

The amount of activated hydrochar yield was calculated by mass loss between hydrochar and activated hydrochar. Activated hydrochar yield was calculated with Equation 4.2:

$$\text{Activated hydrochar yield, \%} = \frac{M_{\text{Activated hydrochar, g}}}{M_{\text{Hydrochar, g}}} \quad (4.2)$$

### 4.3.3 Characterizations

#### 4.3.3.1 Elemental analysis

Elemental analyses of the biomasses and hydrochars were performed on a LECO CHNS 628 elemental analyzer. The percentages of carbon (C), nitrogen (N) and hydrogen (H) contents of the biomasses and hydrochars were determined. Elemental fractions were determined by combustion at high temperature ( $1000 - 1100^{\circ}\text{C}$ ). 1.5 g of sample was burned by oxygen. In elemental analysis, the percentage amounts of carbon (C), hydrogen (H), and nitrogen (N) in the sample were taken from the device via carbon dioxide ( $\text{CO}_2$ ), hydrogen ( $\text{H}_2$ ), dihydrogen oxide ( $\text{H}_2\text{O}$ ), nitrogen ( $\text{N}_2$ ) gases resulting from the combustion of carbon. In the system, carbon and hydrogen were determined by infrared absorption and nitrogen was determined by the thermal conductivity detector.

#### **4.3.3.2 Proximate analysis**

For all biomass and hydrochar samples, moisture content was determined by using a thermogravimetric analyzer (Seiko, TG/DTA 6300) based on American Society for Testing and Materials (ASTM) E871-82 method (ASTM, 2013a); the volatile matter was determined based on ASTM E872-82 method (ASTM, 2013b); ash content was determined based on ASTM E1755-01 method (ASTM, 2015b). The fixed carbon content was calculated from the difference.

#### **4.3.3.3 Determination of extractives in biomass**

Extractives in biomasses were determined according to American Society for Testing and Materials (ASTM) E1690 – 08. Ethanol was used as a solvent. 7 g moisture-free biomass was weighed and placed in a thimble. Thimble was placed in 100 mL Soxhlet apparatus. Several boiling chips were placed in 250 mL flask. Soxhlet and flask were connected. 160 mL of 190 proof ethanol was added to Soxhlet. Soxhlet and condenser were connected. The system was heated at reflux for 6 h. After 6 h, the thimble was washed with 50 mL of ethanol and filtrated. Then, thimble and sample were dried at room temperature. The dried sample was weighed. This process was applied to each biomass. Extraction of biomass was calculated by mass loss between moisture-free biomass and extractive-free biomass (ASTM, 2016).

#### **4.3.3.4 Determination of klason lignin in biomass**

Klason lignin in biomass was determined according to Technical Association of the Pulp and Paper Industry (TAPPI) Test Method T 222 om-02 – Acid-Insoluble Lignin in Wood and Pulp. 1 g extractives-free biomass was weighed and placed in a flask. 15 mL sulphuric acid ( $\text{H}_2\text{SO}_4$ ) (72%) solution was added to the flask. The flask was held in a water bath for 2 h at 20°C. After 2 h, 560 mL distilled water and magnetic stirring bar added to the flask. Flask and condenser were connected. Flask was boiled for 4 h at 100°C and 600 rpm on a magnetic stirrer. After 4 h, the sample was washed until sulphate ( $\text{SO}_4^-$ ) ion removal and filtrated. Then, the sample was dried at room temperature. The dried sample was weighed. This process was applied to each biomass. Klason lignin of biomass was calculated by mass loss between extractives-free biomass and klason lignin-free biomass (TAPPI, 2006).

#### **4.3.3.5 Heating value**

The gross calorific value of samples were determined using an adiabatic mode bomb calorimeter (IKA C 5003) as described in ASTM D5865 (ASTM, 2013c).

#### **4.3.3.6 Fourier transform infrared spectroscopy (FT-IR)**

Fourier Transform Infrared Spectroscopy (FT-IR) basically measures the vibration frequency of bonds in molecules. Since the vibration frequency is directly proportional to the number of waves, the scaling is done based on the number of waves. Organic functional groups in raw biomass samples and their hydrochars and activated hydrochars were characterized by using FT-IR Fourier transform infrared spectroscopy (Perkin Elmer, Spectrum 100) in the region of 650-4000  $\text{cm}^{-1}$ .

#### **4.3.3.7 Thermogravimetric and derivative thermogravimetric analyses (TGA/DTG)**

In a thermogravimetric analysis, mass loss is recorded while the sample is heated to the desired temperatures, starting from ambient conditions under the presence of the desired atmosphere (inert, air, oxygen). The graph drawn by the mass against the temperature is called the thermogravimetric curve and is used to interpret thermal degradation properties. Thermogravimetric and Derivative Thermogravimetric Analyses (TGA/DTG) of biomasses and hydrochars were performed on Seiko, TG/DTG 6300 Thermogravimetric and Derivative Thermogravimetric Analyser. Pyrolysis (under  $\text{N}_2$  atmosphere) and combustion (in the presence of air) characteristics of biomass samples and hydrochars were investigated. The samples used in TG/DTG analyzer were less than 3 mg to prevent the heat and mass transfer limitations.

For pyrolysis behaviour and the volatile matter content, the sample was heated to 105°C at a heating rate of 10°C/min, kept at temperature for 10 min. Then the sample was heated at a heating rate of 40°C/min up to 750°C, and the sample was kept at that temperature for 7 min.

For combustion behaviour and ash content, the sample was heated to 600°C at a heating rate of 40°C/min, and the sample was kept at that temperature for 7 min.



#### **4.3.3.8 Scanning electron microscopy (SEM)**

Scanning electron microscopy (SEM) is used to investigate the morphology and topology of the macro, meso, micro, nano-sized sample surfaces. SEM works with the principle of scanning the surface with a high-energy electron beam focusing on a very small area. Image formation in SEM is based on the principle of collecting and examining the signals generated by the atomic interactions of the electron beam with the surface. Surface morphologies of raw biomasses, hydrochars and activated hydrochars were investigated on FEI Inc., Inspect S50 SEM. The gold sputter coating was applied to samples for 6 min before characterization. Samples were scanned under 20 kV in the high vacuum mode using secondary electrons with different magnifications.

#### **4.3.3.9 Brunauer-Emmett-Teller (BET) surface area analysis**

Brunauer-Emmett-Teller (BET), surface area measurements by physical adsorption method on solid or powder samples can detect macro, meso and micro pores sizes and pore size distribution at low pressures and high resolution. Prior to the analysis, the samples were placed in a degassing unit that was vacuum-heated for purification; then the samples were analyzed with nitrogen gas which was used as the adsorbate. As a result of this analysis, an "adsorption isotherm" was obtained which indicates how much nitrogen the substance holds at which pressure. Once the adsorption isotherm appeared, the BET surface area (single and multi point), micropores size distribution (0.5 nm – 2 nm), mesopore size distribution (2 nm – 50 nm), total pore volume and average pore size of the solids can be calculated. The surface area and pore structure characteristic of activated hydrochars were determined by Quantachrome-Autosorb iQ BET analyzer at 77 K. Before BET surface analysis, samples were degassed at 180°C for 10 h. The BET surface area and total pore volume were determined at relative pressure ( $P/P_0$ ) values ranging from 0.79 to 21.95 and relative pressure of 0.99 with the Brunauer-Emmett-Teller (BET) method, respectively. Micropore volume and micropore area were determined by V-t method.



## 5. RESULT AND DISCUSSION

### 5.1 Fuel Characteristics of Lignocellulosic Biomass Samples and Their Hydrochars

As previously explained, biomass includes moisture in the structure with different proportions. Due to the reason that hydrothermal carbonization bases on solid conversion, it is very important to figure out solid content before HTC. Total solid biomasses were ranked between 98.74% (wood dust) and 78.32% (hazelnut husk). The wood dust was followed by apricot seed (96.13%), olive pomace (95.92%), tea stalk (94.97%) and walnut shell (89.33%).

As stated in literature part, lignin is the key structure in solid conversion yield. Table 5.1 shows the extractives and lignin contents of biomass samples. The ethanol – soluble extractives contents of raw biomasses were between 0% and 4%. Walnut shell had the highest klason lignin content with 69.94%, while wood dust had the least klason lignin content with 28.46%. Walnut shell was followed by tea stalk (61.32%), hazelnut husk (58.96), olive pomace (48.99%) and apricot seed (40.18%).

**Table 5.1 :** Extractives and klason lignin contents of raw biomasses.

Raw biomass	Extractives (%) <sup>1</sup>	Klason lignin (%)
Wood dust	1.86	28.46
Walnut shell	0	69.94
Tea stalk	0	61.32
Olive pomace	1.71	48.99
Apricot seed	4	40.18
Hazelnut husk	0	58.96

<sup>1</sup>Ethanol – soluble extractives

Table 5.2 shows proximate and ultimate analyses, biomass contents and heating values of lignocellulosic biomass samples and their corresponding hydrochars. Elemental analysis indicated that carbon content of all hydrochars was increased but there was a clear difference between the percentage increase values. Since the hydrothermal carbonization conditions were same, this increase was due to the structure of biomass samples. Olive pomace had the highest percentage increase in carbon content with

30%, while wood dust had the least percentage increase with 14%. The percentage increase in carbon content was ranked from highest to lowest as: Olive pomace (31%) > walnut shell (22%) > hazelnut husk (17%) > apricot seed (18%) > tea stalk (16%) > wood dust (14%). With the lowest Klason lignin content, it was not surprising to see the wood dust at the last end of the ranking. Due to hydrolysis and dehydration reactions in HTC, the hydrogen contents decreased. Wood dust had the most decrease in hydrogen content (21%), while hazelnut husk had the least decrease in hydrogen (3.38%). The percentage decrease in hydrogen content was ranked from highest to lowest as: Wood dust (21%) > olive pomace (9.8%) > tea stalk (7.95%) > walnut shell (5.56%) > apricot seed (3.93%) > hazelnut husk (3.38%). Nitrogen content varied with biomass and it was determined that it was ranged between 0.09% (wood dust) and 2.73% (tea stalk) in raw biomass samples. Nakason et al. (2017) investigated the hydrochar obtained from cassava rhizome and after hydrothermal carbonization, determined that the carbon content increased, while hydrogen and oxygen contents decreased, thereby, H/C and O/C ratios were also reduced.

Lignocellulosic biomass is composed of hemicellulose, cellulose, lignin, extractives and ash in different proportions (Kumar et al., 2018). Due to its heterogeneous structure, each component react differently under hydrothermal conditions. In terms of thermal stability, hemicellulose has the least and lignin has the highest thermal stability (Grønli et al., 2002; Libra et al., 2011). Under hydrothermal conditions, a rapid hemicellulose hydrolysis was observed, which was also verified by FTIR spectra. Cellulose degradation was not observed due to its thermal stability up to 230°C. Falco et al. (2011) also reported that cellulose degradation was observed at reaction temperatures above 230°C and the retention time of 240 min. In the case of lignin degradation, higher temperatures (>250 °C) are required, where the degree of degradation depends on the type of lignin (Yu et al., 2008; Funke and Ziegler, 2010). Due to hemicellulose hydrolysis during the hydrothermal carbonization, all hydrochar samples had less volatile content compared to their corresponding biomass. Wood dust had the highest volatile content (79.8%) with the most decrease in hydrogen (21%), while hazelnut husk had the least volatile matter content (54%) with the least decrease in hydrogen (3.38%), in biomasses. Due to hemicellulose hydrolysis all hydrochar samples had less volatile content compared to their corresponding biomass. By hydrothermal carbonization, volatile matter content decreased between 2.80% and

11.83%. Wood dust hydrochar had the highest volatile matter content with 72.5%, while hazelnut husk hydrochar had the least volatile matter content with 49.3%, in hydrochars.

As seen from the proximate analysis, all hydrochar samples, except hazelnut husk hydrochar, had higher fixed carbon content after HTC. Lignin, which is hardly changed under hydrothermal conditions, is the main reason of higher fixed carbon content (Kruse et al., 2013). Hazelnut husk had the highest fixed carbon content with 36.5%, while wood dust had the least the highest fixed carbon content with 10.5%. After hydrothermal carbonization, walnut shell hydrochar had the highest fixed carbon with 42.4%, while wood dust hydrochar had the least fixed carbon with 18.3%.

As a result of higher carbon content and lower volatile matter, heating value of all hydrochar samples were higher than their corresponding biomass. Apricot seed had the highest heating value with 4715 cal/g, while hazelnut husk had the least heating value with 4078 cal/g in the raw biomasses. Olive pomace hydrochar had the highest heating value with 6106 cal/g, while wood dust hydrochar had the least heating value with 4923 cal/g in the hydrochars. With hydrothermal carbonization, the carbon content of all biomasses increased and this changing in carbon content provided an increase in heating value. Since hydrothermal carbonization conditions were the same and increases in carbon contents and heating values for every biomass were different, it is possible to say that these increases were highly dependent on the structure of biomass. Olive pomace had the highest percentage increase in carbon content and heating value with 30%, while wood dust had the least percentage increase with 14%. Olive pomace was followed by the walnut shell (21%), hazelnut husk (20%), apricot seed (19%), tea stalk (17%), respectively. It should be noted that all of the hydrochars had the heating values as high as bituminous coal. Gao et al. (2016a) determined that after the hydrothermal carbonization process applied to the eucalyptus bark at different temperatures and retention times, the amount of carbon and the heating value increased in relation to each other. Chen et al. (2018) performed a similar study for sweet potato paste, and after the hydrothermal carbonization, while the amount of carbon increased, hydrogen and oxygen decreased and the heating value increased due to these elemental changes. These increases in the heating value and carbon content increased the solid fuel quality.

**Table 5.2 :** Proximate and ultimate analyses, biomass contents and heating values of lignocellulosic biomass samples and their corresponding hydrochars.

	Wood dust		Walnut shell		Tea stalk		Olive pomace		Apricot seed		Hazelnut husk	
	Raw	Hydrochar	Raw	Hydrochar	Raw	Hydrochar	Raw	Hydrochar	Raw	Hydrochar	Raw	Hydrochar
Proximate analyses												
Moisture (%)	2.3	2.5	5.2	2.1	5.6	2.1	2.1	1.5	1.6	1.8	4.4	3.1
Volatile matter (%)	79.8	72.5	57.1	55.5	60.8	55.5	73.1	65.3	78.6	69.3	54	49.3
Fixed carbon (%)	10.5	18.3	33.4	42.4	27.1	38.5	24.7	27.7	17.1	19.6	36.5	35.8
Ash (%)	7.4	6.7	4.3	0	6.5	8.4	0.1	5.5	2.7	9.3	5.1	11.8
Ultimate analyses												
C (%)	45.6	52	44.6	53.7	47.1	54.8	46.6	61.1	48.9	57.6	45.7	53.5
H (%)	6.1	4.8	5.6	5.3	5.8	5.4	5.9	6.4	5.9	5.7	5.3	5.1
N (%)	0.09	0.04	0.66	0.87	2.7	2.9	1.4	0.9	0.25	0.33	1.7	1.5
Biomass content												
Extractives (%)	1.9	nd. <sup>1</sup>	0	nd. <sup>1</sup>	0	nd. <sup>1</sup>	1.7	nd. <sup>1</sup>	4	nd. <sup>1</sup>	0	nd. <sup>1</sup>
Klason lignin (%)	28.5	nd. <sup>1</sup>	69.9	nd. <sup>1</sup>	61.3	nd. <sup>1</sup>	48.9	nd. <sup>1</sup>	40.2	nd. <sup>1</sup>	58.9	nd. <sup>1</sup>
Heating value (cal/g)												
	4314	4923	4188	5126	4598	5382	4695	6106	4715	5647	4078	5013

<sup>1</sup>nd: Not determined

Table 5.3 shows the mass yields of lignocellulosic hydrochars and their corresponding activated hydrochars. The mass yields of hydrochar varied with the type of biomass. The mass yields of hydrochar ranged between 55.7% (wood dust) and 71% (tea stalk). Hydrochar synthesis from agricultural wastes showed similar mass yields while wood based hydrochar production had lower yield. The hydrochar yield of biomass samples were ranked from lowest to highest as wood dust < walnut shell < apricot seed < olive pomace = hazelnut husk < tea stalk. After tea stalk, hydrochar yields were ranked from high to low as olive pomace (65.8%), hazelnut husk (65.8%), walnut shell (64.8%) and apricot seed (60.8%), respectively. As seen from Table 5.3, the mass yields of activated hydrochar were also depending on biomass type. The mass yields of activated hydrochar ranged between 24.4% (wood dust) and 41.5% (tea stalk). Activated hydrochar yield were ranked from lowest to highest as wood dust<hazelnut husk< apricot seed<walnut shell<olive pomace<tea stalk. After tea stalk, activated hydrochar yields were ranked from high to low as olive pomace (34.4%), walnut shell (34%), apricot seed (33.2%) and hazelnut husk (32%) respectively. The wood dust had the least hydrochar and activated hydrochar yields with 55.64% and 24.4%, respectively. Wood dust with at least carbon (45.58%), fixed carbon (10.5%), klason lignin (28.5%) and the highest volatile matter (79.8%) had the lowest hydrochar and activated hydrochar yields. Besides, the tea stalk, which had a greater amount of carbon (47.14%), fixed carbon (27.1%), klason lignin (61.32%) and a lower amount of volatile matter (60.8%), had the highest hydrochar and activated hydrochar yields. Hydrochar and activated hydrochar yields changed proportionally within themselves.

**Table 5.3 :** The mass yields of lignocellulosic hydrochars and their corresponding activated hydrochars.

Sample	Wood dust		Walnut shell		Tea stalk		Olive pomace		Apricot seed		Hazelnut husk	
	HC <sup>1</sup>	AHC <sup>2</sup>	HC <sup>1</sup>	AHC <sup>2</sup>	HC <sup>1</sup>	AHC <sup>2</sup>	HC <sup>1</sup>	AHC <sup>2</sup>	HC <sup>1</sup>	AHC <sup>2</sup>	HC <sup>1</sup>	AHC <sup>2</sup>
Yield (%)	55.7	24.4	64.8	34	71	41.5	65.8	34.4	60.8	33.2	65.8	32

<sup>1</sup>HC: Hydrochar, <sup>2</sup>AHC: Activated hydrochar

Excluding drying step, pyrolysis is a single stage reaction, which gives information about thermal degradation under inert atmosphere. This information also points out the volatile matter of the material. In all of the samples investigated, pyrolysis took place

in a single step, where the maximum mass loss rates were observed at different temperatures.

Pyrolysis behaviour of wood dust and wood dust hydrochar are shown in Figure 5.1. The pyrolysis of wood dust and its hydrochar had one stage, which devolatilization. The mass loss due to devolatilization was higher in wood dust (79.8%) than its hydrochar (72.5%). The shoulder which was seen in DTG curve of wood dust at around 300°C, was not seen in the DTG curve of wood dust hydrochar due to decomposition of hemicellulose during hydrothermal carbonization. Similar profile was also detected by Saffe et al. (2019), who investigated thermogravimetric analysis of sawdust. In that study the shoulder indicating hemicellulose was observable in raw material but it was not observed after thermal treatment. The maximum mass loss temperature of wood dust was shifted from 380°C to 386.67°C and the temperature range of the mass loss was shifted from 256.67°C – 406.67°C to 330°C – 420°C with hydrothermal carbonization. The reason for the shift to the higher value was that degradation of lignin-rich wood dust hydrochar required higher temperatures.

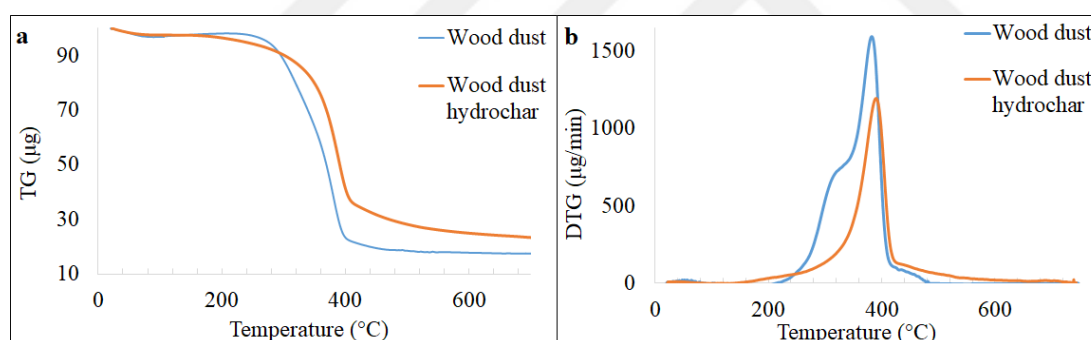


**Figure 5.1 :** The a) TG and b) DTG curves of pyrolysis of wood dust and wood dust hydrochar.

The TG and DTG curves of pyrolysis of walnut shell and walnut shell hydrochar are shown in Figure 5.2. The weight losses due to moisture removal of walnut shell and its hydrochar were 5.2% and 2.1%, respectively. The weight loss due to devolatilization was higher in the walnut shell with 57.1% than its hydrochar with 42.4%. The shoulder that refers to the hemicellulose degradation of walnut shell at around 250°C, was not seen in the DTG curve of walnut shell hydrochar. The temperature where the maximum mass loss was observed for walnut shell was shifted from 350°C to 370°C and the temperature range of the mass loss was shifted from 206.67°C – 403.33°C to 300°C – 416.67°C with hydrothermal carbonization.



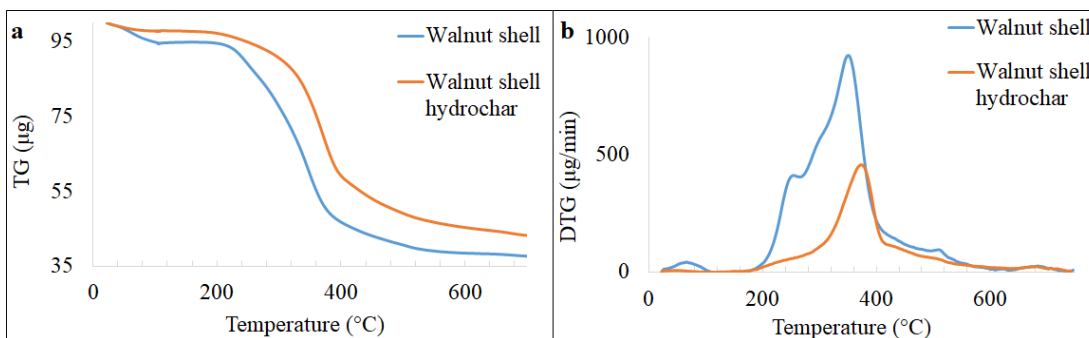


**Figure 5.2 :** The a) TG and b) DTG curves of pyrolysis of walnut shell and walnut shell hydrochar.

The TG and DTG curves of pyrolysis of tea stalk and tea stalk hydrochar are shown in Figure 5.3. The weight losses due to moisture removal of tea stalk and its hydrochar were 5.6% and 2.1%, respectively. The weight loss due to devolatilization was higher in tea stalk with 60.8% than its hydrochar with 55.5%. The shoulder that refers to the hemicellulose content of tea stalk at around 280°C, was not seen in the DTG curve of tea stalk hydrochar due to the deformation of hemicellulose with hydrothermal carbonization. The maximum mass loss temperature of tea stalk was shifted from 363.34°C to 372°C and the temperature range of the mass loss was shifted from 300°C – 400°C to 292.5°C – 458.1°C with hydrothermal carbonization. In addition, because of the degradation, the intensity of the DTG curve of hydrochar decreased. The reason for the shift to the higher value was that tea stalk hydrochar had lower volatile matter content compared to raw tea stalk and degradation of hemicellulose content of tea stalk by hydrothermal carbonization. Similar profile was also detected by Gao et al. (2016b), who investigated the thermal behaviours of various biomass sources. In that study, the shift to a higher temperature for all biomass sources was observed.

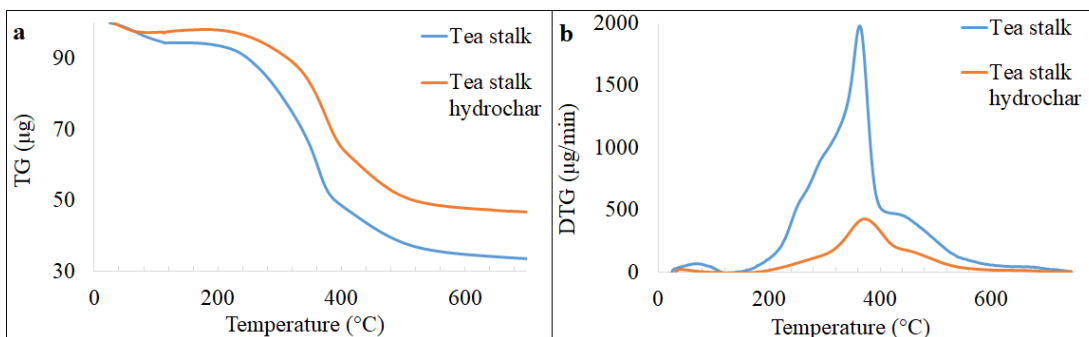


**Figure 5.3 :** The a) TG and b) DTG curves of pyrolysis of tea stalk and tea stalk hydrochar.

The TG and DTG curves of pyrolysis of olive pomace and olive pomace hydrochar are shown in Figure 5.4. The pyrolysis of olive pomace and its hydrochar had one stage, which devolatilization. The weight losses due to moisture removal of olive pomace and its hydrochar were 2.1% and 1.5%, respectively. The weight loss due to devolatilization was higher in olive pomace with 73.1% than its hydrochar with 65.3%. The shoulder that refers to the hemicellulose content of olive pomace at around 300°C, was not seen in the DTG curve of olive pomace hydrochar due to the deformation of hemicellulose with hydrothermal carbonization. Petrović et al. (2016) examined the hydrothermal carbonization of grape pomace as agricultural and lignocellulosic biomass and its pyrolysis behaviour. They determined that raw grape pomace had shoulder, while its hydrochar had no shoulder due to degradation of hemicellulose by HTC, in DTG curves. The maximum mass loss temperature of olive pomace was shifted from 346.67°C to 384°C and the temperature range of the mass loss was shifted from 236.67°C – 516.67°C to 318.6°C – 429.4°C with hydrothermal carbonization. The reason for the shift to the higher value was that olive pomace hydrochar had lower volatile matter content compared to raw olive pomace and degradation of hemicellulose content of olive pomace by hydrothermal carbonization.

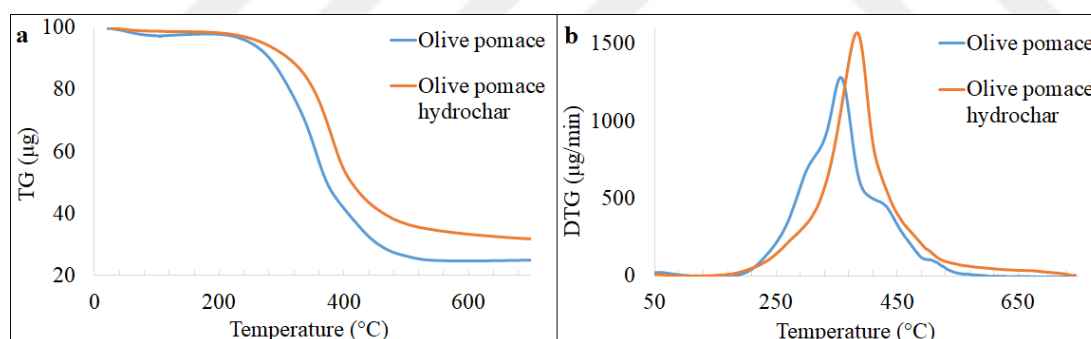


**Figure 5.4 :** The a) TG and b) DTG curves of pyrolysis of olive pomace and olive pomace hydrochar.

The TG and DTG curves of pyrolysis of apricot seed and apricot seed hydrochar are shown in Figure 5.5. As seen from Figure 5.5, hemicellulose and cellulose degradation occurred in a wider temperature range (200-300°C) for apricot seed samples. In the case of its hydrochar, the degradation was smoothly shifted to higher temperatures. The absence of shoulder in the DTG curve of hydrochar was due to the hemicellulose degradation at hydrothermal conditions. The weight loss due to devolatilization was higher in apricot seed (78.6%) than its hydrochar (69.3%). The maximum mass loss

temperature of apricot seed was shifted from 370°C to 373.33°C. The reason for the shift to the higher value was that apricot seed hydrochar had lower volatile matter content compared to raw apricot seed.

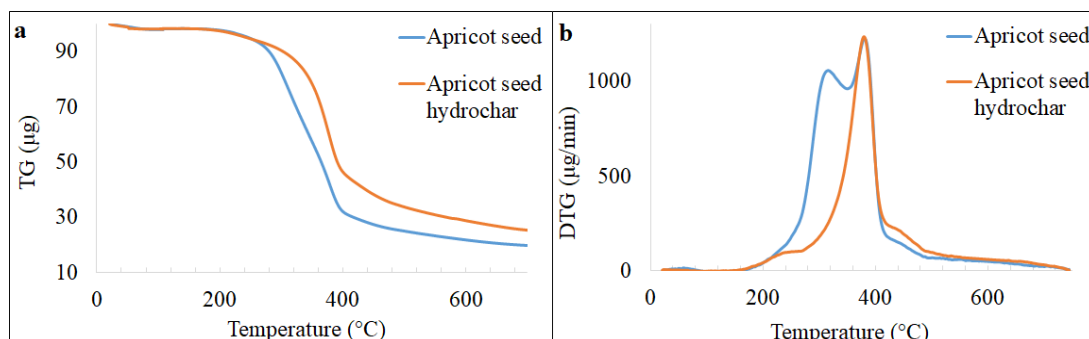


**Figure 5.5 :** The a) TG and b) DTG curves of pyrolysis of apricot seed and apricot seed hydrochar.

The TG and DTG curves of pyrolysis of hazelnut husk and hazelnut husk hydrochar are shown in Figure 5.6. The mass loss due to devolatilization was higher in hazelnut husk with 54% than its hydrochar with 49.3%. The maximum mass loss temperature of hazelnut husk was shifted from 326.67°C to 356.67°C and the temperature range of the mass loss was shifted from 206.67°C – 386.67°C to 276.67°C – 450°C with hydrothermal carbonization.

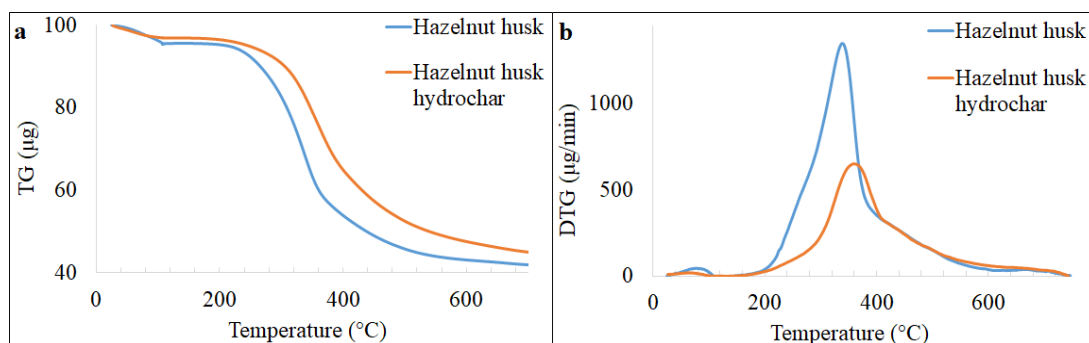


**Figure 5.6 :** The a) TG and b) DTG curves of pyrolysis of hazelnut husk and hazelnut husk hydrochar.

The combustion process mainly consists of three stages, which includes: stage 1 – drying (moisture removal), stage 2 – volatile release (devolatilization) and combustion of volatiles (a homogeneous reaction) and stage 3 – oxidation of char (a heterogeneous reaction). In terms of stages, both biomass samples and their hydrochars represented

same combustions steps, where only temperature intervals of the corresponding combustion stages changed.

Ignition temperature ( $T_i$ ), burnout temperature ( $T_b$ ) and the temperature at maximum weight loss rate ( $T_{max}$ ) are the important characteristics of solid fuel, which are determined by using TG-DTG curves.  $T_i$ , the temperature at which a solid fuel starts burning, is directly affected by the volatile matter and moisture content of biomass. Burnout temperature indicates the temperature where the combustion reaction is completed, and this temperature is mainly affected by the type of solid fuel. In this study,  $T_i$  and  $T_b$  temperatures were determined by using the intersection method (Li et al, 2009; Qin and Thunman, 2015).

The TG and DTG curves of combustion of wood dust and wood dust hydrochar are shown in Figure 5.7. The combustion of wood dust and its hydrochar had 3 stages, which include drying, devolatilization and combustion of volatiles and oxidation of char steps. The weight losses in the drying step were 3.7% for wood dust and 2.5% for its hydrochar. The weight loss due to devolatilization and combustion of volatiles was higher in wood dust with 64.4% than its hydrochar with 52.7%. This is expected due to higher volatile matter content of wood dust. Due to the higher fixed carbon content of hydrochar, it had higher weight loss with 38.1% than raw biomass with 24.5%. The ignition temperature of wood dust was shifted from 300°C to 315.75°C with hydrothermal carbonization. In addition, the shoulder that refers to the hemicellulose degradation of wood dust around 300°C, was not seen in the DTG curve of hydrochar. The reason for the shift to the higher value was that wood dust hydrochar had lower volatile matter content compared to raw wood dust and lower volatile matter content resulted with higher ignition temperature. Besides, wood dust and its hydrochar had the highest ignition temperatures although they had the highest volatile matter contents compared to other biomass samples and their hydrochars. That could be explained by the structural difference between woody biomass and agricultural biomass. Higher ignition temperature is useful in reducing the risk of self-ignition and allows using hydrochar as solid fuel. The burnout temperature of wood dust was shifted from 544.73°C to 571.05°C with hydrothermal carbonization. Wood dust and its hydrochar completed the oxidation reaction at lower burnout temperatures as compared to agricultural biomass samples. The temperatures of maximum mass loss rate of wood dust and its hydrochar, were 360.53°C and 350°C.

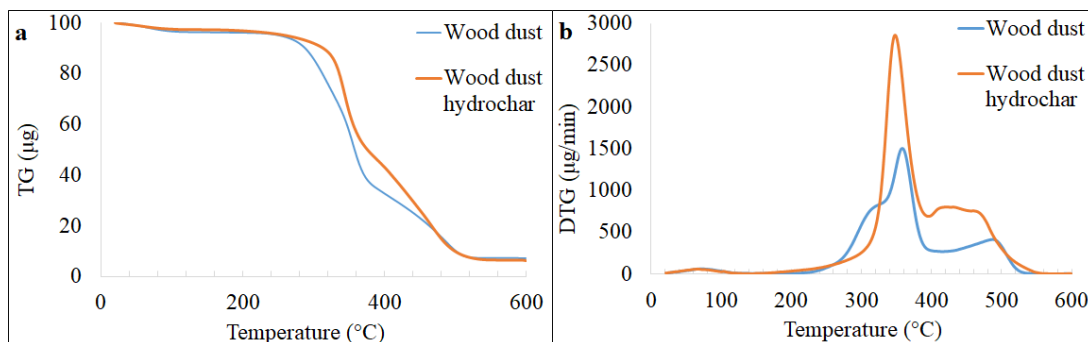


**Figure 5.7 :** The a) TG and b) DTG curves of combustion of wood dust and wood dust hydrochar.

The TG and DTG curves of combustion of walnut shell and walnut shell hydrochar are shown in Figure 5.8. The combustion of walnut shell and its hydrochar had 3 stages, which include drying, devolatilization and combustion of volatiles and oxidation of char steps. The weight losses in the drying step were 6.8% for walnut shell and 1.3% for its hydrochar. This is expected due to dehydration during HTC. The weight loss due to devolatilization and combustion of volatiles was higher in the walnut shell with 56.8% than its hydrochar with 55.5%. Due to the higher fixed carbon content of hydrochar, it had higher weight loss with 43.2% than raw biomass with 32.1%. The ignition temperature of the walnut shell was shifted from 257.89°C to 278.94°C with hydrothermal carbonization. Also, the shoulder that refers to the hemicellulose content of walnut shell around 240°C, was not seen in the DTG curve of walnut shell hydrochar due to the degradation of hemicellulose with hydrothermal carbonization. The reason for the shift to the higher value was that walnut shell hydrochar had lower volatile matter content compared to raw walnut shell and degradation of hemicellulose content of walnut shell by hydrothermal carbonization. The burnout temperature of the walnut shell was shifted from 573.68°C to 555.26°C with hydrothermal carbonization. After hydrothermal carbonization, the oxidation of char took place in a wide temperature range due to its high lignin content. Chen et al. (2015) showed the thermogravimetric analysis of various lignocellulosic biomass sources and stated that degradation of lignin occurs at a wide temperature range. The temperature, where the maximum mass loss rate was observed, were 315.79°C for walnut shell and 327.11°C for its hydrochar.

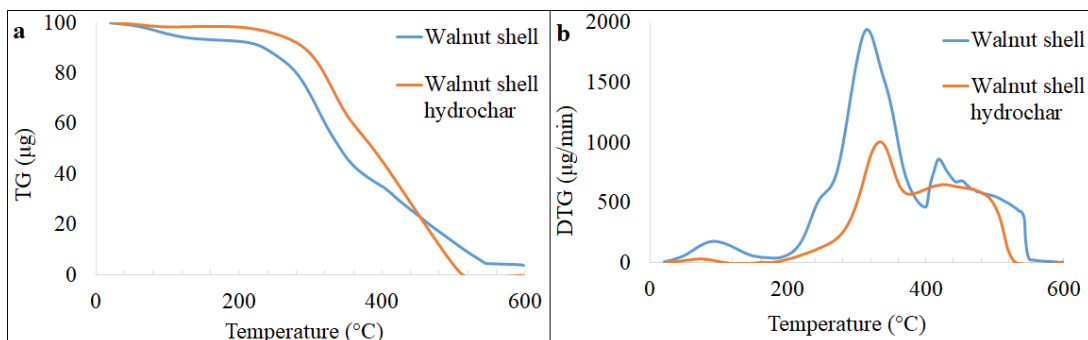


**Figure 5.8 :** The a) TG and b) DTG curves of combustion of walnut shell and walnut shell hydrochar.

The TG and DTG curves of combustion of tea stalk and tea stalk hydrochar are shown in Figure 5.9. Three-staged combustion is observed for both tea stalk and its hydrochar. The weight losses in the drying step were 3.7% for tea stalk and 2.6% for its hydrochar. The weight loss due to devolatilization and combustion of volatiles was higher in tea stalk with 66.7% than its hydrochar with 44.4%. Due to the higher fixed carbon content of hydrochar, it had higher weight loss with 44.6% than raw biomass with 23.1%. The ignition temperature of tea stalk was shifted from 263.16°C to 276.32°C with hydrothermal carbonization. The reason for the shift to the higher value was that tea stalk hydrochar had lower volatile matter content compared to raw tea stalk. It was also shown and concluded by the study of Gao et al. (2016b). The burnout temperature of tea stalk was shifted from 592.11°C to 542.11°C with hydrothermal carbonization. After hydrothermal carbonization, the intensity of the DTG curve decreased due to degradation. The temperature of maximum mass loss rate of tea stalk and its hydrochar, were 315.79°C and 313.16°C.

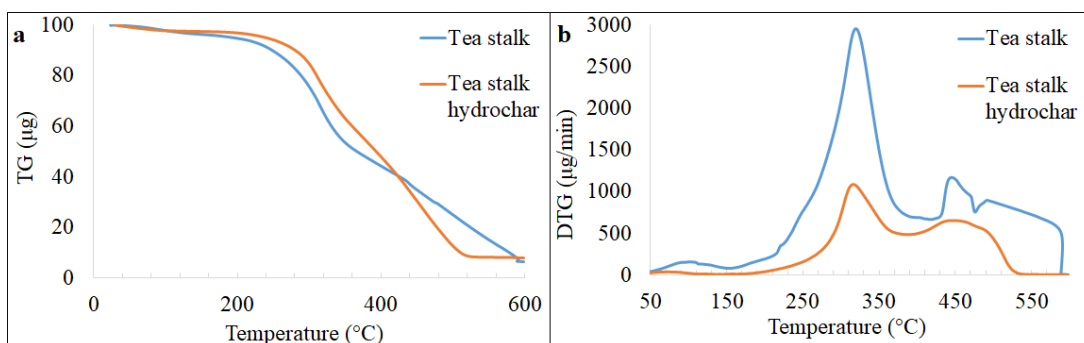


**Figure 5.9 :** The a) TG and b) DTG curves of combustion of tea stalk and tea stalk hydrochar.

The TG and DTG curves of combustion of olive pomace and olive pomace hydrochar are shown in Figure 5.10. Three-staged combustion is observed for both olive pomace and its hydrochar. The weight losses in the drying step were 4.1% for olive pomace and 1.2% for its hydrochar. This is expected due to dehydration during HTC. The weight loss due to devolatilization and combustion of volatiles was higher in olive pomace with 58.6% than its hydrochar with 46.1%. Due to the higher fixed carbon content of hydrochar, it had higher weight loss with 48.4% than raw biomass with 37.2%. The ignition temperature of olive pomace was shifted from 265.79°C to 289.47°C with hydrothermal carbonization. In addition, the shoulder that refers to the hemicellulose content of olive pomace around 300°C, was not seen in the DTG curve of olive pomace hydrochar due to the deformation of hemicellulose with hydrothermal carbonization. The reason for the shift to the higher value was that olive pomace hydrochar had lower volatile matter content compared to raw olive pomace and degradation of hemicellulose content of olive pomace by hydrothermal carbonization. The burnout temperature of olive pomace was shifted from 565.79°C to 586.84°C with hydrothermal carbonization. The temperatures, where the maximum mass loss rate was observed, were 331.58°C for olive pomace and 336.84°C for its hydrochar.

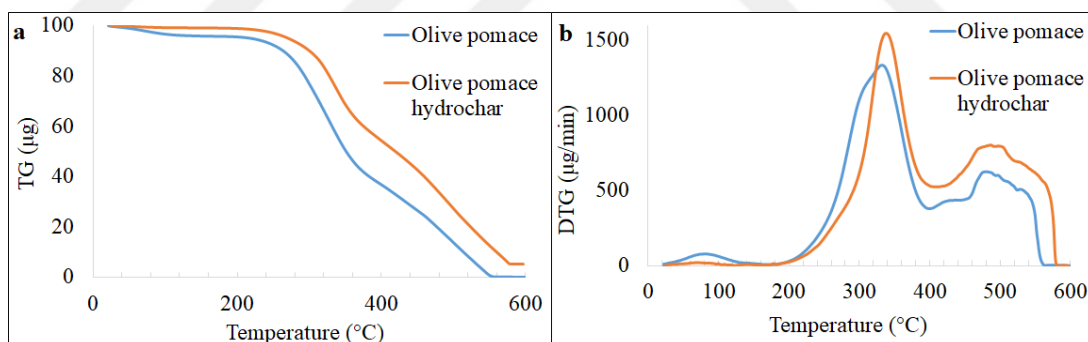


**Figure 5.10 :** The a) TG and b) DTG curves of combustion of olive pomace and olive pomace hydrochar.

The TG and DTG curves of combustion of apricot seed and apricot seed hydrochar are shown in Figure 5.11. Three-staged combustion is observed for both apricot seed and its hydrochar. The weight losses in the drying step were 1.8% for apricot seed and 1% for its hydrochar. The weight loss due to devolatilization and combustion of volatiles was higher in apricot seed with 63.1% than its hydrochar with 45.5%. Due to the higher fixed carbon content of hydrochar, it had higher weight loss with 44.2% than raw biomass with 32.4%. The ignition temperature of apricot seed was shifted from



271.05°C to 294.74°C after HTC. In addition, the shoulder that refers to the hemicellulose content of apricot seed around 300°C, was not seen in the DTG curve of apricot seed hydrochar due to the degradation of hemicellulose with hydrothermal carbonization. The burnout temperature of apricot seed was shifted from 536.84°C to 584.24°C with hydrothermal carbonization. After hydrothermal carbonization, the oxidation of char took place in a wide temperature range. Lignin is resistant to degradation due to light and heavy components in its complex branched structure and oxidation of lignin occurs a wide temperature range (Kok and Ozgur, 2017). The temperature, where the maximum mass loss rate was observed, were 331.58°C for apricot seed and 323.68°C for its hydrochar.

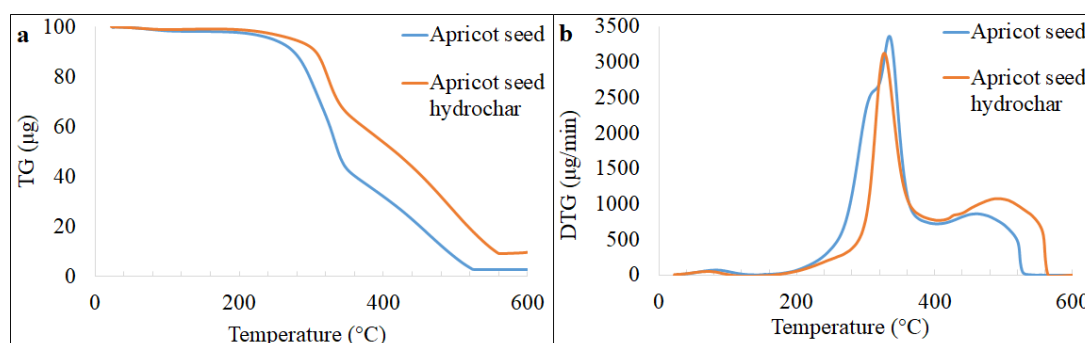


**Figure 5.11 :** The a) TG and b) DTG curves of combustion of apricot seed and apricot seed hydrochar.

The TG and DTG curves of combustion of hazelnut husk and hazelnut husk hydrochar are shown in Figure 5.12. Three-staged combustion is observed for both hazelnut husk and its hydrochar. The weight losses in the drying step were 5.8% for hazelnut husk and 3.5% for its hydrochar. The weight loss due to devolatilization and combustion of volatiles was higher in hazelnut husk with 48.9% than its hydrochar with 42.3%. The weight losses in the oxidation of char step were 42.4% for hydrochar and 40.2% for hazelnut husk. The ignition temperature of hazelnut husk was shifted from 260.53°C to 268.42°C with hydrothermal carbonization. The reason for the shift to the higher value was that hazelnut husk hydrochar had lower volatile matter content compared to raw hazelnut husk and degradation of hemicellulose content of hazelnut husk by hydrothermal carbonization. The burnout temperature of hazelnut husk was shifted from 560.53°C to 550°C with hydrothermal carbonization. The temperatures, with maximum mass losses of hazelnut husk and its hydrochar, were also 315.79°C and 305.26°C. Lignin content of hydrochar was conserved after hydrothermal



carbonization and the peak seen at 410.53°C in the DTG curve of hydrochar is due to the reactivity of lignin.

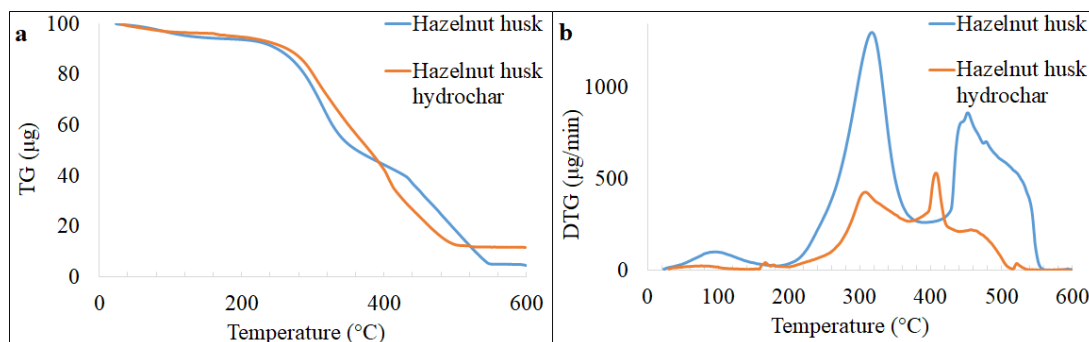


**Figure 5.12 :** The a) TG and b) DTG curves of combustion of hazelnut husk and hazelnut husk hydrochar.

As summary of the comparison of  $T_i$ ,  $T_b$  and  $T_{max}$  values are given in Table 5.4. As seen in Table 5.4, all hydrochar samples had higher ignition temperatures as compared to their original biomass samples. Since the hydrochar samples had lower volatile matter content compared to their original biomass, their ignition temperatures were shifted to higher values. Table 5.4 points out the clear difference between the ignition temperatures of woody biomass and agricultural wastes, and also their hydrochars. As both woody biomass and agricultural biomass samples were considered, wood dust and its hydrochar had the highest ignition temperatures although it had the highest volatile matter content. This could be explained by the structural difference of woody biomass and the ignition temperature of the volatile compounds released from the woody biomass. Among the agricultural biomass samples, walnut shell (which has the highest Klason lignin content) had the lowest ignition temperature; apricot seed (which has the lowest Klason lignin content) had the highest ignition temperature. Higher ignition temperatures are useful in reducing the risk of self-ignition, which is observed in biomass samples with high volatile matter content and low moisture content.

In the case of burnout temperatures, wood dust completed the oxidation reaction at lower temperatures as compared to agricultural biomass samples. Burnout temperature of the agricultural biomass ranged between 536-592°C. Unlike biomass samples, hydrochars of agricultural biowastes had variable burnout temperatures, showing no consistence with the structural units of biomass. Hydrothermal carbonization is also known to decrease the char reactivity due to alkali and alkaline earth metal removal under hydrothermal conditions (Stirling et al, 2018).

**Table 5.4 : Combustion characteristics.**

	Wood dust		Walnut shell		Tea stalk		Olive pomace		Apricot seed		Hazelnut husk	
	Raw	Hydrochar	Raw	Hydrochar	Raw	Hydrochar	Raw	Hydrochar	Raw	Hydrochar	Raw	Hydrochar
T <sub>i</sub> (°C)	300	315.8	257.9	278.9	263.2	276.3	265.8	289.5	271.1	294.7	260.5	268.4
T <sub>b</sub> (°C)	544.7	571.1	573.7	555.3	592.1	542.1	565.8	586.8	536.8	584.2	560.5	550
T <sub>max</sub> (°C)	360.5	350	315.8	327.1	315.8	313.2	331.6	336.8	331.6	323.7	315.8	305.3

## 5.2 Surface Characteristics of Hydrochars and Activated Hydrochars

Comparative FT-IR spectra of the biomass samples, hydrochars and activated hydrochars are shown in Figure 5.13.

In all biomass samples, the band at 3000-3600  $\text{cm}^{-1}$  indicated the O – H stretching vibration in the hydroxyl or carboxyl groups (Yin et al, 2016). Only the walnut shell, tea stalks, olive pomace and apricot seed hydrochars showed a decrease in the intensity of the band between 3000 – 3600  $\text{cm}^{-1}$  and showed an intense peak at 3665  $\text{cm}^{-1}$ , which indicated the – OH stretching of the inner-surface hydroxyl groups (Kloprogge, 2017) and usually seen vibrating at a wavelength of 3555.6  $\text{cm}^{-1}$  (Hadjiivanov, 2014). The stretching vibration of aliphatic C – H was observable at around 2900  $\text{cm}^{-1}$  (Zhao et al, 2017). This peak became intense in the hydrochar samples due to the presence of aliphatic and aromatic structures in hydrochar. The C = O stretching of the hemicellulose, which appeared approximately at 1729  $\text{cm}^{-1}$  in the spectra of wood dust, hazelnut husk, walnut shell and apricot seed, was completely disappeared in their corresponding hydrochars. It is the evidence of hemicellulose degradation, which occurred above 200°C, under hydrothermal conditions (Petrović et al, 2016; Liu et al, 2018). The symmetrical C – O stretching vibration at 1030  $\text{cm}^{-1}$ , which was observable in cellulose, hemicellulose and lignin structures of all biomasses, appeared in hydrochars at 1030  $\text{cm}^{-1}$ , 1050  $\text{cm}^{-1}$  and 1100  $\text{cm}^{-1}$ . Moreover, an increase in the aromatic structure in all hydrochars was seen at approximately 1600  $\text{cm}^{-1}$ , which indicated C = C and C = O stretching vibrations. G (guaiacyl) unit of lignin was partially degraded in almost all biomass samples, which was observed by the decrease in the intensity of the vibration at 1230  $\text{cm}^{-1}$ . The partial degradation of lignin under hydrothermal conditions was also observed by other studies (Cai et al, 2016).

As a result of activation with KOH, some vibrations disappeared and appeared, while some peaks shifted. The aliphatic C – H stretching vibration, which was observable at 2900  $\text{cm}^{-1}$ , was only observable in olive pomace and hazelnut husk activated hydrochars. All activated hydrochars had C  $\equiv$  C stretching vibration of alkyne groups, which was seen at 2300  $\text{cm}^{-1}$  (Islam et al, 2017b). The band at 1990 – 1690  $\text{cm}^{-1}$  indicated the C = C stretching vibration in carbonyl groups (Qian et al, 2018). The aromatic C = C peak at 1600  $\text{cm}^{-1}$  in hydrochars shifted to 1570  $\text{cm}^{-1}$  and its intensity increased (Kazak et al, 2018). The peak that indicated G (guaiacyl) unit in the structure

of lignin in hydrochars at  $1230\text{ cm}^{-1}$  disappeared after activation. That also showed that the lignin structure was degraded after activation.

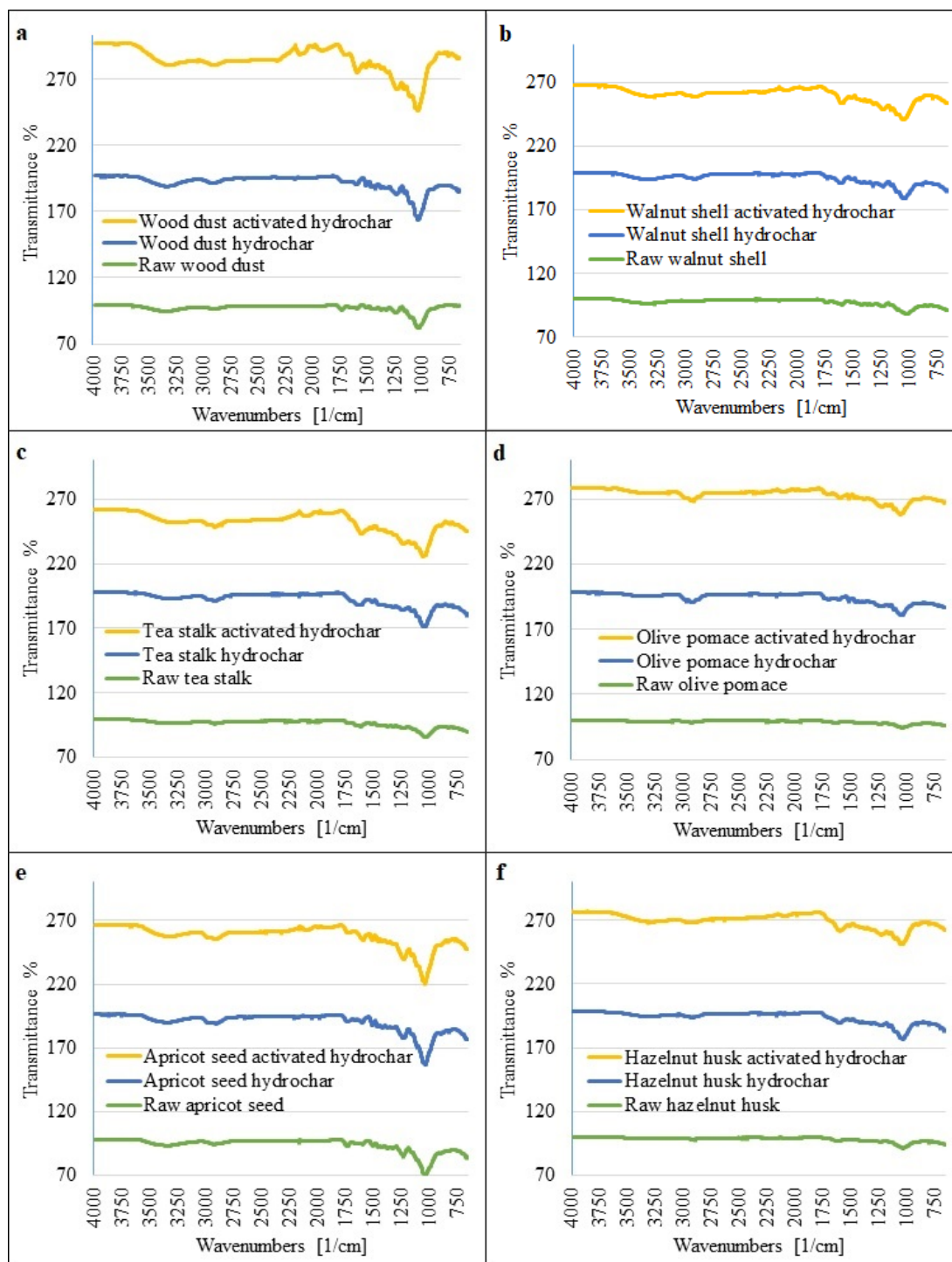


**Figure 5.13 :** Comparative FT-IR spectra of the biomasses, hydrochars and activated hydrochars of **a)** wood dust, **b)** walnut shell, **c)** tea stalk, **d)** olive pomace, **e)** apricot seed and **f)** hazelnut husk.

Surface morphologies of raw biomasses, hydrochars and activated hydrochars are shown in Figure 5.14 – 5.19. The structural difference observed in the hydrochars and activated hydrochars of the woody biomass and agricultural residues are remarkable.

Raw wood dust showed a uniformly fibrous and non-porous structure as seen in Figure 5.14 (a-c). After HTC, the wood dust hydrochar had small diameter, circular, thick-walled and slightly porous structure as seen in Figure 5.14 (d-f). In addition, mainly due to hemicellulose hydrolysis, a mixture of disordered fibers was preserved and the surface was seemed to be softened. After activation with KOH, wood dust activated hydrochar showed a randomly distributed porous structure (Figure 5.14 (g-i)). Moreover, the pores of wood dust activated hydrochar were of different sizes and shapes.

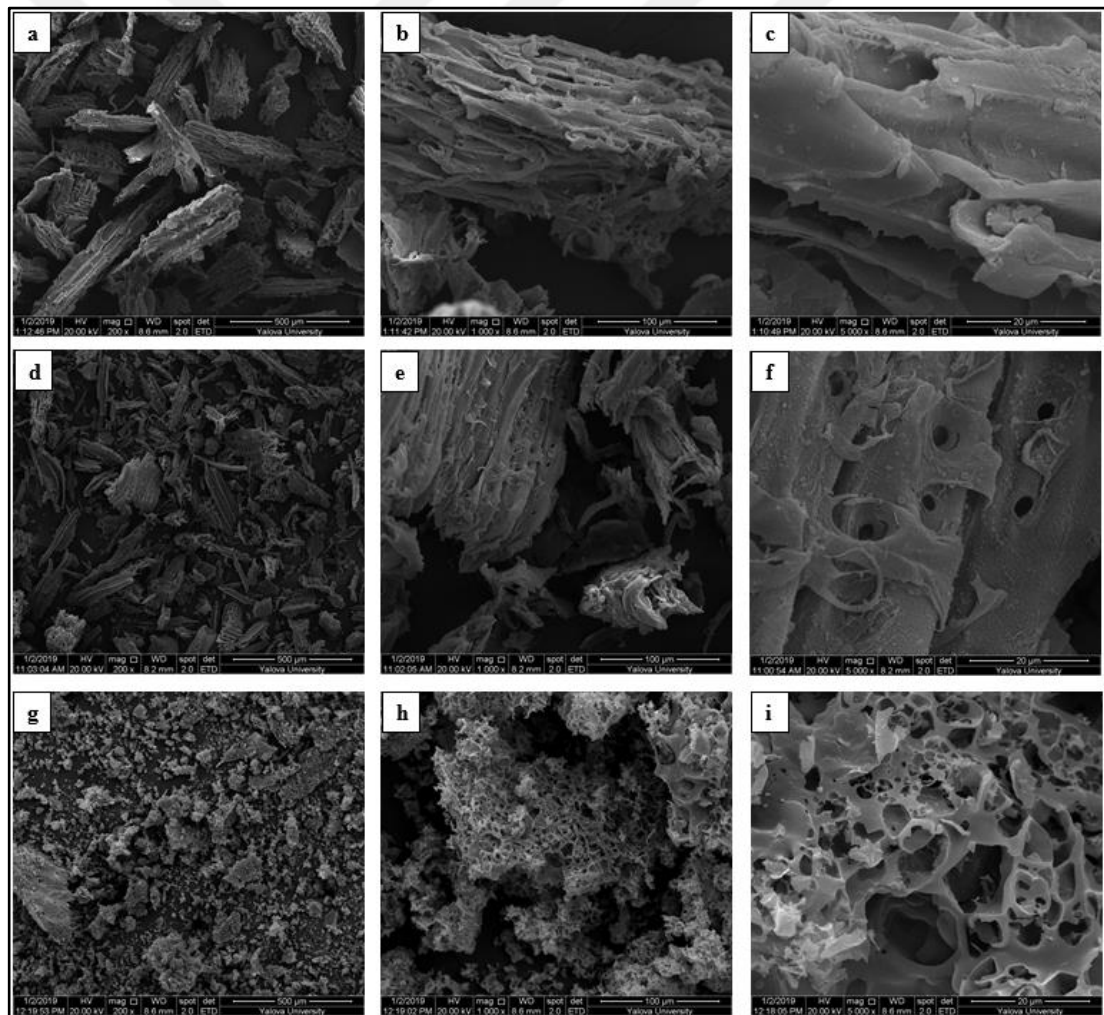


**Figure 5.14 :** SEM images of (a-c) raw wood dust, (d-f) wood dust hydrochar and (g-i) wood dust activated hydrochar with x200, x1000 and x5000 magnifications.

Except from tea stalk and olive pomace, the fibrous structure was not observed in agricultural biomass samples. As seen in Figure 5.15 (a-c), raw walnut shell had circular porous and layered structure. After hydrothermal carbonization, circular pores in the walnut shell hydrochar were increased and the surface structure became softer and thinner (see in Figure 5.15 (d-f)). As seen in Figure 5.15 (g-i), the sponge-like surface with a decreased pore size structure was detected after activation.

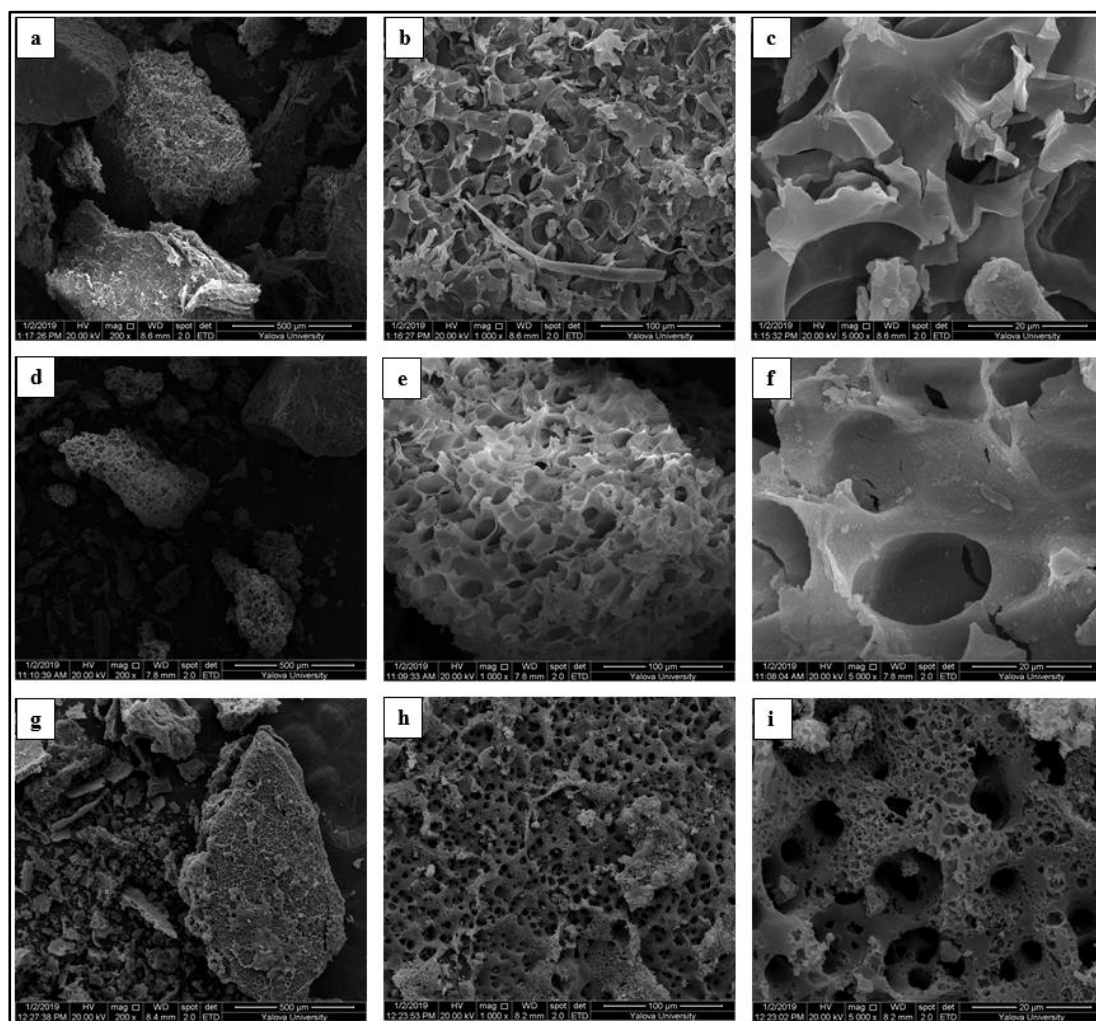


**Figure 5.15 :** SEM images of (a-c) raw walnut shell, (d-f) walnut shell hydrochar and (g-i) walnut shell activated hydrochar with x200, x1000 and x5000 magnifications.

Raw tea stalk showed fibrous and non-porous structure like wood dust, as seen in Figure 5.16 (a-c). Its hydrochar showed honeycomb shaped and thick-walled pores, which can be seen in Figure 5.16 (d-f). However, fibrous structures were also observable due to the high lignin content of raw tea stalk. After activation, the sponge-like surface structure was detected as seen in Figure 5.16 (g-i). Moreover, there was a

clear increase in porosity and a decrease in pore size. Due to the high lignin content of the tea stalk, it was possible to see particles that remained on the surface in Figure 5.16 (i).

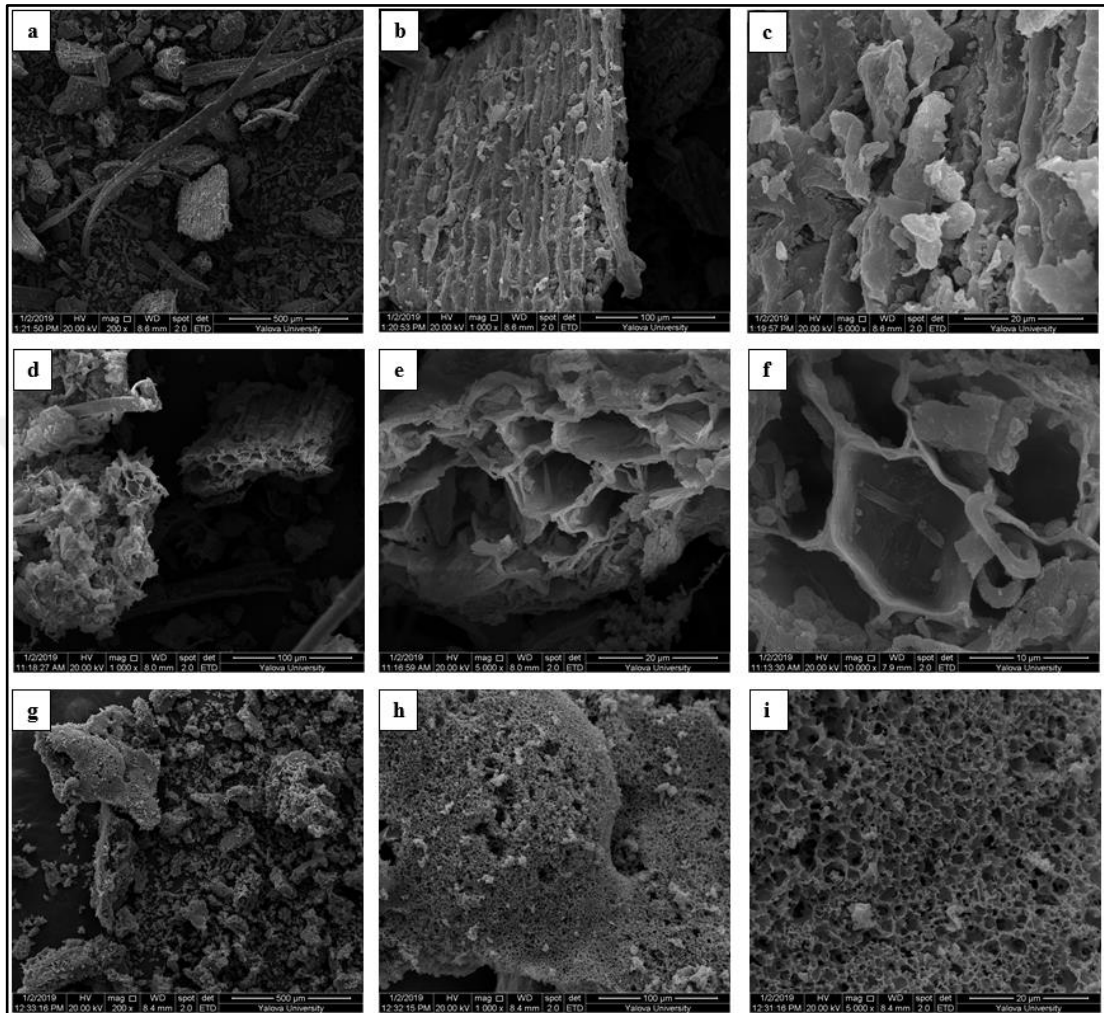


**Figure 5.16 :** SEM images of (a-c) raw tea stalk, (d-f) tea stalk hydrochar and (g-i) tea stalk activated hydrochar with x200, x1000, x5000 and x10k.

Raw olive pomace showed non-porous fibrous structure as seen in Figure 5.17 (a-c). As observable from Figure 5.17 (d-f), olive pomace hydrochar had thick – walled structure with channels and pores. However, spherical structures were also formed and there were undegraded fibrous structures. After activation, the surface became thinner and soft as seen in Figure 5.17 (g-i). Moreover, sponge-like structure with a lower pore size was observable.



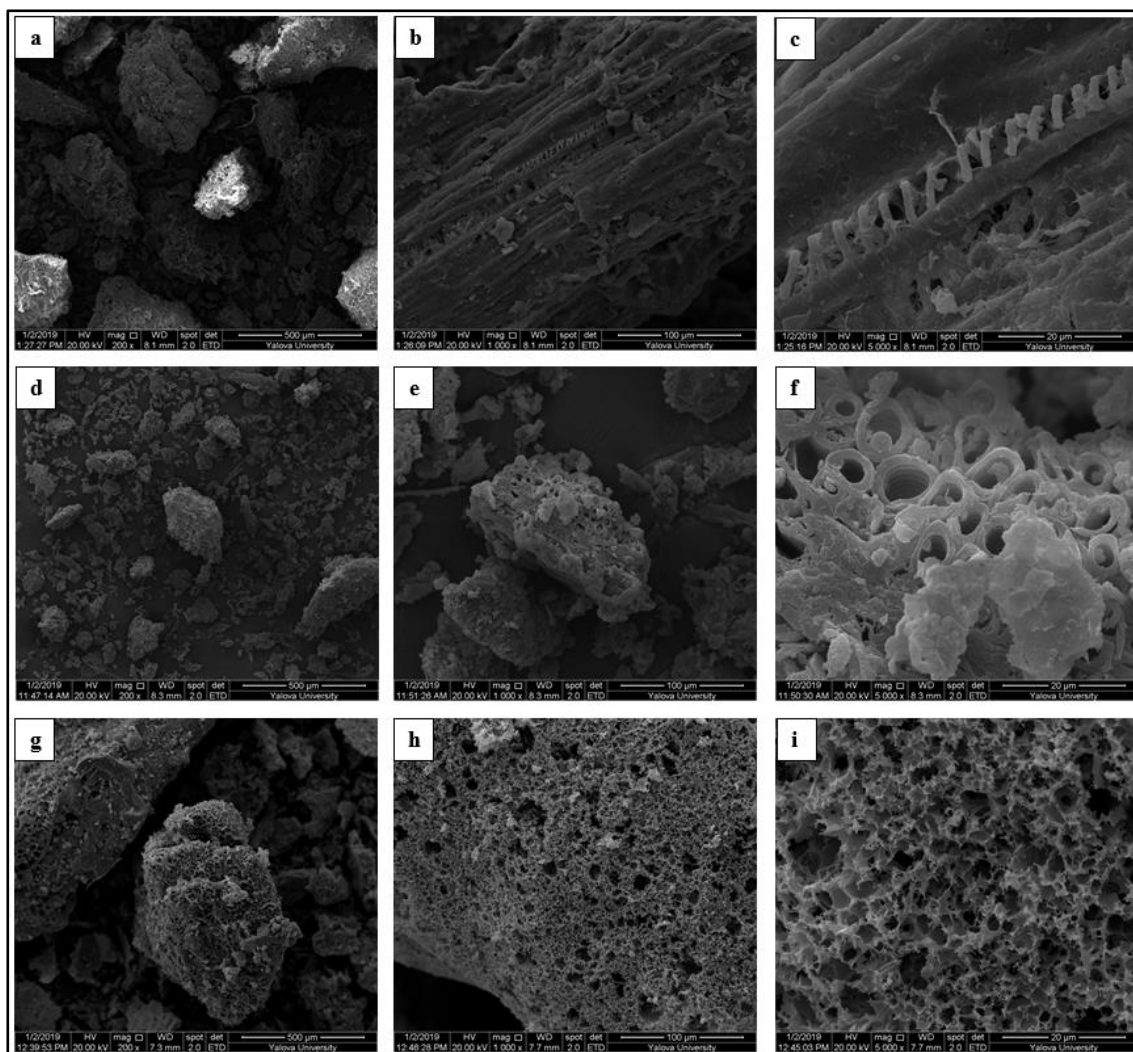


**Figure 5.17 :** SEM images of (a-c) raw olive pomace, (d-f) olive pomace hydrochar and (g-i) olive pomace activated hydrochar with x200, x1000 and x5000 magnifications.

The raw apricot seed had layered and non – porous structure as seen in Figure 5.18 (a-c). Its hydrochar showed a less porous structure with several microspheres (see in Figure 5.18 (d-f)). As stated in the study of Sevilla and Fuertes (2009), carbonaceous microspheres were observable in the cellulose hydrochars, which was mainly due to hydrothermal reactions of cellulose starting at 220°C (Figure 5.18 (f)). In apricot seed activated hydrochar, porosity was increased, and surface was softened as seen in Figure 5.18 (g-i). The microspheres were not observed, but randomly distributed and nonhomogeneous pores were detected.



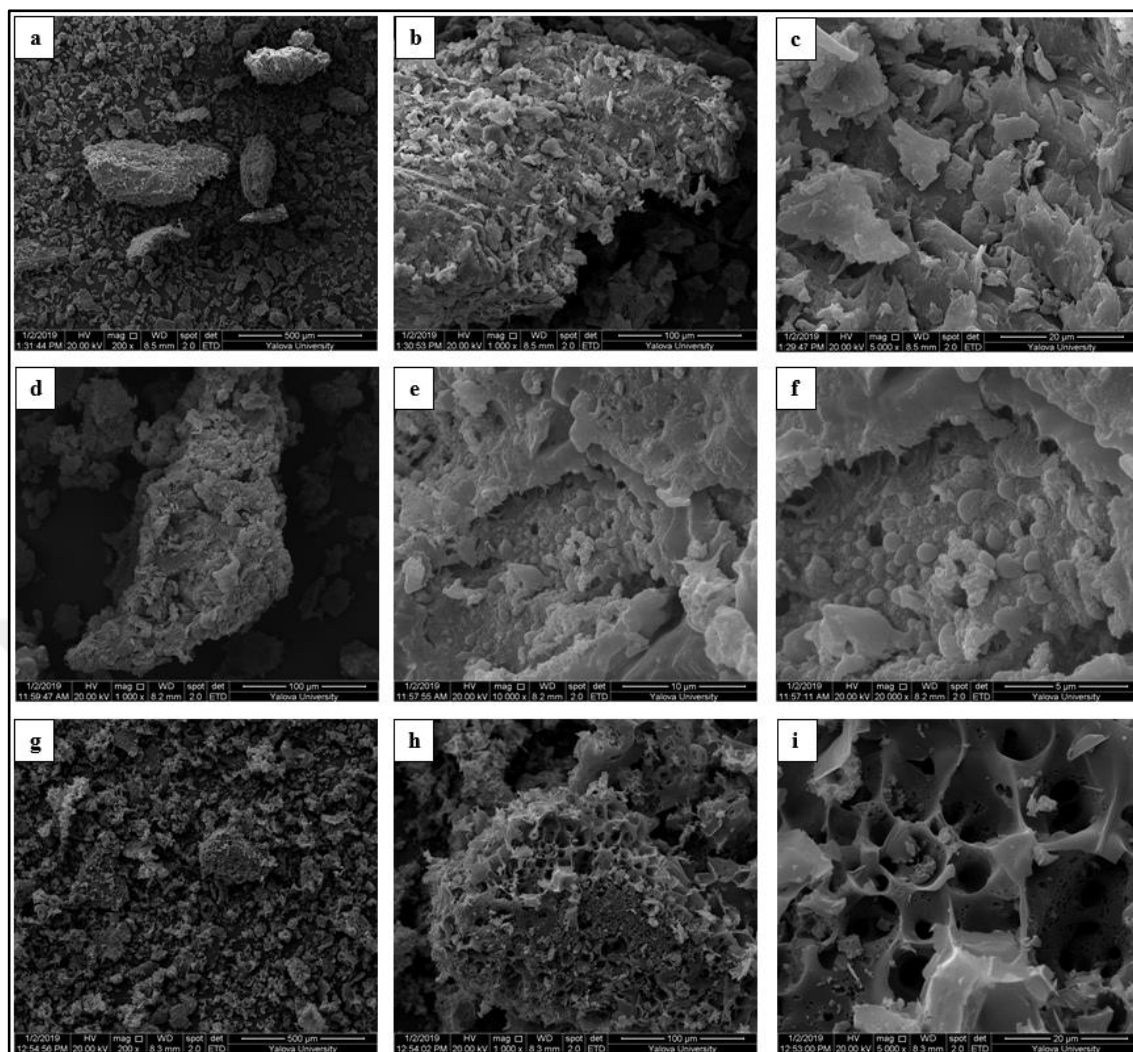


**Figure 5.18 :** SEM images of (a-c) raw apricot seed, (d-f) apricot seed hydrochar and (g-i) apricot seed activated hydrochar with x200, x1000, x5000, x10k and x20k magnifications.

Figure 5.19 shows that raw hazelnut husk had layered-structure. But it is possible to see small pores also in the raw hazelnut husk (see in Figure 5.19 (c)). While the hazelnut husk hydrochar had a small amount of thick-walled and circular pores, it is also possible to see lignin structure after hydrothermal carbonization (see in Figure 5.19 (d-f)). After activation with KOH, the surface became softer and the porosity was increased (Figure 5.19 (g-i)). Moreover, the disorder in the size and shape of the pores were remarkable in Figure 5.19 (h, i).

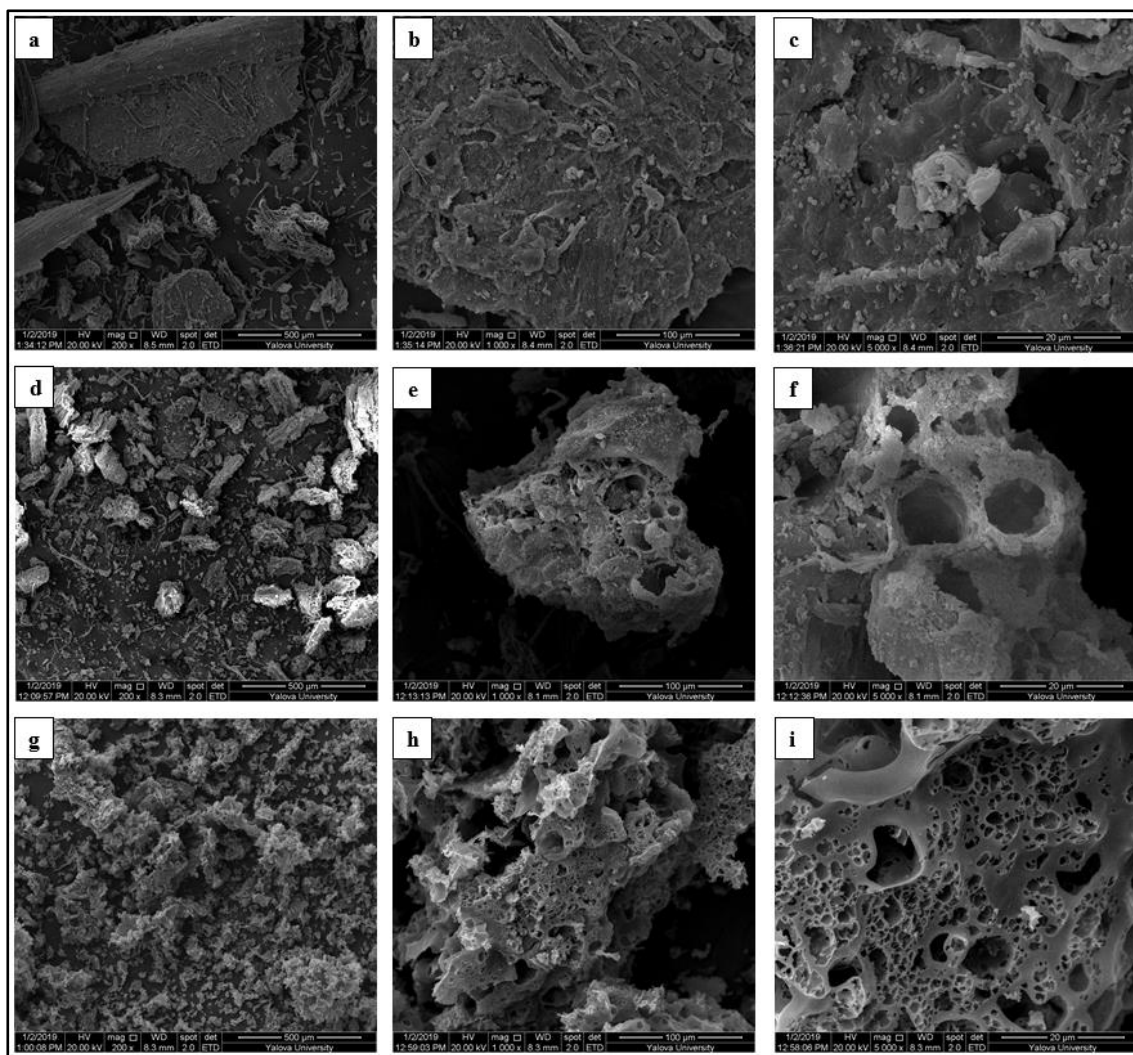


**Figure 5.19 :** SEM images of (a-c) raw hazelnut husk, (d-f) hazelnut husk hydrochar and (g-i) hazelnut husk activated hydrochar with x200, x1000 and x5000 magnifications.

Many researchers, who applied hydrothermal carbonization and activation to various biomass resources, observed similar results about surface morphologies. Sevilla and Fuertes (2011) investigated surface morphology of barley straw hydrochar and found out that the fibrous structure was softened due to the degradation of hemicellulose and cellulose, and carbon spheres were formed while raw biomass skeleton was preserved. Cai et al. (2016) determined that the well-defined and glossy surface of the biomass was changed due to the degradation of cellulose and hemicellulose the partial degradation of lignin. Wang et al. (2015) concluded that the surface morphologies of hydrochars were affected from the biomass type and that not every biomass hydrochar has spherical structure. Regmi et al. (2012) observed that the activated carbon derived from the switchgrass hydrochar was more porous than its hydrochar. The reason of the

porosity was explained by the effect of KOH, which broke the ether linkages of lignin due to lignin selectivity.

Specific surface areas and pores of activated hydrochars were carried out using N<sub>2</sub> adsorption-desorption measurement at 77°K and isotherms were prepared by using these data. The N<sub>2</sub> adsorption-desorption isotherms of activated hydrochars are shown in Figure 5.20. All activated hydrochars showed Type I isotherm according to the IUPAC classification, which typically refers to microporous materials (Zhu et al, 2015; Wang et al, 2015; IUPAC, 1985). Sharp knee indicated that the microporous structures of activated hydrochars at the low relative pressure in the adsorption isotherms. The initial parts of the adsorption isotherms indicated that the micropores were filled by N<sub>2</sub> gas, whereas, at higher relative pressures, the isotherms followed a horizontal plateau. Adsorption and desorption may follow different paths called hysteresis in the relative pressure zone and hysteresis gives information about surface morphology and pore structure. The Type I isotherm is associated with H4 type hysteresis and show that the activated hydrochars have microporous structures. (Gregg and Sign, 1982; IUPAC, 1985; Lowell et al, 2004). In addition, activated hydrochars of hazelnut husk, walnut shell and tea stalk had similar and the highest N<sub>2</sub> adsorptions, while activated hydrochar of wood dust had the least N<sub>2</sub> adsorption. After hazelnut husk, walnut shell and tea stalk, the N<sub>2</sub> adsorption was ranked from high to low as apricot seed activated hydrochar and olive pomace activated hydrochar.

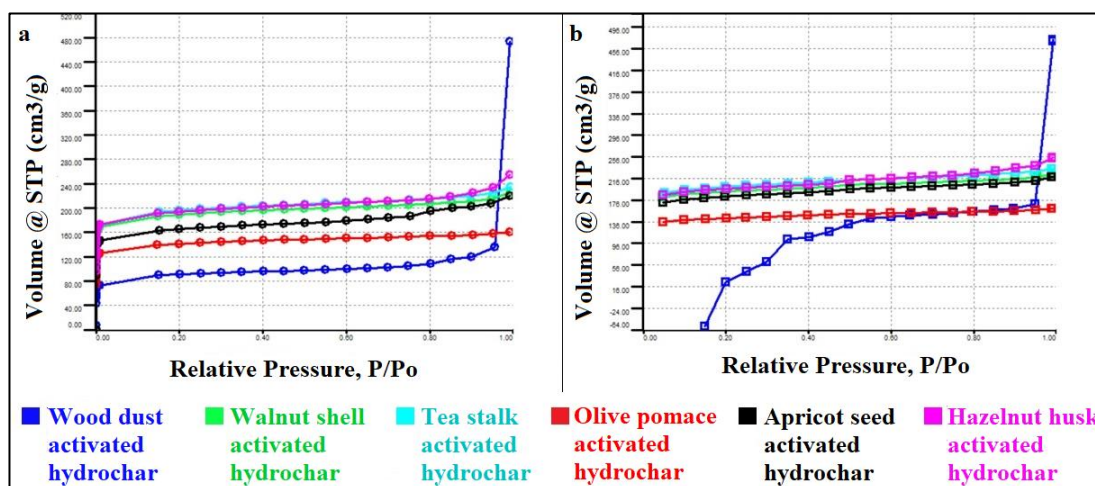


**Figure 5.20 :** The N<sub>2</sub> a) adsorption and b) desorption isotherms of activated hydrochars.

The textural properties of activated hydrochars are shown in Table 5.5. Activated hydrochar of tea stalk had the highest BET surface area with 666.7 m<sup>2</sup>/g, while activated hydrochar of wood dust had least BET surface area with 308.929 m<sup>2</sup>/g. After tea stalk, the BET surface area was ranked from high to low as walnut shell activated hydrochar (642.644 m<sup>2</sup>/g), hazelnut husk activated hydrochar (631.262 m<sup>2</sup>/g), apricot seed activated hydrochar (583.227 m<sup>2</sup>/g) and olive pomace activated hydrochar (473.774 m<sup>2</sup>/g). The percentage of micropore area to BET surface area varied between 84% and 88.5%. Activated hydrochars of agricultural residues such as walnut shell, tea stalk, olive pomace, apricot seed and hazelnut husk had similar micropore area/BET surface area ratios, while activated hydrochar of woody biomass had the least ratio with 84%. The wood dust activated hydrochar had the highest total pore volume with 0.73 cm<sup>3</sup>/g, while had the least micropore volume with 0.12 cm<sup>3</sup>/g. Agricultural residues based activated hydrochars had similar total pore and micropore volumes. Total pore volumes were ranked between 0.25 cm<sup>3</sup>/g (olive pomace) and 0.39 cm<sup>3</sup>/g (hazelnut husk), while micropore volumes were ranked between 0.20 cm<sup>3</sup>/g (olive pomace) and 0.27 cm<sup>3</sup>/g (tea stalk and hazelnut husk), for agricultural residue based activated hydrochars. Since all the experimental conditions for both hydrothermal carbonization and activation were the same, the difference in surface properties and porosity of the activated hydrochars were resulting from the biomass structure. Agricultural residues have lignin structures, which are more easily degradable than woody biomass (Wang et al, 2015; Regmi et al, 2012; Hu et al, 2008a). As seen in Table 5.4, average pore sizes ranged from 1.05 nm to 4.74 nm. Activated hydrochars of agricultural residues had an average pore size ranging from 1.05 nm to 1.25 nm and the pores were in micropore structure, while activated wood dust hydrochar had larger pores with an average pore size of 4.74 nm and it was in mesopore structure. The pore sizes of activated hydrochars of agricultural based were smaller than 2 nm and therefore they had micropore structures, while the pore size of activated hydrochar of wood dust was wider than 2 nm and therefore it had mesopore structure (IUPAC, 1985).

**Table 5.5** : Textural properties of activated hydrochars.

Activated hydrochar	BET Surface area (m <sup>2</sup> /g)	Micropore area (m <sup>2</sup> /g)	Total pore volume (cm <sup>3</sup> /g)	Micropore volume (cm <sup>3</sup> /g)	Average pore size (nm)
Wood dust	308.9	259.4	0.73	0.12	4.74
Walnut shell	642.6	568.5	0.35	0.26	1.08
Tea stalk	666.7	588.7	0.36	0.27	1.08
Olive pomace	473.8	420.8	0.25	0.20	1.05
Apricot seed	583.2	506.1	0.34	0.22	1.16
Hazelnut husk	631.3	550.1	0.39	0.27	1.25

Liu et al. (2018) carried out hydrothermal carbonization to corn straw and corncob for 5 h at 200°C and activation to hydrochars for 2 h at 650°C without using an activating agent. BET surface areas of corn straw and corncob activated carbons were 367.3 m<sup>2</sup>/g and 142.6 m<sup>2</sup>/g, respectively, and the activated hydrochars were used for removal of pollutants. The study of Liu et al. (2018), which was performed under similar conditions with the present study (but without KOH), showed that the surface area could be increased by the use of KOH as an activation agent. Adinata et al. (2007) performed chemical activation to the raw palm shell for 2 h at 600°C with K<sub>2</sub>CO<sub>3</sub>. Any additional carbonization process was not implemented before the activation. Activated carbon of palm shell had a BET surface area of 319 m<sup>2</sup>/g. Nowicki et al. (2010) carried out the pyrolysis of the walnut shell at 400°C for 60 min and then subjected to chemical activation with KOH at 500°C for 30 min. Activated carbon of walnut shell had 490 m<sup>2</sup>/g of BET surface area and 2 nm of average pore size. Elshafei et al. (2016) performed the pyrolysis of the artichoke peel for 1 h at 500°C under a nitrogen atmosphere and chemical activation with ZnCl<sub>2</sub> for 1 h at 800°C. They obtained activated carbon of artichoke peel with 245.2 m<sup>2</sup>/g of BET surface area. Although the activation at high temperature was applied, the pre-carbonization process as hydrothermal carbonization or pyrolysis is also quite important. Hydrothermal carbonization is preferred to pyrolysis as it can be carried out at mild temperatures. When the BET surface area, micropore area and volume were compared with other studies (Adinata et al, 2007; Nowicki et al, 2010; ElShafei et al, 2017) it can be generalized that hydrothermal carbonization prior to activation had a positive effect in increasing the surface area and microporous structure.



## 6. CONCLUSIONS

In this study, hydrochars and activated hydrochars were obtained from lignocellulosic biomass sources (wood dust, walnut shell, tea stalk, olive pomace, apricot seed and hazelnut husk) by hydrothermal carbonization and activation in the presence of KOH. The fuel and surface properties of the hydrochars and the textural and surface characteristics of activated hydrochars were investigated.

As the wood dust, walnut shell, tea stalk, olive pomace, apricot seed and hazelnut husk biomass samples and their corresponding hydrochar were compared, the improvement of the fuel quality after HTC was remarkable. All hydrochars had lower volatile matters and hydrogen contents, higher fixed carbon contents and higher net calorific values. Olive pomace had the highest percentage increase in carbon content and heating value with 30%, while wood dust had the least percentage increase with 14%. Olive pomace was followed by the walnut shell (21%), hazelnut husk (20%), apricot seed (19%), tea stalk (17%), respectively. Among all, olive pomace hydrochar had the highest carbon content (61.1%) and a heating value of 6106 cal/g. It should be noted that all of the hydrochars had the heating values as high as bituminous coal.

In all of the lignocellulosic biomass sources and their hydrochars investigated, pyrolysis took place in a single step, where the maximum mass loss rates were observed at different temperatures. Temperatures, where maximum loss rates of all samples were shifted to higher values after HTC. The combustion of all lignocellulosic biomass sources and their hydrochars had 3 stages, which include drying, devolatilization and combustion of volatiles and oxidation of char steps. All hydrochar samples had higher ignition temperatures as compared to their original biomass samples. Since the hydrochar samples had lower volatile matter content compared to their original biomass, their ignition temperatures were shifted to higher values. In the case of burnout temperatures, wood dust completed the oxidation reaction at lower temperatures as compared to agricultural biomass samples. Burnout temperature of the agricultural biomass ranged between 536-592°C. Unlike biomass samples, hydrochars

of agricultural biowastes had variable burnout temperatures, showing no consistence with the structural units of biomass.

The impacts of chemical activation with KOH and how the porous structure was affected from the biomass type were observable from the SEM images and BET analysis. Upon hydrothermal carbonization, all hydrochars represented significant amount of circular and thick-walled porous structure except tea stalk hydrochar, which had honeycomb shaped pores. Chemical activation KOH caused lignin degradation by breaking the ester bonds, which enhanced the formation of porous structure. Activated hydrochars demonstrated BET surface areas of between 308.9 m<sup>2</sup>/g and 666.7 m<sup>2</sup>/g (activated hydrochar of wood dust and tea stalk), and total pore volumes of between 0.25 cm<sup>3</sup>/g and 0.73 cm<sup>3</sup>/g (activated hydrochar of olive pomace and wood dust). The average pore size distribution of the activated hydrochars was ranging between 1.05 nm (olive pomace) and 4.74 nm (wood dust). All agricultural based activated hydrochars had similar average pore size distribution of 1.05 – 1.25 nm, which falls in the range of microporous structure. With the average pore size of 4.74 nm, activated hydrochar of wood dust can be classified under the mesoporous structure.

This study clearly points out that biomass type definitely affected fuel properties of hydrochars and the porous structure of the activated hydrochars.



## REFERENCES

- Abdullah, N., & Gerhauser, H.** (2008). Bio-oil derived from empty fruit bunches. *Fuel*, 87(12), 2606-2613. doi: 10.1016/j.fuel.2008.02.011
- Abel, S., Peters, A., Trinks, S., Schonsky, H., Facklam, M., & Wessolek, G.** (2013). Impact of biochar and hydrochar addition on water retention and water repellency of sandy soil. *Geoderma*, 202-203, 183-191. doi: 10.1016/j.geoderma.2013.03.003
- Abnisa, F., Daud, W., Husin, W., & Sahu, J.** (2011). Utilization possibilities of palm shell as a source of biomass energy in Malaysia by producing bio-oil in pyrolysis process. *Biomass And Bioenergy*, 35(5), 1863-1872. doi: 10.1016/j.biombioe.2011.01.033
- Adams, P., Bridgwater, T., Lea-Langton, A., Ross, A., & Watson, I.** (2018). Biomass Conversion Technologies. *Greenhouse Gases Balances Of Bioenergy Systems*, 107-139. doi: 10.1016/b978-0-08-101036-5.00008-2
- Adinata, D., Wandaud, W., & Aroua, M.** (2007). Preparation and characterization of activated carbon from palm shell by chemical activation with  $K_2CO_3$ . *Bioresource Technology*, 98(1), 145-149. doi: 10.1016/j.biortech.2005.11.006
- Ahmed, M.** (2017). Adsorption of quinolone, tetracycline, and penicillin antibiotics from aqueous solution using activated carbons: Review. *Environmental Toxicology And Pharmacology*, 50, 1-10. doi: 10.1016/j.etap.2017.01.004
- Akhtar, J., & Saidina Amin, N.** (2012). A review on operating parameters for optimum liquid oil yield in biomass pyrolysis. *Renewable And Sustainable Energy Reviews*, 16(7), 5101-5109. doi: 10.1016/j.rser.2012.05.033
- Albanese, L., Baronti, S., Liguori, F., Meneguzzo, F., Barbaro, P., & Vaccari, F.** (2019). Hydrodynamic cavitation as an energy efficient process to increase biochar surface area and porosity: A case study. *Journal Of Cleaner Production*, 210, 159-169. doi: 10.1016/j.jclepro.2018.10.341
- American Society for Testing and Materials (ASTM).** (2013a). E871-82 Standard test method for moisture analysis of particulate wood fuels.
- American Society for Testing and Materials (ASTM).** (2013b). E872-82 Standard test method for volatile matter in the analysis of particulate wood fuels.
- American Society for Testing and Materials (ASTM).** (2013c). D5865-13 Standard test method for gross calorific value of coal and coke.
- American Society for Testing and Materials (ASTM).** (2015a). E1756 – 08 Standard test method for determination of total solids in biomass.
- American Society for Testing and Materials (ASTM).** (2015b). E1755-01 Standard test method for ash in biomass.

- American Society for Testing and Materials (ASTM).** (2016). E1690 – 08 Standard test method for determination of ethanol extractives in biomass.
- Ando, H., Sakaki, T., Kokusho, T., Shibata, M., Uemura, Y., & Hatate, Y.** (2000). Decomposition Behavior of Plant Biomass in Hot-Compressed Water. *Industrial & Engineering Chemistry Research*, 39(10), 3688-3693. doi: 10.1021/ie0000257
- Ao, W., Fu, J., Mao, X., Kang, Q., Ran, C., & Liu, Y.** (2018). Microwave assisted preparation of activated carbon from biomass: A review. *Renewable And Sustainable Energy Reviews*, 92, 958-979. doi: 10.1016/j.rser.2018.04.051
- Arami-Niya, A., Daud, W., & Mjalli, F.** (2010). Using granular activated carbon prepared from oil palm shell by ZnCl<sub>2</sub> and physical activation for methane adsorption. *Journal Of Analytical And Applied Pyrolysis*, 89(2), 197-203. doi: 10.1016/j.jaap.2010.08.006
- Arami-Niya, A., Daud, W., & Mjalli, F.** (2011). Comparative study of the textural characteristics of oil palm shell activated carbon produced by chemical and physical activation for methane adsorption. *Chemical Engineering Research And Design*, 89(6), 657-664. doi: 10.1016/j.cherd.2010.10.003
- Arami-Niya, A., Wan Daud, W., S. Mjalli, F., Abnisa, F., & Shafeeyan, M.** (2012). Production of microporous palm shell based activated carbon for methane adsorption: Modeling and optimization using response surface methodology. *Chemical Engineering Research And Design*, 90(6), 776-784. doi: 10.1016/j.cherd.2011.10.001
- Arshadi, M., & Sellstedt, A.** (2008). Production of Energy from Biomass. In: Clark, E., & Deswarte, C., editors. *Introduction to Chemicals from Biomass*. John Wiley & Sons.
- Aworn, A., Thiravetyan, P., & Nakbanpote, W.** (2008). Preparation and characteristics of agricultural waste activated carbon by physical activation having micro- and mesopores. *Journal Of Analytical And Applied Pyrolysis*, 82(2), 279-285. doi: 10.1016/j.jaap.2008.04.007
- Bargmann, I., Rillig, M., Kruse, A., Greef, J., & Kücke, M.** (2013). Effects of hydrochar application on the dynamics of soluble nitrogen in soils and on plant availability. *Journal Of Plant Nutrition And Soil Science*, 177(1), 48-58. doi: 10.1002/jpln.201300069
- Barroso-Bogeat, A., Alexandre-Franco, M., Fernández-González, C., Macías-García, A., & Gómez-Serrano, V.** (2015). Temperature dependence of the electrical conductivity of activated carbons prepared from vine shoots by physical and chemical activation methods. *Microporous And Mesoporous Materials*, 209, 90-98. doi: 10.1016/j.micromeso.2014.07.023
- Basso, D., Patuzzi, F., Castello, D., Baratieri, M., Rada, E., Weiss-Hortala, E., & Fiori, L.** (2016). Agro-industrial waste to solid biofuel through hydrothermal carbonization. *Waste Management*, 47, 114-121. doi: 10.1016/j.wasman.2015.05.013
- Basso, D., Weiss-Hortala, E., Patuzzi, F., Castello, D., Baratieri, M., & Fiori, L.** (2015). Hydrothermal carbonization of off-specification compost: A byproduct

of the organic municipal solid waste treatment. *Bioresource Technology*, 182, 217-224. doi: 10.1016/j.biortech.2015.01.118

- Basu, P.** (2013). *Biomass gasification and pyrolysis*. Burlington, MA: Academic Press.
- Benadjemia, M., Millière, L., Reinert, L., Benderdouche, N., & Duclaux, L.** (2011). Preparation, characterization and Methylene Blue adsorption of phosphoric acid activated carbons from globe artichoke leaves. *Fuel Processing Technology*, 92(6), 1203-1212. doi: 10.1016/j.fuproc.2011.01.014
- Benavente, V., Calabuig, E., & Fullana, A.** (2015). Upgrading of moist agro-industrial wastes by hydrothermal carbonization. *Journal Of Analytical And Applied Pyrolysis*, 113, 89-98. doi: 10.1016/j.jaap.2014.11.004
- Berge, N., Ro, K., Mao, J., Flora, J., Chappell, M., & Bae, S.** (2011). Hydrothermal Carbonization of Municipal Waste Streams. *Environmental Science & Technology*, 45(13), 5696-5703. doi: 10.1021/es2004528
- Bicu, I., & Mustata, F.** (2013). Optimization of isolation of cellulose from orange peel using sodium hydroxide and chelating agents. *Carbohydrate Polymers*, 98(1), 341-348. doi: 10.1016/j.carbpol.2013.06.009
- Blazsó, M., Jakab, E., Vargha, A., Székely, T., Zoebel, H., Klare, H., & Keil, G.** (1986). The effect of hydrothermal treatment on a Merseburg lignite. *Fuel*, 65(3), 337-341. doi: 10.1016/0016-2361(86)90292-9
- Bobleter, O.** (1994). Hydrothermal degradation of polymers derived from plants. *Progress In Polymer Science*, 19(5), 797-841. doi: 10.1016/0079-6700(94)90033-7
- Bonn, G., Concini, R., & Bobleter, O.** (1983). Hydrothermolysis - a new process for the utilization of Biomass. *Wood Science And Technology*, 17(3), 195-202. doi: 10.1007/bf00372318
- Bonn, G., Schwald, W., & Bobleter, O.** (1985). Hydrothermolysis of Short Rotation Forestry Plants. In: Palz, W., Coombs, J., & Hall, D.O., editor. *Energy from Biomass 3rd E.C. Conference - Proceedings of the International Conference on Biomass*. Venice, Italy.
- Boyjoo, Y., Cheng, Y., Zhong, H., Tian, H., Pan, J., & Pareek, V.** (2017). From waste Coca Cola® to activated carbons with impressive capabilities for CO<sub>2</sub> adsorption and supercapacitors. *Carbon*, 116, 490-499. doi: 10.1016/j.carbon.2017.02.030
- Briscoe, J., Marinovic, A., Sevilla, M., Dunn, S., & Titirici, M.** (2015). Biomass-Derived Carbon Quantum Dot Sensitizers for Solid-State Nanostructured Solar Cells. *Angewandte Chemie International Edition*, 54(15), 4463-4468. doi: 10.1002/anie.201409290
- Butler, J.** (2018). *Carbon Dioxide Equilibria and Their Applications*. Milton: Routledge.
- Cai, J., Li, B., Chen, C., Wang, J., Zhao, M., & Zhang, K.** (2016). Hydrothermal carbonization of tobacco stalk for fuel application. *Bioresource Technology*, 220, 305-311. doi: 10.1016/j.biortech.2016.08.098

- Calderon Moreno, J., & Yoshimura, M.** (2001). Hydrothermal Processing of High-Quality Multiwall Nanotubes from Amorphous Carbon. *Journal Of The American Chemical Society*, 123(4), 741-742. doi: 10.1021/ja003008h
- Cao, L., Luo, G., Zhang, S., & Chen, J.** (2016). Bio-oil production from eight selected green landscaping wastes through hydrothermal liquefaction. *RSC Advances*, 6(18), 15260-15270. doi: 10.1039/c5ra24760h
- Carvalho, A., Cardoso, B., Pires, J., & Brotas de Carvalho, M.** (2003). Preparation of activated carbons from cork waste by chemical activation with KOH. *Carbon*, 41(14), 2873-2876. doi: 10.1016/s0008-6223(03)00323-3
- Cazetta, A., Vargas, A., Nogami, E., Kunita, M., Guilherme, M., & Martins, A.** (2011). NaOH-activated carbon of high surface area produced from coconut shell: Kinetics and equilibrium studies from the methylene blue adsorption. *Chemical Engineering Journal*, 174(1), 117-125. doi: 10.1016/j.cej.2011.08.058
- Chandra, T., Mirna, M., Sunarso, J., Sudaryanto, Y., & Ismadji, S.** (2009). Activated carbon from durian shell: Preparation and characterization. *Journal Of The Taiwan Institute of Chemical Engineers*, 40(4), 457-462. doi: 10.1016/j.jtice.2008.10.002
- Chang, C., Chang, C., & Tsai, W.** (2000). Effects of Burn-off and Activation Temperature on Preparation of Activated Carbon from Corn Cob Agrowaste by CO<sub>2</sub> and Steam. *Journal Of Colloid And Interface Science*, 232(1), 45-49. doi: 10.1006/jcis.2000.7171
- Chang, S., & Zainal, Z.** (2019). Activated Carbon for Supercapacitors. *Synthesis, Technology And Applications Of Carbon Nanomaterials*, 309-334. doi: 10.1016/b978-0-12-815757-2.00012-7
- Chen, J., Yang, J., Hu, G., Hu, X., Li, Z., & Shen, S.** (2016). Enhanced CO<sub>2</sub> Capture Capacity of Nitrogen-Doped Biomass-Derived Porous Carbons. *ACS Sustainable Chemistry & Engineering*, 4(3), 1439-1445. doi: 10.1021/acssuschemeng.5b01425
- Chen, X., Lin, Q., He, R., Zhao, X., & Li, G.** (2017). Hydrochar production from watermelon peel by hydrothermal carbonization. *Bioresource Technology*, 241, 236-243. doi: 10.1016/j.biortech.2017.04.012
- Chen, X., Ma, X., Peng, X., Lin, Y., & Yao, Z.** (2018). Conversion of sweet potato waste to solid fuel via hydrothermal carbonization. *Bioresource Technology*, 249, 900-907. doi: 10.1016/j.biortech.2017.10.096
- Chen, Y., Tshabalala, M., Gao, J., Stark, N., Fan, Y., & Ibach, R.** (2014). Thermal behavior of extracted and delignified pine wood flour. *Thermochimica Acta*, 591, 40-44. doi: 10.1016/j.tca.2014.06.012
- Chen, Y., Zhu, Y., Wang, Z., Li, Y., Wang, L., & Ding, L.** (2011). Application studies of activated carbon derived from rice husks produced by chemical-thermal process—A review. *Advances In Colloid And Interface Science*, 163(1), 39-52. doi: 10.1016/j.cis.2011.01.006
- Chen, Z., Hu, M., Zhu, X., Guo, D., Liu, S., & Hu, Z.** (2015). Characteristics and kinetic study on pyrolysis of five lignocellulosic biomass via

thermogravimetric analysis. *Bioresource Technology*, 192, 441-450. doi: 10.1016/j.biortech.2015.05.062

- Chomiak, K., Gryglewicz, S., Kierzek, K., & Machnikowski, J.** (2017). Optimizing the properties of granular walnut-shell based KOH activated carbons for carbon dioxide adsorption. *Journal Of CO<sub>2</sub> Utilization*, 21, 436-443. doi: 10.1016/j.jcou.2017.07.026
- Chowdhury, Z., Abd Hamid, S., Das, R., Hasan, M., Zain, S., Khalid, K., & Uddin, M.** (2013). Preparation of Carbonaceous Adsorbents from Lignocellulosic Biomass and Their Use in Removal of Contaminants from Aqueous Solution. *Bioresources*, 8(4). doi: 10.15376/biores.8.4.6523-6555
- Chung, J., Breulmann, M., Clemens, A., Fühner, C., Foppen, J., & Lens, P.** (2016). Simultaneous removal of rotavirus and adenovirus from artificial ground water using hydrochar derived from swine feces. *Journal Of Water And Health*, 14(5), 754-767. doi: 10.2166/wh.2016.010
- Chung, J., Foppen, J., Gerner, G., Krebs, R., & Lens, P.** (2015). Removal of rotavirus and adenovirus from artificial ground water using hydrochar derived from sewage sludge. *Journal Of Applied Microbiology*, 119(3), 876-884. doi: 10.1111/jam.12863
- Coronella, C.J., Lynam, J.G., Reza, M.T., & Uddin, M.H.** (2014). Hydrothermal Carbonization of Lignocellulosic Biomass. In: Jin, F, editor. *Application of hydrothermal reactions to biomass conversion*. Berlin, Heidelberg: Springer.
- Couto, G., Dessimoni, A., Bianchi, M., Perígolo, D., & Trugilho, P.** (2012). Use of sawdust Eucalyptus sp. in the preparation of activated carbons. *Ciência E Agrotecnologia*, 36(1), 69-77. doi: 10.1590/s1413-70542012000100009
- Cui, X., Antonietti, M., & Yu, S.** (2006). Structural Effects of Iron Oxide Nanoparticles and Iron Ions on the Hydrothermal Carbonization of Starch and Rice Carbohydrates. *Small*, 2(6), 756-759. doi: 10.1002/sml.200600047
- Danish, M., & Ahmad, T.** (2018). A review on utilization of wood biomass as a sustainable precursor for activated carbon production and application. *Renewable And Sustainable Energy Reviews*, 87, 1-21. doi: 10.1016/j.rser.2018.02.003
- Davis, N.** (1980). Use of carbon for the precipitation of gold from solution and subsequent burning. US.
- Delgado, L., Charles, P., Glucina, K., & Morlay, C.** (2012). The removal of endocrine disrupting compounds, pharmaceutically activated compounds and cyanobacterial toxins during drinking water preparation using activated carbon—A review. *Science Of The Total Environment*, 435-436, 509-525. doi: 10.1016/j.scitotenv.2012.07.046
- Demir-Cakan, R., Baccile, N., Antonietti, M., & Titirici, M.** (2009). Carboxylate-Rich Carbonaceous Materials via One-Step Hydrothermal Carbonization of Glucose in the Presence of Acrylic Acid. *Chemistry Of Materials*, 21(3), 484-490. doi: 10.1021/cm802141h
- Ding, L., Wang, Z., Li, Y., Du, Y., Liu, H., & Guo, Y.** (2012). A novel hydrochar and nickel composite for the electrochemical supercapacitor electrode material. *Materials Letters*, 74, 111-114. doi: 10.1016/j.matlet.2012.01.070

- Ding, L., Zou, B., Li, Y., Liu, H., Wang, Z., & Zhao, C.** (2013a). The production of hydrochar-based hierarchical porous carbons for use as electrochemical supercapacitor electrode materials. *Colloids And Surfaces A: Physicochemical And Engineering Aspects*, 423, 104-111. doi: 10.1016/j.colsurfa.2013.02.003
- Ding, L., Zou, B., Liu, H., Li, Y., Wang, Z., & Su, Y.** (2013b). A new route for conversion of corncob to porous carbon by hydrolysis and activation. *Chemical Engineering Journal*, 225, 300-305. doi: 10.1016/j.cej.2013.03.090
- Dinjus, E., Kruse, A., & Tröger, N.** (2011). Hydrothermal Carbonization - 1. Influence of Lignin in Lignocelluloses. *Chemical Engineering & Technology*, 34(12), 2037-2043. doi: 10.1002/ceat.201100487
- Donar, Y., Çağlar, E., & Sınağ, A.** (2016). Preparation and characterization of agricultural waste biomass based hydrochars. *Fuel*, 183, 366-372. doi: 10.1016/j.fuel.2016.06.108
- Duan, X., Yuan, C., Jing, T., & Yuan, X.** (2019). Removal of elemental mercury using large surface area micro-porous corn cob activated carbon by zinc chloride activation. *Fuel*, 239, 830-840. doi: 10.1016/j.fuel.2018.11.017
- Edelstein, A.** (2001). Nanomaterials. *Encyclopedia of materials*, 5916-5927. Amsterdam: Elsevier.
- El-Hendawy, A., Samra, S., & Girgis, B.** (2001). Adsorption characteristics of activated carbons obtained from corncobs. *Colloids And Surfaces A: Physicochemical And Engineering Aspects*, 180(3), 209-221. doi: 10.1016/s0927-7757(00)00682-8
- ElShafei, G., ElSherbiny, I., Darwish, A., & Philip, C.** (2017). Artichoke as a non-conventional precursor for activated carbon: Role of the activation process. *Journal Of Taibah University For Science*, 11(5), 677-688. doi: 10.1016/j.jtusci.2016.04.006
- Erdogan, E., Atila, B., Mumme, J., Reza, M., Toptas, A., Elibol, M., & Yanik, J.** (2015). Characterization of products from hydrothermal carbonization of orange pomace including anaerobic digestibility of process liquor. *Bioresource Technology*, 196, 35-42. doi: 10.1016/j.biortech.2015.06.115
- Fakkaew, K., Koottatep, T., & Polprasert, C.** (2015). Effects of hydrolysis and carbonization reactions on hydrochar production. *Bioresource Technology*, 192, 328-334. doi: 10.1016/j.biortech.2015.05.091
- Falco, C., Baccile, N., & Titirici, M.** (2011). Morphological and structural differences between glucose, cellulose and lignocellulosic biomass derived hydrothermal carbons. *Green Chemistry*, 13(11), 3273. doi: 10.1039/c1gc15742f
- Falco, C., Sieben, J., Brun, N., Sevilla, M., van der Maelen, T., & Morallón, E.** (2013). Hydrothermal Carbons from Hemicellulose-Derived Aqueous Hydrolysis Products as Electrode Materials for Supercapacitors. *Chemsuschem*, 6(2), 374-382. doi: 10.1002/cssc.201200817
- Fan, Y., Liu, P., Huang, Z., Jiang, T., Yao, K., & Han, R.** (2015). Porous hollow carbon spheres for electrode material of supercapacitors and support material of dendritic Pt electrocatalyst. *Journal Of Power Sources*, 280, 30-38. doi: 10.1016/j.jpowsour.2015.01.096

- Fang, J., Gao, B., Chen, J., & Zimmerman, A.** (2015). Hydrochars derived from plant biomass under various conditions: Characterization and potential applications and impacts. *Chemical Engineering Journal*, 267, 253-259. doi: 10.1016/j.cej.2015.01.026
- Fang, J., Zhan, L., Ok, Y., & Gao, B.** (2018). Minireview of potential applications of hydrochar derived from hydrothermal carbonization of biomass. *Journal Of Industrial And Engineering Chemistry*, 57, 15-21. doi: 10.1016/j.jiec.2017.08.026.
- Feng, S., Li, W., Wang, J., Song, Y., Elzatahry, A., Xia, Y., & Zhao, D.** (2014). Hydrothermal synthesis of ordered mesoporous carbons from a biomass-derived precursor for electrochemical capacitors. *Nanoscale*, 6(24), 14657-14661. doi: 10.1039/c4nr05629a
- Fernandez, M., Ledesma, B., Román, S., Bonelli, P., & Cukierman, A.** (2015). Development and characterization of activated hydrochars from orange peels as potential adsorbents for emerging organic contaminants. *Bioresource Technology*, 183, 221-228. doi: 10.1016/j.biortech.2015.02.035
- Fiori, L., Basso, D., Castello, D., & Baratieri, M.** (2014). Hydrothermal carbonization of biomass: design of a batch reactor and preliminary experimental results. *Chemical Engineering Transactions*, 37, 55-60. doi: 10.3303/CET1437010
- Flora, J., Lu, X., Li, L., Flora, J., & Berge, N.** (2013). The effects of alkalinity and acidity of process water and hydrochar washing on the adsorption of atrazine on hydrothermally produced hydrochar. *Chemosphere*, 93(9), 1989-1996. doi: 10.1016/j.chemosphere.2013.07.018
- Franciski, M., Peres, E., Godinho, M., Perondi, D., Foletto, E., Collazzo, G., & Dotto, G.** (2018). Development of CO<sub>2</sub> activated biochar from solid wastes of a beer industry and its application for methylene blue adsorption. *Waste Management*, 78, 630-638. doi: 10.1016/j.wasman.2018.06.040
- Fu, K., Yue, Q., Gao, B., Wang, Y., & Li, Q.** (2017). Activated carbon from tomato stem by chemical activation with FeCl<sub>2</sub>. *Colloids And Surfaces A: Physicochemical And Engineering Aspects*, 529, 842-849. doi: 10.1016/j.colsurfa.2017.06.064
- Funke, A., & Ziegler, F.** (2010). Hydrothermal carbonization of biomass: A summary and discussion of chemical mechanisms for process engineering. *Biofuels, Bioproducts And Biorefining*, 4(2), 160-177. doi: 10.1002/bbb.198
- Funke, A., Mumme, J., Koon, M., & Diakité, M.** (2013). Cascaded production of biogas and hydrochar from wheat straw: Energetic potential and recovery of carbon and plant nutrients. *Biomass And Bioenergy*, 58, 229-237. doi: 10.1016/j.biombioe.2013.08.018
- Gañan, J., González-García, C., González, J., Sabio, E., Macías-García, A., & Díaz-Díez, M.** (2004). Preparation of activated carbons from bituminous coal pitches. *Applied Surface Science*, 238(1-4), 347-354. doi: 10.1016/j.apsusc.2004.05.222

- Gani, A., & Naruse, I.** (2007). Effect of cellulose and lignin content on pyrolysis and combustion characteristics for several types of biomass. *Renewable Energy*, *32*(4), 649-661. doi: 10.1016/j.renene.2006.02.017
- Gao, F., Shao, G., Qu, J., Lv, S., Li, Y., & Wu, M.** (2015). Tailoring of porous and nitrogen-rich carbons derived from hydrochar for high-performance supercapacitor electrodes. *Electrochimica Acta*, *155*, 201-208. doi: 10.1016/j.electacta.2014.12.069
- Gao, P., Zhou, Y., Meng, F., Zhang, Y., Liu, Z., Zhang, W., & Xue, G.** (2016a). Preparation and characterization of hydrochar from waste eucalyptus bark by hydrothermal carbonization. *Energy*, *97*, 238-245. doi: 10.1016/j.energy.2015.12.123
- Gao, Y., Yu, B., Wu, K., Yuan, Q., Wang, X., & Chen, H.** (2016b). Physicochemical, Pyrolytic, and Combustion Characteristics of Hydrochar Obtained by Hydrothermal Carbonization of Biomass. *Bioresources*, *11*(2). doi: 10.15376/biores.11.2.4113-4133
- George, C., Wagner, M., Kücke, M., & Rillig, M.** (2012). Divergent consequences of hydrochar in the plant–soil system: Arbuscular mycorrhiza, nodulation, plant growth and soil aggregation effects. *Applied Soil Ecology*, *59*, 68-72. doi: 10.1016/j.apsoil.2012.02.021
- Ghanim, B., Pandey, D., Kwapinski, W., & Leahy, J.** (2016). Hydrothermal carbonisation of poultry litter: Effects of treatment temperature and residence time on yields and chemical properties of hydrochars. *Bioresource Technology*, *216*, 373-380. doi: 10.1016/j.biortech.2016.05.087
- Gogotsi, Y., & Yoshimura, M.** (1994). Formation of carbon films on carbides under hydrothermal conditions. *Nature*, *367*(6464), 628-630. doi: 10.1038/367628a0
- González-García, P.** (2018). Activated carbon from lignocellulosics precursors: A review of the synthesis methods, characterization techniques and applications. *Renewable And Sustainable Energy Reviews*, *82*, 1393-1414. doi: 10.1016/j.rser.2017.04.117
- Goudriaan, F., & Peferoen, D.** (1990). Liquid fuels from biomass via a hydrothermal process. *Chemical Engineering Science*, *45*(8), 2729-2734. doi: 10.1016/0009-2509(90)80164-a
- Goyal, H., Seal, D., & Saxena, R.** (2008). Bio-fuels from thermochemical conversion of renewable resources: A review. *Renewable And Sustainable Energy Reviews*, *12*(2), 504-517. doi: 10.1016/j.rser.2006.07.014
- Gozaydin, G., & Yuksel, A.** (2017). Valorization of hazelnut shell waste in hot compressed water. *Fuel Processing Technology*, *166*, 96-106. doi: 10.1016/j.fuproc.2017.05.034
- Gregg, S., & Sing, K.** (1995). Adsorption, surface area and porosity. London: Academic Press.
- Grønli, M., Várhegyi, G., & Di Blasi, C.** (2002). Thermogravimetric Analysis and Devolatilization Kinetics of Wood. *Industrial & Engineering Chemistry Research*, *41*(17), 4201-4208. doi: 10.1021/ie0201157



- Guney, M.** (2013). Utilization of hazelnut husk as biomass. *Sustainable Energy Technologies And Assessments*, 4, 72-77. doi: 10.1016/j.seta.2013.09.004
- Guo, H., Bi, C., Zeng, C., Ma, W., Yan, L., Li, K., & Wei, K.** (2018). Camellia oleifera seed shell carbon as an efficient renewable bio-adsorbent for the adsorption removal of hexavalent chromium and methylene blue from aqueous solution. *Journal Of Molecular Liquids*, 249, 629-636. doi: 10.1016/j.molliq.2017.11.096
- Gupta, T.** (2017). Historical Production and Use of Carbon Materials: The Activated Carbon. *Carbon*, 47-70. doi: 10.1007/978-3-319-66405-7\_2
- Hadjiivanov, K.** (2014). Identification and Characterization of Surface Hydroxyl Groups by Infrared Spectroscopy. In: Friederike C. Jentoft, editor, *Advances in Catalysis, Burlington*. Academic Press. 57 99-318.
- Hammud, H., Shmait, A., & Hourani, N.** (2015). Removal of Malachite Green from water using hydrothermally carbonized pine needles. *RSC Advances*, 5(11), 7909-7920. doi: 10.1039/c4ra15505j
- Hao, W., Björkman, E., Lilliestråle, M., & Hedin, N.** (2013). Activated carbons prepared from hydrothermally carbonized waste biomass used as adsorbents for CO<sub>2</sub>. *Applied Energy*, 112, 526-532. doi: 10.1016/j.apenergy.2013.02.028
- Hao, W., Björkman, E., Lilliestråle, M., & Hedin, N.** (2014). Activated Carbons for Water Treatment Prepared by Phosphoric Acid Activation of Hydrothermally Treated Beer Waste. *Industrial & Engineering Chemistry Research*, 53(40), 15389-15397. doi: 10.1021/ie5004569
- He, C., Giannis, A., & Wang, J.** (2013). Conversion of sewage sludge to clean solid fuel using hydrothermal carbonization: Hydrochar fuel characteristics and combustion behavior. *Applied Energy*, 111, 257-266. doi: 10.1016/j.apenergy.2013.04.084
- Heilmann, S., Davis, H., Jader, L., Lefebvre, P., Sadowsky, M., & Schendel, F.** (2010). Hydrothermal carbonization of microalgae. *Biomass And Bioenergy*, 34(6), 875-882. doi: 10.1016/j.biombioe.2010.01.032
- Heilmann, S., Molde, J., Timler, J., Wood, B., Mikula, A., & Vozhdayev, G.** (2014). Phosphorus Reclamation through Hydrothermal Carbonization of Animal Manures. *Environmental Science & Technology*, 48(17), 10323-10329. doi: 10.1021/es501872k
- Henriksson, G., Li, J., Zhang, L., & Lindström, M.** (2010). Lignin Utilization. *Thermochemical Conversion Of Biomass To Liquid Fuels And Chemicals*, 222-262. doi: 10.1039/9781849732260-00222
- Hoekman, S., Broch, A., & Robbins, C.** (2011). Hydrothermal Carbonization (HTC) of Lignocellulosic Biomass. *Energy & Fuels*, 25(4), 1802-1810. doi: 10.1021/ef101745n
- Holtzapple, M.T.** (2003). Hemicelluloses. *Encyclopedia of Food Sciences and Nutrition*, 3060–3071. doi:10.1016/b0-12-227055-x/00589-7
- Hu, B., Yu, S., Wang, K., Liu, L., & Xu, X.** (2008a). Functional carbonaceous materials from hydrothermal carbonization of biomass: an effective chemical process. *Dalton Transactions*, (40), 5414. doi: 10.1039/b804644c

- Hu, Y., Demir-Cakan, R., Titirici, M., Müller, J., Schlögl, R., Antonietti, M., & Maier, J.** (2008b). Superior Storage Performance of a Si@SiO<sub>x</sub>/C Nanocomposite as Anode Material for Lithium-Ion Batteries. *Angewandte Chemie International Edition*, 47(9), 1645-1649. doi: 10.1002/anie.200704287
- Huff, M., Kumar, S., & Lee, J.** (2014). Comparative analysis of pinewood, peanut shell, and bamboo biomass derived biochars produced via hydrothermal conversion and pyrolysis. *Journal Of Environmental Management*, 146, 303-308. doi: 10.1016/j.jenvman.2014.07.016
- Idrees, M., Rangari, V., & Jeelani, S.** (2018). Sustainable packaging waste-derived activated carbon for carbon dioxide capture. *Journal Of CO<sub>2</sub> Utilization*, 26, 380-387. doi: 10.1016/j.jcou.2018.05.016
- Inagaki, M., Kang, F., Toyoda, M., & Konno, H.** (2014). Introduction. *Advanced Materials Science And Engineering Of Carbon*, 1-13. doi: 10.1016/b978-0-12-407789-8.00001-6
- Inoue, S., Hanaoka, T., & Minowa, T.** (2002). Hot Compressed Water Treatment for Production of Charcoal from Wood. *Journal of Chemical Engineering of Japan*, 35(10), 1020-1023. doi: 10.1252/jcej.35.1020
- Inoue, S., Uno, S., & Minowa, T.** (2008). Carbonization of Cellulose Using the Hydrothermal Method. *Journal Of Chemical Engineering Of Japan*, 41(3), 210-215. doi: 10.1252/jcej.07we230
- Ioannidou, O., & Zabaniotou, A.** (2007). Agricultural residues as precursors for activated carbon production—A review. *Renewable and Sustainable Energy Reviews*, 11(9), 1966-2005. doi: 10.1016/j.rser.2006.03.013
- Islam, M., Ahmed, M., Khanday, W., Asif, M., & Hameed, B.** (2017a). Mesoporous activated coconut shell-derived hydrochar prepared via hydrothermal carbonization-NaOH activation for methylene blue adsorption. *Journal Of Environmental Management*, 203, 237-244. doi: 10.1016/j.jenvman.2017.07.029
- Islam, M., Ahmed, M., Khanday, W., Asif, M., & Hameed, B.** (2017b). Mesoporous activated carbon prepared from NaOH activation of rattan (*Lacosperma secundiflorum*) hydrochar for methylene blue removal. *Ecotoxicology And Environmental Safety*, 138, 279-285. doi: 10.1016/j.ecoenv.2017.01.010
- Islam, M., Benhouria, A., Asif, M., & Hameed, B.** (2015a). Methylene blue adsorption on factory-rejected tea activated carbon prepared by conjunction of hydrothermal carbonization and sodium hydroxide activation processes. *Journal Of The Taiwan Institute Of Chemical Engineers*, 52, 57-64. doi: 10.1016/j.jtice.2015.02.010
- Islam, M., Tan, I., Benhouria, A., Asif, M., & Hameed, B.** (2015b). Mesoporous and adsorptive properties of palm date seed activated carbon prepared via sequential hydrothermal carbonization and sodium hydroxide activation. *Chemical Engineering Journal*, 270, 187-195. doi: 10.1016/j.cej.2015.01.058
- International Union of Pure and Applied Chemistry (IUPAC).** (1985). Reporting physisorption data for gas/solid systems with special reference to the

determination of surface area and porosity, commission on colloid and surface chemistry including catalysis. *Pure Appl. Chem.* 57, 603.

- Jain, A., Balasubramanian, R., & Srinivasan, M.** (2015). Tuning hydrochar properties for enhanced mesopore development in activated carbon by hydrothermal carbonization. *Microporous And Mesoporous Materials*, 203, 178-185. doi: 10.1016/j.micromeso.2014.10.036
- Jain, A., Balasubramanian, R., & Srinivasan, M.** (2016). Hydrothermal conversion of biomass waste to activated carbon with high porosity: A review. *Chemical Engineering Journal*, 283, 789-805. doi: 10.1016/j.cej.2015.08.014
- Jamari, S., & Howse, J.** (2012). The effect of the hydrothermal carbonization process on palm oil empty fruit bunch. *Biomass And Bioenergy*, 47, 82-90. doi: 10.1016/j.biombioe.2012.09.061
- Kambo, H., & Dutta, A.** (2015). A comparative review of biochar and hydrochar in terms of production, physico-chemical properties and applications. *Renewable And Sustainable Energy Reviews*, 45, 359-378. doi: 10.1016/j.rser.2015.01.050
- Kammann, C., Ratering, S., Eckhard, C., & Müller, C.** (2012). Biochar and Hydrochar Effects on Greenhouse Gas (Carbon Dioxide, Nitrous Oxide, and Methane) Fluxes from Soils. *Journal Of Environment Quality*, 41(4), 1052. doi: 10.2134/jeq2011.0132
- Kar, Y.** (2011). Co-pyrolysis of walnut shell and tar sand in a fixed-bed reactor. *Bioresource Technology*, 102(20), 9800-9805. doi: 10.1016/j.biortech.2011.08.022
- Kazak, O., Eker, Y., Bingol, H., & Tor, A.** (2018). Preparation of chemically-activated high surface area carbon from waste vinasse and its efficiency as adsorbent material. *Journal Of Molecular Liquids*, 272, 189-197. doi: 10.1016/j.molliq.2018.09.085
- Kaźmierczak, J., Nowicki, P., & Pietrzak, R.** (2012). Sorption properties of activated carbons obtained from corn cobs by chemical and physical activation. *Adsorption*, 19(2-4), 273-281. doi: 10.1007/s10450-012-9450-y
- Khezami, L., Ould-Dris, A., & Capart, R.** (2007). Activated carbon from thermo-compressed wood and other lignocellulosic precursors. *Bioresources*, 2(2), 193-209. doi: 10.15376/biores.2.2.193-209
- Kloprogge, J.T.** (2017). Raman Spectroscopy of Clay Minerals, *Developments in Clay Science*. 8, 150-199.
- Kok, M., & Ozgur, E.** (2017). Characterization of lignocellulose biomass and model compounds by thermogravimetry. *Energy Sources, Part A: Recovery, Utilization, And Environmental Effects*, 39(2), 134-139. doi: 10.1080/15567036.2016.1214643
- Kou, L., Song, Y., Zhang, X., & Tan, T.** (2017). Comparison of four types of energy grasses as lignocellulosic feedstock for the production of bio-ethanol. *Bioresource Technology*, 241, 424-429. doi: 10.1016/j.biortech.2017.04.078
- Köseođlu, E., & Akmil-Başar, C.** (2015). Preparation, structural evaluation and adsorptive properties of activated carbon from agricultural waste

- biomass. *Advanced Powder Technology*, 26(3), 811-818. doi: 10.1016/j.appt.2015.02.006
- Kruse, A., Funke, A., & Titirici, M.** (2013). Hydrothermal conversion of biomass to fuels and energetic materials. *Current Opinion In Chemical Biology*, 17(3), 515-521. doi: 10.1016/j.cbpa.2013.05.004
- Kumar, A., & Jena, H.** (2016). Preparation and characterization of high surface area activated carbon from Fox nut (*Euryale ferox*) shell by chemical activation with  $H_3PO_4$ . *Results In Physics*. doi: 10.1016/j.rinp.2016.03.006
- Kumar, A., & Jena, H.** (2017). Adsorption of Cr(VI) from aqueous solution by prepared high surface area activated carbon from Fox nutshell by chemical activation with  $H_3PO_4$ . *Journal Of Environmental Chemical Engineering*, 5(2), 2032-2041. doi: 10.1016/j.jece.2017.03.035
- Kumar, M., Olajire Oyedun, A., & Kumar, A.** (2018). A review on the current status of various hydrothermal technologies on biomass feedstock. *Renewable And Sustainable Energy Reviews*, 81, 1742-1770. doi: 10.1016/j.rser.2017.05.270
- Kumar, S., Loganathan, V., Gupta, R., & Barnett, M.** (2011). An Assessment of U(VI) removal from groundwater using biochar produced from hydrothermal carbonization. *Journal Of Environmental Management*, 92(10), 2504-2512. doi: 10.1016/j.jenvman.2011.05.013
- Kwiatkowski, M., & Broniek, E.** (2017). An analysis of the porous structure of activated carbons obtained from hazelnut shells by various physical and chemical methods of activation. *Colloids And Surfaces A: Physicochemical And Engineering Aspects*, 529, 443-453. doi: 10.1016/j.colsurfa.2017.06.028
- Le Van, K., & Luong Thi, T.** (2014). Activated carbon derived from rice husk by NaOH activation and its application in supercapacitor. *Progress In Natural Science: Materials International*, 24(3), 191-198. doi: 10.1016/j.pnsc.2014.05.012
- Ledesma, B., Olivares-Marín, M., Álvarez-Murillo, A., Roman, S., & Nabais, J.** (2018). Method for promoting in-situ hydrochar porosity in hydrothermal carbonization of almond shells with air activation. *The Journal Of Supercritical Fluids*, 138, 187-192. doi: 10.1016/j.supflu.2018.04.018
- Lee, J., Lee, K., Sohn, D., Kim, Y., & Park, K.** (2018a). Hydrothermal carbonization of lipid extracted algae for hydrochar production and feasibility of using hydrochar as a solid fuel. *Energy*, 153, 913-920. doi: 10.1016/j.energy.2018.04.112
- Lee, K., Park, C., & Kim, J.** (2018b). Synthesis of ZnO/activated carbon with high surface area for supercapacitor electrodes. *Colloids And Surfaces A: Physicochemical And Engineering Aspects*, 555, 482-490. doi: 10.1016/j.colsurfa.2018.06.077
- Li, B., Zhang, H., Wang, D., Lv, H., & Zhang, C.** (2017). Agricultural waste-derived activated carbon for high performance lithium-ion capacitors. *RSC Advances*, 7(60), 37923-37928. doi: 10.1039/c7ra06680e
- Li, Q., Zhao, C., Chen, X., Wu, W., & Li, Y.** (2009). Comparison of pulverized coal combustion in air and in  $O_2/CO_2$  mixtures by thermo-gravimetric

analysis. *Journal Of Analytical And Applied Pyrolysis*, 85(1-2), 521-528. doi: 10.1016/j.jaap.2008.10.018

- Li, Y., Liu, H., Xiao, K., Liu, X., Hu, H., Li, X., & Yao, H.** (2019). Correlations between the physicochemical properties of hydrochar and specific components of waste lettuce: Influence of moisture, carbohydrates, proteins and lipids. *Bioresource Technology*, 272, 482-488. doi: 10.1016/j.biortech.2018.10.066
- Liang, J., Qiao, S., Lu, G., & Hulicova-Jurcakova, D.** (2012). Carbon-based Catalyst Support in Fuel Cell Applications. *Novel Carbon Adsorbents*, 549-581. doi: 10.1016/b978-0-08-097744-7.00018-1
- Libera, J., & Gogotsi, Y.** (2001). Hydrothermal synthesis of graphite tubes using Ni catalyst. *Carbon*, 39(9), 1307-1318. doi: 10.1016/s0008-6223(00)00263-3
- Libra, J., Ro, K., Kammann, C., Funke, A., Berge, N., & Neubauer, Y.** (2011). Hydrothermal carbonization of biomass residuals: a comparative review of the chemistry, processes and applications of wet and dry pyrolysis. *Biofuels*, 2(1), 71-106. doi: 10.4155/bfs.10.81
- Lima, H., Maniezzo, R., Llop, M., Kupfer, V., Arroyo, P., & Guilherme, M.** (2019). Synthesis and characterization of pecan nutshell-based adsorbent with high specific area and high methylene blue adsorption capacity. *Journal Of Molecular Liquids*, 276, 570-576. doi: 10.1016/j.molliq.2018.12.010
- Lin, Q., Zhang, C., Wang, X., Cheng, B., Mai, N., & Ren, J.** (2019). Impact of activation on properties of carbon-based solid acid catalysts for the hydrothermal conversion of xylose and hemicelluloses. *Catalysis Today*, 319, 31-40. doi: 10.1016/j.cattod.2018.03.070
- Lin, Y., Ma, X., Peng, X., & Yu, Z.** (2016). A mechanism study on hydrothermal carbonization of waste textile. *Energy & Fuels*, 30(9), 7746-7754. doi: 10.1021/acs.energyfuels.6b01365
- Liu, M., Yan, Y., Zhang, L., Wang, X., & Wang, C.** (2012). Hydrothermal preparation of carbon nanosheets and their supercapacitive behavior. *Journal Of Materials Chemistry*, 22(23), 11458. doi: 10.1039/c2jm31484c
- Liu, Y., Huo, Z., Song, Z., Zhang, C., Ren, D., Zhong, H., & Jin, F.** (2019). Preparing a magnetic activated carbon with expired beverage as carbon source and KOH as activator. *Journal Of The Taiwan Institute Of Chemical Engineers*, 96, 575-587. doi: 10.1016/j.jtice.2018.11.017
- Liu, Y., Ma, S., & Chen, J.** (2018). A novel pyro-hydrochar via sequential carbonization of biomass waste: Preparation, characterization and adsorption capacity. *Journal Of Cleaner Production*, 176, 187-195. doi: 10.1016/j.jclepro.2017.12.090
- Liu, Y., Yao, S., Wang, Y., Lu, H., Brar, S., & Yang, S.** (2017). Bio- and hydrochars from rice straw and pig manure: Inter-comparison. *Bioresource Technology*, 235, 332-337. doi: 10.1016/j.biortech.2017.03.103
- Liu, Z., Quek, A., Kent Hoekman, S., & Balasubramanian, R.** (2013). Production of solid biochar fuel from waste biomass by hydrothermal carbonization. *Fuel*, 103, 943-949. doi: 10.1016/j.fuel.2012.07.069

- Long, H., Li, X., Wang, H., & Jia, J.** (2013). Biomass resources and their bioenergy potential estimation: A review. *Renewable And Sustainable Energy Reviews*, 26, 344-352. doi: 10.1016/j.rser.2013.05.035
- Lowell, S., Shield, J.E., Thomas, M.A., & Thommes, M.** (2004). Characterization of Porous Solids and Powders: Surface Area, Pore Size and Density. Published by Kluwer Academic Publishers, ISBN: 978-90-481-6633-6, 350s., 12-14.
- Lu, X., & Berge, N.** (2014). Influence of feedstock chemical composition on product formation and characteristics derived from the hydrothermal carbonization of mixed feedstocks. *Bioresource Technology*, 166, 120-131. doi: 10.1016/j.biortech.2014.05.015
- Lua, A., & Guo, J.** (2001). Preparation and characterization of activated carbons from oil-palm stones for gas-phase adsorption. *Colloids And Surfaces A: Physicochemical And Engineering Aspects*, 179(2-3), 151-162. doi: 10.1016/s0927-7757(00)00651-8
- Ma, X., Li, L., Chen, R., Wang, C., Zhou, K., & Li, H.** (2018). Porous carbon materials based on biomass for acetone adsorption: Effect of surface chemistry and porous structure. *Applied Surface Science*, 459, 657-664. doi: 10.1016/j.apsusc.2018.07.170
- Mäkelä, M., Benavente, V., & Fullana, A.** (2016). Hydrothermal carbonization of industrial mixed sludge from a pulp and paper mill. *Bioresource Technology*, 200, 444-450. doi: 10.1016/j.biortech.2015.10.062
- Makowski, P., Demir Cakan, R., Antonietti, M., Goettmann, F., & Titirici, M.** (2008). Selective partial hydrogenation of hydroxy aromatic derivatives with palladium nanoparticles supported on hydrophilic carbon. *Chemical Communications*, (8), 999. doi: 10.1039/b717928f
- Malghani, S., Gleixner, G., & Trumbore, S.** (2013). Chars produced by slow pyrolysis and hydrothermal carbonization vary in carbon sequestration potential and greenhouse gases emissions. *Soil Biology And Biochemistry*, 62, 137-146. doi: 10.1016/j.soilbio.2013.03.013
- Mamaní, A., Sardella, M., Giménez, M., & Deiana, C.** (2019). Highly microporous carbons from olive tree pruning: Optimization of chemical activation conditions. *Journal Of Environmental Chemical Engineering*, 7(1), 102830. doi: 10.1016/j.jece.2018.102830
- Maniatis, K.** (2001). Progress in biomass gasification: An overview. In: Bridgwater, A, editor. *Progress in thermochemical biomass conversion*. Oxford: Blackwell Science.
- Manyà, J., González, B., Azuara, M., & Arner, G.** (2018). Ultra-microporous adsorbents prepared from vine shoots-derived biochar with high CO<sub>2</sub> uptake and CO<sub>2</sub>/N<sub>2</sub> selectivity. *Chemical Engineering Journal*, 345, 631-639. doi: 10.1016/j.cej.2018.01.092
- Marques, S., Mestre, A., Machuqueiro, M., Gotvajn, A., Marinšek, M., & Carvalho, A.** (2018). Apple tree branches derived activated carbons for the removal of  $\beta$ -blocker atenolol. *Chemical Engineering Journal*, 345, 669-678. doi: 10.1016/j.cej.2018.01.076

- Masselter, S., Zemann, A., & Bobleter, O.** (1995). Analysis of lignin degradation products by capillary electrophoresis. *Chromatographia*, *40*(1-2), 51-57. doi: 10.1007/bf02274608.
- McDougall, G.** (1991). The physical nature and manufacture of activated carbon. *Journal Of The Southern African Institute Of Mining And Metallurgy*, *91*(4), 109-120.
- Menéndez-Díaz, J.A., & Martín-Gullón, I.** (2006). Types of carbon adsorbents and their production. In: Bandosz, T, editor. *Activated carbon surfaces in environmental remediation*. Amsterdam: Elsevier.
- Mestre, A., Bexiga, A., Proença, M., Andrade, M., Pinto, M., & Matos, I.** (2011). Activated carbons from sisal waste by chemical activation with K<sub>2</sub>CO<sub>3</sub>: Kinetics of paracetamol and ibuprofen removal from aqueous solution. *Bioresource Technology*, *102*(17), 8253-8260. doi: 10.1016/j.biortech.2011.06.024
- Mumme, J., Eckervogt, L., Pielert, J., Diakité, M., Rupp, F., & Kern, J.** (2011). Hydrothermal carbonization of anaerobically digested maize silage. *Bioresource Technology*, *102*(19), 9255-9260. doi: 10.1016/j.biortech.2011.06.099
- Nahil, M., & Williams, P.** (2012). Pore characteristics of activated carbons from the phosphoric acid chemical activation of cotton stalks. *Biomass And Bioenergy*, *37*, 142-149. doi: 10.1016/j.biombioe.2011.12.019
- Nakason, K., Panyapinyopol, B., Kanokkantapong, V., Viriya-empikul, N., Kraithong, W., & Pavasant, P.** (2018). Characteristics of hydrochar and liquid fraction from hydrothermal carbonization of cassava rhizome. *Journal Of The Energy Institute*, *91*(2), 184-193. doi: 10.1016/j.joei.2017.01.002
- Nascimento, S., & Rezende, C.** (2018). Combined approaches to obtain cellulose nanocrystals, nanofibrils and fermentable sugars from elephant grass. *Carbohydrate Polymers*, *180*, 38-45. doi: 10.1016/j.carbpol.2017.09.099
- Nizamuddin, S., Baloch, H., Griffin, G., Mubarak, N., Bhutto, A., & Abro, R.** (2017). An overview of effect of process parameters on hydrothermal carbonization of biomass. *Renewable And Sustainable Energy Reviews*, *73*, 1289-1299. doi: 10.1016/j.rser.2016.12.122
- Nizamuddin, S., Mubarak, N., Tiripathi, M., Jayakumar, N., Sahu, J., & Ganesan, P.** (2016). Chemical, dielectric and structural characterization of optimized hydrochar produced from hydrothermal carbonization of palm shell. *Fuel*, *163*, 88-97. doi: 10.1016/j.fuel.2015.08.057
- Nowicki, P., Pietrzak, R., & Wachowska, H.** (2010). Sorption properties of active carbons obtained from walnut shells by chemical and physical activation. *Catalysis Today*, *150*(1-2), 107-114. doi: 10.1016/j.cattod.2009.11.009
- Olivares-Marín, M., Fernández-González, C., Macías-García, A., & Gómez-Serrano, V.** (2006a). Preparation of activated carbons from cherry stones by activation with potassium hydroxide. *Applied Surface Science*, *252*(17), 5980-5983. doi: 10.1016/j.apsusc.2005.11.018

- Olivares-Marín, M., Fernández-González, C., Macías-García, A., & Gómez-Serrano, V.** (2006b). Preparation of activated carbon from cherry stones by chemical activation with ZnCl<sub>2</sub>. *Applied Surface Science*, 252(17), 5967-5971. doi: 10.1016/j.apsusc.2005.11.008
- Ould-Idriss, A., Stitou, M., Cuerda-Correa, E., Fernández-González, C., Macías-García, A., Alexandre-Franco, M., & Gómez-Serrano, V.** (2011). Preparation of activated carbons from olive-tree wood revisited. II. Physical activation with air. *Fuel Processing Technology*, 92(2), 266-270. doi: 10.1016/j.fuproc.2010.05.018
- Overend, R., Milne, T., & Mudge, L.** (1985). *Fundamentals of thermochemical biomass conversion*. London: Elsevier.
- Pala, M., Kantarli, I., Buyukisik, H., & Yanik, J.** (2014). Hydrothermal carbonization and torrefaction of grape pomace: A comparative evaluation. *Bioresource Technology*, 161, 255-262. doi: 10.1016/j.biortech.2014.03.052
- Pallarés, J., González-Cencerrado, A., & Arauzo, I.** (2018). Production and characterization of activated carbon from barley straw by physical activation with carbon dioxide and steam. *Biomass And Bioenergy*, 115, 64-73. doi: 10.1016/j.biombioe.2018.04.015
- Pandolfo, A., & Hollenkamp, A.** (2006). Carbon properties and their role in supercapacitors. *Journal Of Power Sources*, 157(1), 11-27. doi: 10.1016/j.jpowsour.2006.02.065
- Paraskeva, P., Kalderis, D., & Diamadopoulos, E.** (2008). Production of activated carbon from agricultural by-products. *Journal Of Chemical Technology & Biotechnology*, 83(5), 581-592. doi: 10.1002/jctb.1847
- Pari, G., Darmawan, S., & Prihandoko, B.** (2014). Porous Carbon Spheres from Hydrothermal Carbonization and KOH Activation on Cassava and Tapioca Flour Raw Material. *Procedia Environmental Sciences*, 20, 342-351. doi: 10.1016/j.proenv.2014.03.043
- Parshetti, G., Chowdhury, S., & Balasubramanian, R.** (2015). Biomass derived low-cost microporous adsorbents for efficient CO<sub>2</sub> capture. *Fuel*, 148, 246-254. doi: 10.1016/j.fuel.2015.01.032
- Parshetti, G., Kent Hoekman, S., & Balasubramanian, R.** (2013). Chemical, structural and combustion characteristics of carbonaceous products obtained by hydrothermal carbonization of palm empty fruit bunches. *Bioresource Technology*, 135, 683-689. doi: 10.1016/j.biortech.2012.09.042
- Pattiya, A.** (2018). Fast pyrolysis. *Direct Thermochemical Liquefaction For Energy Applications*, 3-28. doi: 10.1016/b978-0-08-101029-7.00001-1
- Pecha, B., & Garcia-Perez, M.** (2015). Pyrolysis of Lignocellulosic Biomass. *Bioenergy*, 413-442. doi: 10.1016/b978-0-12-407909-0.00026-2
- Pereira, P., Oliveira, T., Rosa, M., Cavalcante, F., Moates, G., & Wellner, N.** (2016). Pectin extraction from pomegranate peels with citric acid. *International Journal Of Biological Macromolecules*, 88, 373-379. doi: 10.1016/j.ijbiomac.2016.03.074



- Petrović, J., Perišić, N., Maksimovic, J., Maksimovic, V., Kragovic, M., & Stojanovic, M.** (2016). Hydrothermal conversion of grape pomace: Detailed characterization of obtained hydrochar and liquid phase. *Journal Of Analytical And Applied Pyrolysis*, *118*, 267-277. doi: 10.1016/j.jaap.2016.02.010
- Pezoti, O., Cazetta, A., Bedin, K., Souza, L., Martins, A., & Silva, T.** (2016). NaOH-activated carbon of high surface area produced from guava seeds as a high-efficiency adsorbent for amoxicillin removal: Kinetic, isotherm and thermodynamic studies. *Chemical Engineering Journal*, *288*, 778-788. doi: 10.1016/j.cej.2015.12.042
- Plaza, M., González, A., Pis, J., Rubiera, F., & Pevida, C.** (2014). Production of microporous biochars by single-step oxidation: Effect of activation conditions on CO<sub>2</sub> capture. *Applied Energy*, *114*, 551-562. doi: 10.1016/j.apenergy.2013.09.058
- Prahas, D., Kartika, Y., Indraswati, N., & Ismadji, S.** (2008). Activated carbon from jackfruit peel waste by H<sub>3</sub>PO<sub>4</sub> chemical activation: Pore structure and surface chemistry characterization. *Chemical Engineering Journal*, *140*(1-3), 32-42. doi: 10.1016/j.cej.2007.08.032
- Qian, H., Yu, S., Luo, L., Gong, J., Fei, L., & Liu, X.** (2006). Synthesis of Uniform Te@Carbon-Rich Composite Nanocables with Photoluminescence Properties and Carbonaceous Nanofibers by the Hydrothermal Carbonization of Glucose. *Chemistry Of Materials*, *18*(8), 2102-2108. doi: 10.1021/cm052848y
- Qian, W., Luo, X., Wang, X., Guo, M., & Li, B.** (2018). Removal of methylene blue from aqueous solution by modified bamboo hydrochar. *Ecotoxicology And Environmental Safety*, *157*, 300-306. doi: 10.1016/j.ecoenv.2018.03.088
- Qin, K., & Thunman, H.** (2015). Diversity of chemical composition and combustion reactivity of various biomass fuels. *Fuel*, *147*, 161-169. doi: 10.1016/j.fuel.2015.01.047
- Rambabu, N., Rao, B., Surisetty, V., Das, U., & Dalai, A.** (2015). Production, characterization, and evaluation of activated carbons from de-oiled canola meal for environmental applications. *Industrial Crops And Products*, *65*, 572-581. doi: 10.1016/j.indcrop.2014.09.046
- Ranzi, E., Faravelli, T., & Manenti, F.** (2016). Pyrolysis, Gasification, and Combustion of Solid Fuels. *Advances In Chemical Engineering*, *49*, 1-94. doi: 10.1016/bs.ache.2016.09.001
- Rashidi, N., & Yusup, S.** (2017). A review on recent technological advancement in the activated carbon production from oil palm wastes. *Chemical Engineering Journal*, *314*, 277-290. doi: 10.1016/j.cej.2016.11.059
- Regmi, P., Garcia Moscoso, J., Kumar, S., Cao, X., Mao, J., & Schafran, G.** (2012). Removal of copper and cadmium from aqueous solution using switchgrass biochar produced via hydrothermal carbonization process. *Journal Of Environmental Management*, *109*, 61-69. doi: 10.1016/j.jenvman.2012.04.047
- Reza, M., Andert, J., Wirth, B., Busch, D., Pielert, J., Lynam, J., & Mumme, J.** (2014a). Hydrothermal Carbonization of Biomass for Energy and Crop Production. *Applied Bioenergy*, *1*(1). doi: 10.2478/apbi-2014-0001

- Reza, M., Lynam, J., Uddin, M., & Coronella, C.** (2013). Hydrothermal carbonization: Fate of inorganics. *Biomass And Bioenergy*, *49*, 86-94. doi: 10.1016/j.biombioe.2012.12.004
- Reza, M., Uddin, M., Lynam, J., Hoekman, S., & Coronella, C.** (2014b). Hydrothermal carbonization of loblolly pine: reaction chemistry and water balance. *Biomass Conversion And Biorefinery*, *4*(4), 311-321. doi: 10.1007/s13399-014-0115-9
- Reza, M., Yang, X., Coronella, C., Lin, H., Hathwaik, U., & Shintani, D.** (2015). Hydrothermal Carbonization (HTC) and Pelletization of Two Arid Land Plants Bagasse for Energy Densification. *ACS Sustainable Chemistry & Engineering*, *4*(3), 1106-1114. doi: 10.1021/acssuschemeng.5b01176
- Rezma, S., Birot, M., Hafiane, A., & Deleuze, H.** (2017). Physically activated microporous carbon from a new biomass source: Date palm petioles. *Comptes Rendus Chimie*, *20*(9-10), 881-887. doi: 10.1016/j.crci.2017.05.003
- Román, S., Valente Nabais, J., Ledesma, B., González, J., Laginhas, C., & Titirici, M.** (2013). Production of low-cost adsorbents with tunable surface chemistry by conjunction of hydrothermal carbonization and activation processes. *Microporous And Mesoporous Materials*, *165*, 127-133. doi: 10.1016/j.micromeso.2012.08.006
- Ruan, S., Wan, J., Fu, Y., Han, K., Li, X., & Chen, J.** (2014). PEGylated Fluorescent Carbon Nanoparticles for Noninvasive Heart Imaging. *Bioconjugate Chemistry*, *25*(6), 1061-1068. doi: 10.1021/bc5001627
- Sabio, E., Álvarez-Murillo, A., Román, S., & Ledesma, B.** (2016). Conversion of tomato-peel waste into solid fuel by hydrothermal carbonization: Influence of the processing variables. *Waste Management*, *47*, 122-132. doi: 10.1016/j.wasman.2015.04.016
- Safari, F., Salimi, M., Tavasoli, A., & Ataei, A.** (2016). Non-catalytic conversion of wheat straw, walnut shell and almond shell into hydrogen rich gas in supercritical water media. *Chinese Journal Of Chemical Engineering*, *24*(8), 1097-1103. doi: 10.1016/j.cjche.2016.03.002
- Saffe, A., Fernandez, A., Mazza, G., & Rodriguez, R.** (2018). Prediction of regional agro-industrial wastes characteristics by thermogravimetric analysis to obtain bioenergy using thermal process. *Energy Exploration & Exploitation*, *37*(1), 544-557. doi: 10.1177/0144598718793908
- Saleh, S., Hansen, B., Jensen, P., & Dam-Johansen, K.** (2013). Influence of Biomass Chemical Properties on Torrefaction Characteristics. *Energy & Fuels*, *27*(12), 7541-7548. doi: 10.1021/ef401788m
- Salman, J.** (2014). Optimization of preparation conditions for activated carbon from palm oil fronds using response surface methodology on removal of pesticides from aqueous solution. *Arabian Journal Of Chemistry*, *7*(1), 101-108. doi: 10.1016/j.arabjc.2013.05.033
- Sánchez, A., Elguézabal, A., & de La Torre Saenz, L.** (2001). CO<sub>2</sub> activation of char from *Quercus agrifolia* wood waste. *Carbon*, *39*(9), 1367-1377. doi: 10.1016/s0008-6223(00)00253-0

- Sartova, K., Omurzak, E., Kambarova, G., Dzhumaev, I., Borkoev, B., & Abdullaeva, Z.** (2019). Activated carbon obtained from the cotton processing wastes. *Diamond And Related Materials*, 91, 90-97. doi: 10.1016/j.diamond.2018.11.011
- Schwald, W., & Bobleter, O.** (1989). Hydrothermolysis of Cellulose Under Static and Dynamic Conditions at High Temperatures. *Journal Of Carbohydrate Chemistry*, 8(4), 565-578. doi: 10.1080/07328308908048017
- Sevilla, M., & Fuertes, A.** (2009). The production of carbon materials by hydrothermal carbonization of cellulose. *Carbon*, 47(9), 2281-2289. doi: 10.1016/j.carbon.2009.04.026.
- Sevilla, M., & Fuertes, A.** (2011). Sustainable porous carbons with a superior performance for CO<sub>2</sub> capture. *Energy & Environmental Science*, 4(5), 1765. doi: 10.1039/c0ee00784f
- Sevilla, M., & Mokaya, R.** (2014). Energy storage applications of activated carbons: supercapacitors and hydrogen storage. *Energy Environ. Sci.*, 7(4), 1250-1280. doi: 10.1039/c3ee43525c
- Sevilla, M., Fuertes, A., & Mokaya, R.** (2011a). High density hydrogen storage in superactivated carbons from hydrothermally carbonized renewable organic materials. *Energy & Environmental Science*, 4(4), 1400. doi: 10.1039/c0ee00347f
- Sevilla, M., Gu, W., Falco, C., Titirici, M., Fuertes, A., & Yushin, G.** (2014). Hydrothermal synthesis of microalgae-derived microporous carbons for electrochemical capacitors. *Journal Of Power Sources*, 267, 26-32. doi: 10.1016/j.jpowsour.2014.05.046
- Sevilla, M., Maciá-Agulló, J., & Fuertes, A.** (2011b). Hydrothermal carbonization of biomass as a route for the sequestration of CO<sub>2</sub>: Chemical and structural properties of the carbonized products. *Biomass And Bioenergy*, 35(7), 3152-3159. doi: 10.1016/j.biombioe.2011.04.032
- Shahraki, Z., Sharififard, H., & Lashanizadegan, A.** (2018). Grape stalks biomass as raw material for activated carbon production: synthesis, characterization and adsorption ability. *Materials Research Express*, 5(5), 055603. doi: 10.1088/2053-1591/aac1cd
- Simsir, H., Eltugral, N., & Karagoz, S.** (2017). Hydrothermal carbonization for the preparation of hydrochars from glucose, cellulose, chitin, chitosan and wood chips via low-temperature and their characterization. *Bioresource Technology*, 246, 82-87. doi: 10.1016/j.biortech.2017.07.018
- Sindhu, R., Binod, P., & Pandey, A.** (2016). Biological pretreatment of lignocellulosic biomass – An overview. *Bioresource Technology*, 199, 76-82. doi: 10.1016/j.biortech.2015.08.030
- Stemann, J., Putschew, A., & Ziegler, F.** (2013). Hydrothermal carbonization: Process water characterization and effects of water recirculation. *Bioresource Technology*, 143, 139-146. doi: 10.1016/j.biortech.2013.05.098
- Stirling, R., Snape, C., & Meredith, W.** (2018). The impact of hydrothermal carbonisation on the char reactivity of biomass. *Fuel Processing Technology*, 177, 152-158. doi: 10.1016/j.fuproc.2018.04.023

- Sun, K., & Jiang, J.** (2010). Preparation and characterization of activated carbon from rubber-seed shell by physical activation with steam. *Biomass And Bioenergy*, 34(4), 539-544. doi: 10.1016/j.biombioe.2009.12.020
- Sun, Y., Gao, B., Yao, Y., Fang, J., Zhang, M., & Zhou, Y.** (2014). Effects of feedstock type, production method, and pyrolysis temperature on biochar and hydrochar properties. *Chemical Engineering Journal*, 240, 574-578. doi: 10.1016/j.cej.2013.10.081
- Sun, Y., Yang, G., Zhang, L., & Sun, Z.** (2017). Preparation of high performance H<sub>2</sub>S removal biochar by direct fluidized bed carbonization using potato peel waste. *Process Safety And Environmental Protection*, 107, 281-288. doi: 10.1016/j.psep.2017.02.018
- Takaya, C., Fletcher, L., Singh, S., Anyikude, K., & Ross, A.** (2016). Phosphate and ammonium sorption capacity of biochar and hydrochar from different wastes. *Chemosphere*, 145, 518-527. doi: 10.1016/j.chemosphere.2015.11.052
- Tan, X., Liu, S., Liu, Y., Gu, Y., Zeng, G., & Hu, X.** (2017). Biochar as potential sustainable precursors for activated carbon production: Multiple applications in environmental protection and energy storage. *Bioresource Technology*, 227, 359-372. doi: 10.1016/j.biortech.2016.12.083
- Tang, D., Luo, Y., Lei, W., Xiang, Q., Ren, W., & Song, W.** (2018). Hierarchical porous carbon materials derived from waste lentinus edodes by a hybrid hydrothermal and molten salt process for supercapacitor applications. *Applied Surface Science*, 462, 862-871. doi: 10.1016/j.apsusc.2018.08.153
- Tang, K., Fu, L., White, R., Yu, L., Titirici, M., Antonietti, M., & Maier, J.** (2012b). Hollow Carbon Nanospheres with Superior Rate Capability for Sodium-Based Batteries. *Advanced Energy Materials*, 2(7), 873-877. doi: 10.1002/aenm.201100691
- Tang, K., White, R., Mu, X., Titirici, M., van Aken, P., & Maier, J.** (2012a). Hollow Carbon Nanospheres with a High Rate Capability for Lithium-Based Batteries. *Chemosphere*, 5(2), 400-403. doi: 10.1002/cssc.201100609
- Technical Association of the Pulp and Paper Industry (TAPPI).** (2006). TAPPI Test method T 222 om-02 – acid – insoluble lignin in wood and pulp.
- Tekin, K., Karagöz, S., & Bektaş, S.** (2014). A review of hydrothermal biomass processing. *Renewable And Sustainable Energy Reviews*, 40, 673-687. doi: 10.1016/j.rser.2014.07.216
- Thomsen, M., Thygesen, A., & Thomsen, A.** (2008). Hydrothermal treatment of wheat straw at pilot plant scale using a three-step reactor system aiming at high hemicellulose recovery, high cellulose digestibility and low lignin hydrolysis. *Bioresource Technology*, 99(10), 4221-4228. doi: 10.1016/j.biortech.2007.08.054
- Tian, D., Xu, Z., Zhang, D., Chen, W., Cai, J., & Deng, H.** (2019). Micro-mesoporous carbon from cotton waste activated by FeCl<sub>3</sub>/ZnCl<sub>2</sub>: Preparation, optimization, characterization and adsorption of methylene blue and eriochrome black T. *Journal Of Solid State Chemistry*, 269, 580-587. doi: 10.1016/j.jssc.2018.10.035

- Titirici, M., & Antonietti, M.** (2010). ChemInform Abstract: Chemistry and Materials Options of Sustainable Carbon Materials Made by Hydrothermal Carbonization. *Cheminform*, *41*(16). doi: 10.1002/chin.201016219
- Titirici, M., Antonietti, M., & Thomas, A.** (2006). A Generalized Synthesis of Metal Oxide Hollow Spheres Using a Hydrothermal Approach. *Chemistry Of Materials*, *18*(16), 3808-3812. doi: 10.1021/cm052768u
- Titirici, M., Thomas, A., & Antonietti, M.** (2007). Back in the black: hydrothermal carbonization of plant material as an efficient chemical process to treat the CO<sub>2</sub> problem?. *New Journal Of Chemistry*, *31*(6), 787. doi: 10.1039/b616045j
- Titirici, M., Thomas, A., & Antonietti, M.** (2007b). Replication and Coating of Silica Templates by Hydrothermal Carbonization. *Advanced Functional Materials*, *17*(6), 1010-1018. doi: 10.1002/adfm.200600501
- Titirici, M., Thomas, A., Yu, S., Müller, J., & Antonietti, M.** (2007c). A Direct Synthesis of Mesoporous Carbons with Bicontinuous Pore Morphology from Crude Plant Material by Hydrothermal Carbonization. *Chemistry Of Materials*, *19*(17), 4205-4212. doi: 10.1021/cm0707408
- Toklu, E.** (2017). Biomass energy potential and utilization in Turkey. *Renewable Energy*, *107*, 235-244. doi: 10.1016/j.renene.2017.02.008
- Toor, S., Rosendahl, L., Hoffmann, J., Pedersen, T., Nielsen, R., & Søgaard, E.** (2014). Hydrothermal Liquefaction of Biomass. *Green Chemistry And Sustainable Technology*, 189-217. doi: 10.1007/978-3-642-54458-3\_9
- Trakal, L., Šigut, R., Šillerová, H., Faturiková, D., & Komárek, M.** (2014). Copper removal from aqueous solution using biochar: Effect of chemical activation. *Arabian Journal Of Chemistry*, *7*(1), 43-52. doi: 10.1016/j.arabjc.2013.08.001
- Tran, H., Huang, F., Lee, C., & Chao, H.** (2017). Activated carbon derived from spherical hydrochar functionalized with triethylenetetramine: synthesis, characterizations, and adsorption application. *Green Processing And Synthesis*, *6*(6). doi: 10.1515/gps-2016-0178
- Tsapekos, P., Kougias, P., Egelund, H., Larsen, U., Pedersen, J., Trénel, P., & Angelidaki, I.** (2017). Improving the energy balance of grass-based anaerobic digestion through combined harvesting and pretreatment. *Anaerobe*, *46*, 131-137. doi: 10.1016/j.anaerobe.2016.12.005
- Tseng, R., & Tseng, S.** (2005). Pore structure and adsorption performance of the KOH-activated carbons prepared from corncob. *Journal Of Colloid And Interface Science*, *287*(2), 428-437. doi: 10.1016/j.jcis.2005.02.033
- Tsukashima, H.** (1967). Alkaline permanganate oxidation of artificial coals prepared from lignin and cellulose. *Fuel*, *46*, 177-185.
- Turley, D.B.** (2009). The Chemical Value of Biomass. In: Clark, J., & Deswarte, F, editors. *Introduction to chemicals from biomass*. Chichester: Wiley.
- Tusi, M., Brandalise, M., Correa, O., Oliveira Neto, A., Linardi, M., & Spinacé, E.** (2007). Preparation of PtRu/carbon hybrids by hydrothermal carbonization process. *Materials Research*, *10*(2), 171-175. doi: 10.1590/s1516-14392007000200013

- Tusi, M., Brandalise, M., Polanco, N., Correa, O., da Silva, A., & Villalba, J.** (2013). Ni/Carbon Hybrid Prepared by Hydrothermal Carbonization and Thermal Treatment as Support for PtRu Nanoparticles for Direct Methanol Fuel Cell. *Journal Of Materials Science & Technology*, 29(8), 747-751. doi: 10.1016/j.jmst.2013.05.004
- Tzvetkov, G., Mihaylova, S., Stoitchkova, K., Tzvetkov, P., & Spassov, T.** (2016). Mechanochemical and chemical activation of lignocellulosic material to prepare powdered activated carbons for adsorption applications. *Powder Technology*, 299, 41-50. doi: 10.1016/j.powtec.2016.05.033
- Uçar, S., & Karagöz, S.** (2009). The slow pyrolysis of pomegranate seeds: The effect of temperature on the product yields and bio-oil properties. *Journal Of Analytical And Applied Pyrolysis*, 84(2), 151-156. doi: 10.1016/j.jaap.2009.01.005
- Ullah, K., Kumar Sharma, V., Dhingra, S., Braccio, G., Ahmad, M., & Sofia, S.** (2015). Assessing the lignocellulosic biomass resources potential in developing countries: A critical review. *Renewable And Sustainable Energy Reviews*, 51, 682-698. doi: 10.1016/j.rser.2015.06.044
- Unur, E.** (2013). Functional nanoporous carbons from hydrothermally treated biomass for environmental purification. *Microporous And Mesoporous Materials*, 168, 92-101. doi: 10.1016/j.micromeso.2012.09.027
- Unur, E., Brutti, S., Panero, S., & Scrosati, B.** (2013). Nanoporous carbons from hydrothermally treated biomass as anode materials for lithium ion batteries. *Microporous And Mesoporous Materials*, 174, 25-33. doi: 10.1016/j.micromeso.2013.02.032
- Uzuner, S., Sharma-Shivappa, R., Cekmecelioglu, D., & Kolar, P.** (2018). A novel oxidative destruction of lignin and enzymatic digestibility of hazelnut shells. *Biocatalysis And Agricultural Biotechnology*, 13, 110-115. doi: 10.1016/j.bcab.2017.12.003
- Vernersson, T., Bonelli, P., Cerrella, E., & Cukierman, A.** (2002). Arundo donax cane as a precursor for activated carbons preparation by phosphoric acid activation. *Bioresource Technology*, 83(2), 95-104. doi: 10.1016/s0960-8524(01)00205-x
- Wang, B., Zhai, Y., Wang, T., Li, S., Peng, C., & Wang, Z.** (2019). Fabrication of bean dreg-derived carbon with high adsorption for methylene blue: Effect of hydrothermal pretreatment and pyrolysis process. *Bioresource Technology*, 274, 525-532. doi: 10.1016/j.biortech.2018.12.022
- Wang, J., & Kaskel, S.** (2012). KOH activation of carbon-based materials for energy storage. *Journal Of Materials Chemistry*, 22(45), 23710. doi: 10.1039/c2jm34066f
- Wang, L., Guo, Y., Zou, B., Rong, C., Ma, X., & Qu, Y.** (2011a). High surface area porous carbons prepared from hydrochars by phosphoric acid activation. *Bioresource Technology*, 102(2), 1947-1950. doi: 10.1016/j.biortech.2010.08.100
- Wang, L., Zhang, Z., Qu, Y., Guo, Y., Wang, Z., & Wang, X.** (2014). A novel route for preparation of high-performance porous carbons from hydrochars by KOH

activation. *Colloids And Surfaces A: Physicochemical And Engineering Aspects*, 447, 183-187. doi: 10.1016/j.colsurfa.2014.01.013

- Wang, M., Xie, R., Chen, Y., Pu, X., Jiang, W., & Yao, L.** (2018a). A novel mesoporous zeolite-activated carbon composite as an effective adsorbent for removal of ammonia-nitrogen and methylene blue from aqueous solution. *Bioresource Technology*, 268, 726-732. doi: 10.1016/j.biortech.2018.08.037
- Wang, T., Zhai, Y., Zhu, Y., Li, C., & Zeng, G.** (2018b). A review of the hydrothermal carbonization of biomass waste for hydrochar formation: Process conditions, fundamentals, and physicochemical properties. *Renewable And Sustainable Energy Reviews*, 90, 223-247. doi: 10.1016/j.rser.2018.03.071
- Wang, X., Hu, C., Xiong, Y., Liu, H., Du, G., & He, X.** (2011b). Carbon-nanosphere-supported Pt nanoparticles for methanol and ethanol electro-oxidation in alkaline media. *Journal Of Power Sources*, 196(4), 1904-1908. doi: 10.1016/j.jpowsour.2010.09.072
- Wang, Y., Yang, R., Li, M., & Zhao, Z.** (2015). Hydrothermal preparation of highly porous carbon spheres from hemp (*Cannabis sativa* L.) stem hemicellulose for use in energy-related applications. *Industrial Crops And Products*, 65, 216-226. doi: 10.1016/j.indcrop.2014.12.008
- Wang, Z., Li, C., Gu, D., & Yin, G.** (2013). Carbon riveted PtRu/C catalyst from glucose in-situ carbonization through hydrothermal method for direct methanol fuel cell. *Journal Of Power Sources*, 238, 283-289. doi: 10.1016/j.jpowsour.2013.03.082
- Wei, L., Sevilla, M., Fuertes, A., Mokaya, R., & Yushin, G.** (2011). Hydrothermal Carbonization of Abundant Renewable Natural Organic Chemicals for High-Performance Supercapacitor Electrodes. *Advanced Energy Materials*. doi: 10.1002/aenm.201000019
- Wiedner, K., Naisse, C., Rumpel, C., Pozzi, A., Wieczorek, P., & Glaser, B.** (2013). Chemical modification of biomass residues during hydrothermal carbonization – What makes the difference, temperature or feedstock?. *Organic Geochemistry*, 54, 91-100. doi: 10.1016/j.orggeochem.2012.10.006
- Wilk, M., & Magdziarz, A.** (2017). Hydrothermal carbonization, torrefaction and slow pyrolysis of *Miscanthus giganteus*. *Energy*, 140, 1292-1304. doi: 10.1016/j.energy.2017.03.031
- Wilk, M., Magdziarz, A., Jayaraman, K., Szymańska-Chargot, M., & Gökalp, I.** (2019). Hydrothermal carbonization characteristics of sewage sludge and lignocellulosic biomass. A comparative study. *Biomass And Bioenergy*, 120, 166-175. doi: 10.1016/j.biombioe.2018.11.016
- Wu, F., & Tseng, R.** (2008). High adsorption capacity NaOH-activated carbon for dye removal from aqueous solution. *Journal Of Hazardous Materials*, 152(3), 1256-1267. doi: 10.1016/j.jhazmat.2007.07.109
- Wu, Q., Yu, S., Hao, N., Wells, T., Meng, X., & Li, M.** (2017). Characterization of products from hydrothermal carbonization of pine. *Bioresource Technology*, 244, 78-83. doi: 10.1016/j.biortech.2017.07.138
- Xue, Y., Gao, B., Yao, Y., Inyang, M., Zhang, M., Zimmerman, A., & Ro, K.** (2012). Hydrogen peroxide modification enhances the ability of biochar

- (hydrochar) produced from hydrothermal carbonization of peanut hull to remove aqueous heavy metals: Batch and column tests. *Chemical Engineering Journal*, 200-202, 673-680. doi: 10.1016/j.cej.2012.06.116
- Yakout, S., & Sharaf El-Deen, G.** (2016). Characterization of activated carbon prepared by phosphoric acid activation of olive stones. *Arabian Journal Of Chemistry*, 9, S1155-S1162. doi: 10.1016/j.arabjc.2011.12.002
- Yan, W., Hastings, J., Acharjee, T., Coronella, C., & Vásquez, V.** (2010). Mass and Energy Balances of Wet Torrefaction of Lignocellulosic Biomass. *Energy & Fuels*, 24(9), 4738-4742. doi: 10.1021/ef901273n
- Yang, G., Song, S., Li, J., Tang, Z., Ye, J., & Yang, J.** (2019). Preparation and CO<sub>2</sub> adsorption properties of porous carbon by hydrothermal carbonization of tree leaves. *Journal Of Materials Science & Technology*, 35(5), 875-884. doi: 10.1016/j.jmst.2018.11.019
- Yang, K., Peng, J., Srinivasakannan, C., Zhang, L., Xia, H., & Duan, X.** (2010). Preparation of high surface area activated carbon from coconut shells using microwave heating. *Bioresource Technology*, 101(15), 6163-6169. doi: 10.1016/j.biortech.2010.03.001
- Yang, T., & Lua, A.** (2003). Characteristics of activated carbons prepared from pistachio-nut shells by physical activation. *Journal Of Colloid And Interface Science*, 267(2), 408-417. doi: 10.1016/s0021-9797(03)00689-1
- Yang, W., Shimanouchi, T., & Kimura, Y.** (2015a). Characterization of the Residue and Liquid Products Produced from Husks of Nuts from *Carya cathayensis* Sarg by Hydrothermal Carbonization. *ACS Sustainable Chemistry & Engineering*, 3(4), 591-598. doi: 10.1021/acssuschemeng.5b00103
- Yang, W., Shimanouchi, T., Iwamura, M., Takahashi, Y., Mano, R., & Takashima, K.** (2015b). Elevating the fuel properties of *Humulus lupulus*, *Plumeria alba* and *Calophyllum inophyllum* L. through wet torrefaction. *Fuel*, 146, 88-94. doi: 10.1016/j.fuel.2015.01.005
- Yang, W., Shimizu, I., Ono, T., & Kimura, Y.** (2014). Preparation of biodegradable foam from walnut shells treated by subcritical water. *Journal Of Chemical Technology & Biotechnology*, 90(1), 44-49. doi: 10.1002/jctb.4451
- Yang, W., Wang, H., Zhang, M., Zhu, J., Zhou, J., & Wu, S.** (2016). Fuel properties and combustion kinetics of hydrochar prepared by hydrothermal carbonization of bamboo. *Bioresource Technology*, 205, 199-204. doi: 10.1016/j.biortech.2016.01.068
- Yazdani, N., & Brown, E.** (2016). Carbon nanofibers in cement composites. *Innovative Developments Of Advanced Multifunctional Nanocomposites In Civil And Structural Engineering*, 47-58. doi: 10.1016/b978-1-78242-326-3.00003-8
- You, P., & Kamarudin, S.** (2017). Recent progress of carbonaceous materials in fuel cell applications: An overview. *Chemical Engineering Journal*, 309, 489-502. doi: 10.1016/j.cej.2016.10.051
- Yu, Y., Lou, X., & Wu, H.** (2008). Some Recent Advances in Hydrolysis of Biomass in Hot-Compressed Water and Its Comparisons with Other Hydrolysis Methods. *Energy & Fuels*, 22(1), 46-60. doi: 10.1021/ef700292p



- Zeng, G., Lou, S., Ying, H., Wu, X., Dou, X., Ai, N., & Wang, J.** (2018). Preparation of Microporous Carbon from *Sargassum horneri* by Hydrothermal Carbonization and KOH Activation for CO<sub>2</sub> Capture. *Journal Of Chemistry*, 2018, 1-11. doi: 10.1155/2018/4319149
- Zeng, L., Lou, X., Zhang, J., Wu, C., Liu, J., & Jia, C.** (2019). Carbonaceous mudstone and lignin-derived activated carbon and its application for supercapacitor electrode. *Surface And Coatings Technology*, 357, 580-586. doi: 10.1016/j.surfcoat.2018.10.041
- Zhang, L., & Zhao, X.** (2009). Carbon-based materials as supercapacitor electrodes. *Chemical Society Reviews*, 38(9), 2520. doi: 10.1039/b813846j
- Zhang, L., Wang, Q., Wang, B., Yang, G., Lucia, L., & Chen, J.** (2015). Hydrothermal Carbonization of Corncob Residues for Hydrochar Production. *Energy & Fuels*, 29(2), 872-876. doi: 10.1021/ef502462p
- Zhang, S., Zhu, X., Zhou, S., Shang, H., Luo, J., & Tsang, D.** (2019). Hydrothermal Carbonization for Hydrochar Production and Its Application. *Biochar From Biomass And Waste*, 275-294. doi: 10.1016/b978-0-12-811729-3.00015-7
- Zhao, P., Shen, Y., Ge, S., Chen, Z., & Yoshikawa, K.** (2014). Clean solid biofuel production from high moisture content waste biomass employing hydrothermal treatment. *Applied Energy*, 131, 345-367. doi: 10.1016/j.apenergy.2014.06.038.
- Zhao, S.X., Ta, N., & Wang, X.D.** (2017). Effect of Temperature on the Structural and Physicochemical Properties of Biochar with Apple Tree Branches as Feedstock Material. *Energies*. 10, 1293. doi: 10.3390/en10091293
- Zheng, A., Zhao, Z., Huang, Z., Zhao, K., Wei, G., & Wang, X.** (2014). Catalytic Fast Pyrolysis of Biomass Pretreated by Torrefaction with Varying Severity. *Energy & Fuels*, 28(9), 5804-5811. doi: 10.1021/ef500892k
- Zhong, C., & Wei, X.** (2004). A comparative experimental study on the liquefaction of wood. *Energy*, 29(11), 1731-1741. doi: 10.1016/j.energy.2004.03.096
- Zhu, X., Liu, Y., Qian, F., Zhou, C., Zhang, S., & Chen, J.** (2015). Role of Hydrochar Properties on the Porosity of Hydrochar-based Porous Carbon for Their Sustainable Application. *ACS Sustainable Chemistry & Engineering*, 3(5), 833-840. doi: 10.1021/acssuschemeng.5b00153
- Zhu, Y., Gao, S., & Hosmane, N.** (2018). Carbonaceous Materials. *Comprehensive Energy Systems*, 40-71. doi: 10.1016/b978-0-12-809597-3.00202-9
- Zhuang, X., Zhan, H., Huang, Y., Song, Y., Yin, X., & Wu, C.** (2018). Conversion of industrial biowastes to clean solid fuels via hydrothermal carbonization (HTC): Upgrading mechanism in relation to coalification process and combustion behavior. *Bioresource Technology*, 267, 17-29. doi: 10.1016/j.biortech.2018.07.002
- Zhuang, X., Zhan, H., Song, Y., He, C., Huang, Y., Yin, X., & Wu, C.** (2019). Insights into the evolution of chemical structures in lignocellulose and non-lignocellulose biowastes during hydrothermal carbonization (HTC). *Fuel*, 236, 960-974. doi: 10.1016/j.fuel.2018.09.019



## CURRICULUM VITAE

**Name Surname:** Sümeyra Seniha BARAN

**Place and Date of Birth:** Giresun / 10.06.1992

**Address:** Kultur Mah. Kumova Sok. Kardelen Sitesi A Blok D:2 Nilufer/BURSA

**E-Mail:** sumeyraseniha@gmail.com

**B.Sc.:** Yalova University – Energy Systems Engineering

### Professional Experience and Rewards:

- Priority Areas Graduate Scholarship – The Scientific and Technological Research Council of Turkey | March 2018 – March 2019
- Production of Bio-Based Porous Carbon Materials from Lignocellulosics – Funded by Yalova University Scientific Research Unit (Project No: 2018/YL/0004) | May 2018 – May 2019
- Biobased Fuel Additive (Alkyl Phenols) from Organosolv Lignin – Funded by Yalova University Scientific Research Unit (Project No: 2017/AP/146) | January 2018 – January 2019

### List of Publications and Patents:

- Kilic, B., Turkdogan, S., Astam, A., Baran, S.S., Asgin, M., Gur, E., & Kocak, Y. (2018). Interfacial engineering of CuO nanorod/ZnO nanowire hybrid nanostructure photoanode in dye-sensitized solar cell. *Journal of Nanoparticle Research*, 20(1). doi: 10.1007/s11051-017-4103-4
- Kilic, B., Turkdogan, S., Astam, A., Baran, S.S., Asgin, M., Cebeci, H., & Urk, D. (2017). Graphene-based copper oxide thin film nanostructures as high-efficiency photocathode for p-type dye-sensitized solar cells. *Journal of Photonics for Energy*, 7(04), 1. doi: 10.1117/1.jpe.7.045502
- Baran, S.S., Aşgin, M., & Kılıç, B. (2017). Synthesis of CuO on ZnO Semiconductor and Investigation of Structural and Optical Properties in Dye Sensitized Solar Cell. *13th Nanoscience & Nanotechnology Conference – Poster Presentation*. October 22-25, 2017 Antalya, Turkey
- Baran, S.S., Aşgin, M., & Kılıç, B. (2017). Synthesizing ZnO Nanoparticle Semiconductor by Electro Plating for Using as Photoanode in Dye Sensitized Solar Cells and Comparing with TiO<sub>2</sub> Semiconductor. *13th Nanoscience & Nanotechnology Conference – Poster Presentation*. October 22-25, 2017 Antalya, Turkey

- Kilic, B., Turkdogan, S., Asgin, M., & Baran, S.S. (2017). Copper Oxide Thin Film and Mesoporous ZnO as a Barrier in Dye-Sensitized Solar Cells. *International Porous & Powder Materials – Oral Presentation*, September 12-15, 2017 Kuşadası, Turkey
- Süngü, D.E., Yakut M.B., Erdem, K., Baran, S.S., & Aşgin, M. (2017). Investigation of Usage, Structural and Optical Characterization of CuO Photo Anode in Dye-Sensitized Solar Cells. *8th National Chemistry Student Congress – Poster Presentation*, May 16-18 Istanbul, Turkey
- Baran, S.S., & Aşgin, M. (2017). The Synthesis of Carbon Nanotubes/Nanowires for Produce High-Efficiency Dye-Sensitized Solar Cell. *8th National Chemistry Student Congress – Poster Presentation*, May 16-18 Istanbul, Turkey
- Öztemur, İ., Karamustafaoglu, T., Baran, S.S., & Aşgin, M. (2017). Using WS<sub>2</sub> Counter Electrode in Dye-Sensitized Solar Cell, Investigating Structural and Optical Characterization. *8th National Chemistry Student Congress – Poster Presentation*, May 16-18 Istanbul, Turkey
- Dilber, S., Bay, O., Efe, Ö., Baran, S.S., & Aşgin, M. (2017). Investigation of Structural and Optical Properties of ZnO/CuO Photo Anode in Dye-Sensitized Solar Cells. *8th National Chemistry Student Congress – Poster Presentation*, May 16-18 Istanbul, Turkey
- Kilic, B., Sezginer, M., Baran, S.S., Hergul, A.S., & Tüzemen, S. (2015). The Synthesis of Carbon Nanotubes/ZnO nanowires for Produce High Efficiency Solar Cell. *11th Nanoscience and Nanotechnology Conference – Poster Presentation*, June 22-25, 2015 Ankara, Turkey

#### **PUBLICATIONS/PRESENTATIONS ON THE THESIS**

- Başakçılardan Kabakcı, S., & Baran, S.S. (2018). Investigation of Thermochemical Characteristics of Various Biomass Hydrochars. *Proceedings Book of 13th National Chemical Engineering Congress*, September 03-06, 2018 Van, Turkey.
- Başakçılardan Kabakcı, S., & Baran, S.S. (2018). Investigation of Thermochemical Characteristics of Various Biomass Hydrochars. *13th National Chemical Engineering Congress – Oral Presentation*, September 03-06, 2018 Van, Turkey.